Summer 2019

Role of Epigenetic, Molecular and Cellular Pathways in the Regulation of Inflammation

William James Becker

ROLE OF EPIGENETIC, MOLECULAR AND CELLULAR PATHWAYS IN THE REGULATION OF INFLAMMATION

by

William James Becker

Bachelor of Science
University of South Carolina, 2014

Submitted in Partial Fulfillment of the Requirements

For the Degree of Doctor of Philosophy in

Biomedical Science

School of Medicine

University of South Carolina

2019

Accepted by:

Mitzi Nagarkatti, Major Professor

Prakash Nagarkatti, Chairman, Examining Committee

Traci Testerman, Committee Member

Mohamad Azhar, Committee Member

Sofia Lizarraga, Committee Member

Cheryl L. Addy, Vice Provost and Dean of the Graduate School

DEDICATION

This work is dedicated to everyone who has helped me throughout my life, particularly my parents, my sister Maggie and her husband Crawford, and Mary Frances. I want to also dedicate this work to my colleagues who shared this journey with me. Last, this work is dedicated to Science and the accumulated understanding of our world that countless others have worked immensely hard to unearth. This work is but a snowflake on the ever-growing apex of humanity's collective knowledge we pass on to future generations.

ACKNOWLEDGEMENTS

I would like to thank my mentors, Dr. Mitzi Nagarkatti and Dr. Prakash Nagarkatti, for their support, wisdom and leadership. I never would have learned about the fascinating world of Immunology if not for them. I want to thank my committee members, Dr. Traci Testerman, Dr. Mohamad Azhar, and Dr. Sofia Lizarraga for their guidance and support. Special thanks to Nicole Holt, Lee Ann Faulling, Tina Akers, and Margaret Whisenant for their service to our department and for their graciousness. I want to thank my fellow graduate students, postdocs, and faculty members from our laboratory for their experience, friendship and support: Kathryn Miranda, Dr. Brandon Busbee, Dr. Alexa Gandy, Dr. Haider Alrafas, Nicholas Dopkins, Dr. Narendra Singh, Wurood Neamah, Osama Abdullah, Muthanna Sultan, Zinah Al-Ghezi, Dr. Marpe Bam, Dr. Xiaoming Yang, Yin Zhong (Linda), Alkeiver Cannon, Bryan Holloman, Amira Mohammed, Dr. Hasan Al-Ghetaa, and past lab members.

I would like to thank my family and my friends for being an infinite fountain of support throughout this journey, I hope they realize this accomplishment is due to their encouragement and love.

ABSTRACT

Dysregulated inflammation is at the heart of countless human diseases. Graft rejection is the process by which an organ from an incompatible donor is rejected by the recipient whose immune cells attack the foreign tissue. Colitis is an inflammatory disorder caused by undue chronic inflammation in the colon and rectum that can progress to cancer. Colitis incidence is on the rise, especially in developing nations and Asia; and the list of patients who need organ transplants grow by the day. Therapies for both graft rejection and colitis are limited to immunosuppressive drugs that leaves patients vulnerable to infection, heart disease, nephrotoxicity and malignancy. Thus, new strategies to address the immunological problems facing these conditions are critical. In this dissertation, we tried to identify epigenetic, molecular, and cellular pathways involved in inflammation as seen during allograft rejection or development of colitis. Data is presented regarding the expression of a pro-inflammatory microRNA cluster that is up-regulated with graft rejection, that when silenced, can provoke anti-inflammatory changes to the transplanted graft, providing a role for epigenetic modulation of inflammation. We also tested the role of cannabinoid receptors in regulating inflammation through use of natural compounds such as Δ^9-tetrahydrocannabinol (THC), found in *Cannabis sativa* plant. THC was highly effective in suppressing colitis through complex pathways involving stimulation of colonocyte mucin production and barrier integrity mediated by tight-junction proteins to provide spatial separation between host and commensal organisms. In addition, THC modulated dendritic cell (DC) phenotype towards increased CD103 expression in the

colonic lamina propria (cLP) and enhanced DC TGF-β1 expression to expand the cLP Tregs. The current study has identified novel pathways of inflammation that can be targeted to benefit patients suffering from inflammatory diseases.

TABLE OF CONTENTS

LIST OF TABLES

LIST OF FIGURES

LIST OF ABBREVIATIONS

AOM ..... Azoxymethane

CB ..... Cannabinoid

CBD ..... Cannabidiol

CC ..... Colon Cancer

CD ..... Crohn's disease

DSS ..... Dextran Sodium Sulfate

ELISA ..... Enzyme-linked Immunosorbant Assay

FT ..... Fecal Transfer

IBD ..... Inflammatory Bowel Disease

IFN ..... Interferon

LCN-2 ..... Lipocalin-2

MDSC ..... Myeloid-derived Suppressor Cells

miR/miRNA ..... MicroRNA

MPO ..... Myeloperoxidase

OUT ..... Operational Taxonomic Unit

PCOA ..... Principle Coordinate Analysis

PCR ..... Polymerase Chain Reaction

SAA ..... Serum Amyloid A

SCFA ..... Short Chain Fatty Acid

TGF-β ..... Transforming Growth Factor Beta

Th ..... T Helper Cell

THC.....Δ9 - tetrahydrocannabinol

TNBS .....2,4,6-Trinitrobenzenesulfonic Acid

TNF ..... Tumor Necrosis Factor

Treg.....T Tegulatory Cell

UC.....Ulcerative colitis

CHAPTER 1

INTRODUCTION

1.1 ALLOGRAFT REJECTION AND ORGAN TRANSPLANTATION

Organ transplantation is a life-saving, ultimate resort for people undergoing end-stage organ failure. Thanks to an armamentarium of immunosuppressive drugs, graft loss due to acute rejection is rare; however, chronic allograft failure persists, and immunosuppression leaves patients vulnerable to infection, heart disease, nephrotoxicity and malignancy, among others (1-2). Exciting developments in the generation of *ex vivo* expanded T regulatory cells (Tregs) are promising candidates for suppressing graft rejection *sans* global immunosuppression (3-6). However, increased attention is needed into the mechanisms that dictate and control the generation of antigen-specific Tregs, to prevent them from reverting to a pro-inflammatory phenotype once they are introduced into the diverse cytokine milieu found *in vivo.* As shown by others, there exists opportunities for Treg differentiation into Th1 and Th17 lymphocytes during inflammation (7-8). In an inflammatory environment, Tregs may undergo reprogramming, wherein the Treg-specific demethylation region (TSDR), which is constitutively demethylated in Tregs, may become methylated, or partially methylated with peripheral Tregs (pTregs), leading to a loss in Foxp3 expression and immunosuppressive activity, conferring an acquired proclivity for graft destruction in the reprogrammed cells (9-10). Investigations in recent years have delved into the factors dictating the differentiation (12-13), generation

(11, 13), and functions (11, 20-22) of Treg cells. Nevertheless, there remains a need for increased attention into the factors that can confer stable Treg suppressive activity.

1.2 MICRORNA

MicroRNAs (miRNAs) are one of the critical players of T cell function and plasticity (16-19). miRNAs are a group of, short, single stranded, ~21 nucleotide-long RNA sequences that bind to the 3' untranslated region (UTR) of target mRNAs through a 6-8 nucleotide 'seed sequence', generally leading to degradation of target mRNA or inhibition of translation (18). MiRNAs are heavily influential in several areas of Treg biology, such as the effect of miR-155 on Treg fitness (21), miR-146a on Treg control of T helper suppression, specifically Th1 responses (22-23) and miR-21's role in Treg expansion (24-25). However, there remains a paucity of information concerning what miRNAs hinder Treg generation in inflammatory models. One factor critical to the development of FoxP3+ regulatory T cells is Transforming Growth Factor-Beta1 (TGF-β1). At first contentious, many studies have since highlighted an indispensable role for TGF-β1 in the differentiation and generation of Tregs. Both thymic intra-medullary naïve CD4 cells (CD4+CD8-CD25-), and peripheral naïve CD4 cells can be differentiated into FoxP3 expressing Tregs after TCR stimulation in the presence of TGF-β1 (14,15).

1.3 TGF-β AND T REGULATORY CELLS

TGF-β1 is a pleiotropic cytokine from the TGF-β signaling pathway superfamily that plays a role in virtually all cell processes starting from development to differentiation and apoptosis (65-68). In the context of immunity, much is known about the anti-inflammatory properties of TGF-β1. It acts through reducing effector cell generation and proliferation as well as by inducing anti-inflammatory Tregs (11,65). Tregs are a CD4+ T

cell subset that express the transcription factor FoxP3 and quench inflammation by inhibiting inflammatory effector cells through a variety of mechanisms including: direct cell-cell contact, increased IL-2 uptake, adenosine release, and TGF-β1 secretion and activation, among others (10-15). Although the types of Tregs are still increasing, they fall into two main subsets, natural and peripheral Tregs, nTregs and pTregs, respectively. Natural or thymic Tregs arise in the thymus and protect the body against auto-immunity after complex interactions with specialized thymic antigen presenting cells (APCs) lead to Tregs with high avidity for self-antigens. Peripheral or induced Tregs, as the name suggests, arise in the periphery through a TGF-β1 dependent mechanism and allows for the tolerance to environmental antigens that are beneficial to the host (10-15,58,60). While the role for TGF-β1 in immunity is established and expanding; another TGF-β superfamily member, TGF-β2, has received a fraction of the interrogation into its immunomodulatory capacity. TGF-β2 is mainly studied in the context of development and Loeys-Dietz syndrome (69,70). Although some studies show anti-inflammatory properties available to TGF-β2 (78,79), and its expression in immune-privileged tissues like the eyes and testes implicate a role for immunity, more work needs to be done to examine its role in Treg induction and the resolution of inflammation.

1.4 COLITIS AND COLITIS-ASSOCIATED COLON CANCER

The mammalian gastro-intestinal (GI) tract provides the architecture for solid and liquid nutrient absorption, while harboring a diverse and vast array of microbes to maximize catabolic potential for the host. The interplay between absorptive epithelial cells, surveilling immune cells and commensals calibrate according to age, diet, genetics, geography, immunity, xenobiotics and numerous other environmental and behavioral

variables (26). A perturbation in any of these factors in the GI tract can cause inflammatory bowel diseases (IBD), encompassing Crohn's disease (CD) and ulcerative colitis (UC). These chronic idiopathic conditions are a major health concern, with prevalence in North America and Europe reaching 3.5 million people (27). Although immunomodulatory corticosteroids, anti-TNFα antibodies and 5-ASA therapies have shown potent remission-inducing ability for IBD patients, they are accompanied by risks for infusion reactions and immunosuppression leading to opportunistic infection and malignancy (28). It has been shown conclusively that, besides the pernicious effects of IBD, those afflicted have an increased risk of developing colorectal cancer (CRC) during their lifetime (29,30).

The precise pathological mechanisms underlying the development and progression of IBD remain unclear, however certain factors predispose or stave off developing disease. Host genetics can predispose an individual to IBD (31,32), and uncontrolled inflammation via mutation or dysregulated immunogenicity to commensals or dietary antigens precludes the causative pathology in IBD (33). Exogenous factors such as diet and microbial community have been recognized as significant contributors to the pathogenesis and prevention of IBD, such that a 'western' diet will predispose an individual to IBD, while a diet high in fiber promotes the production of mucus to protect gut epithelial lining and provide a matrix and substrate for which beneficial bacteria can flourish (34-36). Although many studies have investigated the specific microbial clades influencing IBD, no consensus has been reached, and the emerging hypothesis is that perturbations to the collective GI microbiome, deemed dysbiosis, contribute to IBD progression (37). The advances in biologics targeting inflammation, and beneficial effects of diet and exercise on IBD have stemmed the incidence of IBD in the westernized world; however, recent

epidemiological data suggest an accelerating incidence of disease in newly industrialized nations and Asia, highlighting a need for therapies and strategies that address multi-faceted mechanisms of disease prevention (27,28,38).

1.5 CANNABINOIDS

Cannabinoids are a class of chemically unique compounds that bind to evolutionarily conserved yet geographically and functionally distinct G protein-coupled receptors: cannabinoid receptors 1 (CB1) and 2 (CB2). The first two exogenous ligands for the cannabinoid receptors to be discovered were Δ9-tetrahydrocannabinol (THC) and cannabidiol (CBD), the two main natural products derived from the plant Cannabis sativa. Investigation into CB1 and CB2 led to the discovery of the endogenous cannabinoids, N-arachidonoyl-ethanolamine (AEA) and 2-arachidonoylglycerol (2-AG), which are synthesized on demand as bioactive lipids from the precursor arachidonic acid (39-41). Many early studies investigated the psychoactive properties of THC, but recent work, along with a plethora of largely anecdotal reports (41,42), have hailed THC, its non-psychoactive cousin CBD, and the endocannabinoids for their therapeutic potential in conditions of autoimmunity, spasticity, nausea and pain management (42,43). Cannabinoid receptor activation leads to a robust anti-inflammatory response, largely characterized by reduced antigen-presenting cell (APC) activation (44), a switch from a T helper 1 (Th1) phenotype to a T helper 2 (Th2) phenotype, and a direct induction of apoptosis in activated T cells (46-48). In the GI tract, cannabinoids exert a host of anti-colitic effects, demonstrated in several models (48-50). Activation of CB2 in the gut prompts anti-inflammatory responses that can ameliorate the symptoms of colitis, while activation of CB1 leads to reduced GI motility, gastric emptying, and increased epithelial integrity (48-52). Further support for

the notion that cannabinoids have therapeutic potential for IBD is that knockout mice lacking CB1 or CB2 develop more severe colitis symptoms (52,53). Despite the plethora of data from pre-clinical studies on the effectiveness of cannabinoids for IBD, only two clinical studies have been conducted, and there remains a lack of understanding how the myriad functions of cannabinoids work collectively to influence colitis development and progression (53-56).

1.6 PROBLEM AND HYPOTHESIS

The process of allograft rejection and colitis are instances of allo- and autoimmunity, respectively, that encompass inflammation and thus treatment modalities that target inflammation are desired. The burden of these conditions on patient quality of life, risk of cancer development, and increasing health care costs are staggering (1-3,26-28). There is an acute need to find remedies that re-program our immune system towards graft acceptance in the case of graft rejection, and to find preventative therapeutic options in the case of colitis. Therefore, we examined how to fine-tune the immune system in the case of graft rejection so that a natural epigenetic change that occurs in the host to dampen anti-inflammatory processes is suppressed, allowing increased Treg induction to stave off graft rejection. We explored the mechanism through which cannabinoids beneficially impact the complex interplay between colonic epithelial cells, underlying immune cells and the commensal microbiota to provide protection from colitis using mouse and human cell lines using CB antagonists, several animal models of colitis, and a model of colitis-associated CRC.

CHAPTER 2

miR-466a TARGETING OF TGF-β2 CONTRIBUTES TO FoxP3+ REGULATORY T CELL DIFFERENTIATION IN A MURINE MODEL OF ALLOGENEIC TRANSPLANTATION[1]

2.1 ABSTRACT

The promise of inducing immunological tolerance through Regulatory T cell (Treg) control of effector T cell function is crucial for developing future therapeutic strategies to treat allograft rejection as well as inflammatory autoimmune diseases. In the current study, we used murine allograft rejection as a model to identify microRNA (miRNA) regulation of Treg differentiation from naïve CD4 cells. We performed miRNA expression array in CD4+ T cells in the draining lymph node (dLN) of mice which received syngeneic or allogeneic grafts to determine the molecular mechanisms that hinder the expansion of Tregs. We identified an increase in miRNA cluster 297-669 (C2MC) after allogeneic transplantation, in CD4+ T cells, such that 10 of the 27 up-regulated miRNAs were all from this cluster, with one of its members, mmu-miR-466a-3p (miR-466a-3p), targeting TGF-β2, as identified through reporter luciferase assay. Transfection of miR-466a-3p in CD4+ T cells led to decreased inducible FoxP3+ Treg generation while inhibiting miR-466a-3p

[1] Becker W, Nagarkatti M, Nagarkatti PS. miR-466a Targeting of TGF-β2 Contributes to FoxP3+ Regulatory T Cell Differentiation in a Murine Model of Allogeneic Transplantation. Front Immunol. 2018;9:688.

expression through Locked Nucleic Acid (LNA) resulted in increased Tregs, and a reduction in effector T cells. Furthermore, in vivo inhibition of miR-466a-3p in an allogeneic skin graft model attenuated T cell response against the graft through an increase in TGF-β2. TGF-β2 was as effective as TGF-β1 at both inducing Tregs, and, through adoptive transfer, mitigating host effector T cell response against the allograft. Collectively, these data demonstrate for the first time a new role for microRNA-466a-3p and TGF-β2 in the regulation of Treg differentiation and thus offers novel avenues to control inflammatory disorders.

2.2 INTRODUCTION

Allograft rejection is a robust T cell-mediated immune response involving activation of a large proportion of T cells that are alloreactive. We used that as model to study how Tregs are silenced. To that end, we performed expression profiling of miRNAs in CD4+ T cells found in the draining lymph node (dLN) of mice that received tail skin allografts to identify miRNA that influence the generation of Tregs. Our results demonstrate that a cluster of miRNA is upregulated after alloantigen exposure, specifically in dLN CD4+ T cells, that act to suppress TGF-β2, resulting in decreased Treg generation and increased inflammation. The accumulated data suggests a unique role for TGF-β2 in the regulation of Tregs and therefore opens new avenues to treat not only allograft rejection but other inflammatory disorders.

2.3 MATERIALS AND METHODS

Animals The University of South Carolina Institutional Animal Care and Use Committee approved all experiments. All mice were housed at the AAALAC-accredited animal facility at the University of South Carolina, School of Medicine (Columbia, SC),

and given ad libitum access to water and normal chow diet. Female C57BL/6 (H-2b wild-type, BL6) and C3H (H-2k, C3H) mice, aged 8-12 weeks, with an average weight of 20g, were obtained from Jackson Laboratories (Bar Harbor, ME, USA). C57BL/6-FoxP3GFP mice were bred and maintained in-house. The number of mice for each experimental cohort is described in the figure legends. Each experiment was repeated at least twice, and in many cases, three or four times.

Skin Transplant, LNA-based Treatment, and Adoptive iTreg Transfer

Transplantation of tail skin from donor (C3H, allograft; C57BL/6, syngeneic graft) to recipient C57BL/6 mice, was carried out as described previously (83). Skin grafts were obtained by excising the tail from donor mice, and splitting the tail into equivalently sized ~1x1 cm2 grafts. Recipient mice were anesthetized by an intraperitoneal injection of ketamine (80mg/kg) and xylazine (12mg/kg) (Southern Anesthesia & Surgical, Columbia, SC) in molecular grade water. Upon sufficient anesthetic depth, mice were shaved and ~1x1 cm2 graft beds were made using curved scissors on the dorsal lateral surface. Donor skin grafts were placed onto the graft beds and mice were bandaged. Mice were monitored and kept in bandages for 7-9 days following skin transplantation surgery. In studies using Locked Nucleic Acid (LNA)-based miRNA inhibitor (anti-miR-466a-3p, Exiqon), the LNA (10mg/kg) was injected i.p. to graft recipient mice 1 day before skin transplant, and then every 3rd day after that until termination of the study. For studies involving expanded iTregs, these cells were cultured as described below, sorted for CD4+, FoxP3-GFP expression using BD FACSAria II, and 1x106 iTregs were adoptively transferred 1 day before skin-grafting. For graft rejection scoring, mice were scored as +/+, viable graft; +/-, partially rejected the graft (>50% scabbed over or necrotic, or >50% reduction in graft

size); or -/-, fully rejected the graft (>80% necrotic). For depicting graft survival, +/+ and +/- skin grafts were considered viable, and -/- skin grafts were considered nonviable. The log-rank method was used to determine differences in graft survival.

Target Prediction and Luciferase Reporter Assays Relevant targets for miR-466a-3p and other miRNAs were investigated by cross-referencing predictions from TargetScan Mouse 6.2 software using a context+ score threshold greater than -0.02 and microRNA.org using a mirSVR score between -1.2 and -0.2. The 3' UTR of candidate gene targets or mutated control were purchased from Integrated DNA Technologies (IDT) and cloned immediately downstream of luciferase in the pMiReport vector (Promega, Madison, WI, USA). Insertion of candidate mRNAs was verified through PCR and agarose gel electrophoresis. For luciferase assays, 2.5 x 105 EL-4 cells were plated in 24-well plates for 24 hr and subsequently transfected with either luciferase reporter constructs, together with miR-466a-3p mimics or the negative scramble control (Qiagen, Valencia, CA) using lipofectamine 3000 (Life Technologies). At 48hr post-transfection, dual luciferase assay system (Promega, Madison, WI, USA) was used to detect luciferase activity. Normalized data were calculated as the quotient of Renilla/firefly luciferase activities. The experiments were performed in duplicate and repeated at least 3 times.

Cell Culture Cells were cultured in a sterile incubator that was maintained at 37°C and 5% CO2. EL-4 cells were cultured in DMEM supplemented with 10% fetal bovine serum, 100 U/mL penicillin and 100 U/mL streptomycin. Primary cells were cultured in complete RPMI supplemented with 10% FBS, 100 U/mL penicillin, 100 U/mL streptomycin (both Gibco), 10mM HEPES (Gibco, Paisley, UK), and 50 μM β-mercaptoethanol (Sigma-Aldrich, Gillingham, UK) (complete medium).

Treg Polarization, CD3/CD28 Stimulation and miRNA Transfection For Treg polarization and CD3/CD28 stimulation studies, naïve lymph nodes were harvested and processed into single-cell suspensions. CD4+ T cells were purified using EasySep PE Positive Selection Kit (Stemcell Technologies, 18557). CD4+ T cell purity was routinely >90% as verified through flow cytometry. Cells (1x 106) were plated in 12 well plates in complete medium supplemented with plate-bound anti-mouse CD3ε, clone 145-2C11 (3µg/mL) in the presence of anti-mouse CD28, clone 37.51 (3µg/mL). For studies examining only CD23/CD28 stimulation, cells were harvested 48hr after plating for downstream analysis. For Treg polarization, cells were plated with recombinant mouse IL-2 (5ng/mL) and recombinant human TGF-β1 (5ng/mL) or recombinant TGF-β2 (5ng/mL) (R&D Systems, Minneapolis, MN) where indicated, in addition to the aforementioned amounts of CD3 and CD28. Five days after plating, cells were harvested for downstream analysis and cell culture supernatants were collected for ELISAs. All cytokines were purchased from Biolegend (San Diego, CA). In both experiments, cells were transfected with either 25 nM miR-466a-3p mimic (UAUACAUACACGCACACAUAAGA), 100nM miR-466a-3p inhibitor (UAUACAUACACGCACACAUAAGA), or 25 nM scramble control, using HiPerfect Transfection Reagent from Qiagen (Valencia, CA). Transfection efficiency was validated using qRT-PCR.

iTreg Generation CD4+ T cells from BL6 FoxP3GFP mice were purified using EasySep PE Positive Selection Kit (Stemcell Technologies, 18557). CD11c+ allogenic APCs were isolated from the spleens of C3H mice using EasySep PE Positive Selection Kit. The cells were co-cultured for 3 days at a ratio of 5:1, T cells : APCs. Additionally, anti-CD3ε (10µg/mL), anti-CD28 (4µg/mL) and IL-2 (5ng/mL) were added to all wells

and TGF-β1 (5ng/mL) and TGF-β2 (5ng/mL) were added where indicated. Cells were co-cultured for 72 hours before being collected for downstream analysis or sorted for purity and injected intravenously.

Alloantigen Co-culture Naïve lymph node cells were harvested and processed through a 100μm cell strainer to make single-cell suspensions. Cells (1x106) were plated in the presence of 50 μg/mL of alloantigen or no antigen (control) in complete RPMI in 12-well plates for 10 days. Fresh medium was added on day 5, and LNA-based miRNA inhibitor (anti-miR-466a-3p, Exiqon, Denmark) and control LNA were added every 3 days at 50 ng/mL. After 10 days, cells were collected for downstream analysis and cell culture supernatants were stored at -20°C before being analyzed by cytokine-specific ELISA for: IFNγ, TNFα, IL-17A, total TGF-β1 (Biolegend, San Diego, Ca), and TGF-β2 (R&D Systems, Minneapolis, MN).

Antigen Preparation (splenocyte lysates) C3H and C57BL/6 mice were euthanized and their spleens were aseptically removed, homogenized, and passed through a 100μm cell strainer to make single-cell suspensions in cold, serum-free media. Red blood cells (RBCs) were lysed and the cell suspension was washed twice with cold serum-free media. Then, cells were re-suspended at a cellular density of 1x108 cells/mL and subjected to 4 freeze (5 min liquid nitrogen) – thaw (10 min 37 °C water bath) cycles. Cells were then sonicated for 5 min, and the lysate was centrifuged at 350g (10 min, 4 °C) and supernatant was recovered. The lysate was filtered with a 0.22 μm microporous membrane, protein concentration was determined using Qubit fluorometer (Thermo Fisher Scientific), and subsequently stored at 4 °C.

Graft Infiltrating Cell Extraction Mice that received a skin-transplant were sacrificed and the transplanted graft was aseptically excised. Grafts were cut longitudinally, minced and digested for 2 hours at 37°C 5% CO2 in PBS containing Type I Collagenase (2.5 mg/mL) and Hyaluronidase (0.25mg/ml) (both from Sigma). Subsequently, graft infiltrating cells (GICs) were obtained by spinning at 1000g for 7min at 4°C before being re-suspended in FACS buffer and live cells enumerated using a hematocytometer, and either stained immediately for flow cytometry or plated overnight to recover GIC culture supernatants. Cell-free culture supernatants were recovered and stored at -20°C before being analyzed by cytokine-specific ELISA.

Flow Cytometry and Antibodies Relevant tissues were harvested and cells were homogenized and subsequently depleted of red blood cells as described above. To analyze immunophenotype surface markers, we stained single cell suspensions using the recommended dilutions indicated on the manufacturer product sheets, and gated them on PE conjugated anti-CD4 (GK1.5) or FITC conjugated anti-CD8α (53-6.7) where indicated. Antibodies used for flow cytometric analysis (BioLegend, San Diego, CA, USA) include Fc block, PE, PE/Cy7 and APC-Cy7 conjugated anti-CD4 (GK1.5), PE and BV421 conjugated CD304 (Neuropilin-1) (3E12), PE conjugated anti-IL-17A (TC11-18H10.1) Alexa Fluor 488 and BV421 conjugated FoxP3 (MF-14), FITC conjugated Helios (22F6), APC conjugated IFNγ (XMG1.2), APC and PerCP-Cy5.5 conjugated LAP (TGF-β1) (TW7-16B4), FITC conjugated CD8α (53-6.7), BV650 conjugated CD223 (LAG-3) (C9B7W), Alexa Fluor 700 conjugated CD49b. PE conjugated IL-10 (JES5-16E3), PE conjugated GATA3 (16E10A23), FITC conjugated T-bet (4B10), APC conjugated CD62L (MEL-14), BV650 conjugated CD278 (ICOS)(DX29), (PE conjugated CD44 (IM7) and

PE/Cy7 and BV786 conjugated CD25 (3C7). Antibodies against nuclear proteins were probed using True-Nuclear Transcription Factor Buffer Set (BioLegend, San Diego, CA, USA) and intracellular cytokine staining was performed using Fixation/Permeabilization Solution Kit (BD, San Jose, CA). The stained cells were then assessed by flow cytometer (FC500; Beckman Coulter, Brea, CA, USA) or BD FACSCelesta (BD, San Jose, CA, USA) and the resulting data analyzed by Cytomics CXP software (Beckman Coulter), DIVA software, or FlowJo. Sorting of cells was performed using a BD FACSAria II (BD, San Jose, CA, USA). The gates were set following exclusion of debris. Additionally, we used positive and negative controls for the fluorophores used. The events were displayed as a dot plots or as a contour maps to show the relative intensity of scatter patterns. The gates were set at around populations of cells with common characteristics such as forward scatter, side scatter and density of marker expression.

miRNA Expression Profiling dLN CD4+ T cells purified to >90% purity using EasySep PE Positive Selection Kit (Stemcell Technologies, 18557) were subject to total RNA isolation using miRNeasy kit (Qiagen, Valencia, CA), following manufacturer's protocol. The concentration and purity of the isolated RNA were determined using a spectrophotometer, and the integrity of the RNA was verified using Agilent Eukaryote Total RNA Nano Series II on an Agilent 2100 BioAnalyzer (Agilent Tech, Palo Alto, CA). Only samples with a RIN value above 8 were used for subsequent processing. Profiling of miRNA expression from samples was performed using the Affymetrix GeneChip miRNA 4.0 array platform (Affymetrix, Santa Clara, CA) at the Johns Hopkins Deep Sequencing and Microarray Core (http://www.microarray.jhmi.edu/) following the manufacturer's protocol. This array version covers all mature miRNA sequences in miRBase Release 20

(http://www.mirbase.org/). The stained chip was scanned on a GeneChip Scanner (Affymetrix) and microarray image data were analyzed using Affymetrix Power Tools (APT) to generate Robust MultiArray Average (RMA) values as well as detection above background (DABG) p-values as well as for normalization and quality control of data. Hybridization signals that that showed aberrant properties and were <3 standard deviations over the mean background value were excluded. Statistical significance (p values) for "detection calls" were determined by Affymetrix test. Probe sets with a p value lower than 0.05 were called present (true). The log-transformed fluorescence intensity values were mean-centered and visualized by heat maps. miRNA fold changes were obtained from the array and miRNAs with only a greater than 1.5-fold change were considered for further analysis. Predicted miRNA targets, alignments, and mirSVR scores were determined using online miRNA databases:microrna.org, and TargetScan Mouse 6.2. Heatmap was made using Genesis software (Graz University of Technology). Ingenuity Pathway Analysis (IPA) (Qiagen, Valencia, CA) was used to identify the molecular and functional annotations and canonical biological pathways potentially influenced by target genes of differentially expressed miRNA. The array data were deposited into the Genome Expression Omnibus (GEO) of NCBI (https://www.ncbi.nlm.nih.gov/geo/) and can be accessed via accession number GSE109160.

Immunoblotting Cell extracts were collected using RIPA lysis buffer supplemented with sodium orthovanadate, PMSF and protease inhibitor (Sigma). Protein concentration was measured using Qubit fluorometer (Thermo Fisher Scientific) and were subjected to gel-electrophoresis and transfer onto a nitrocellulose membrane. Blots were blocked with 5% BSA in TBST, washed, and probed overnight at 4 °C with antibodies

against TGFβ2 (1:1000, R&D Systems, MAB73461), TGFβR3 (1:2000, R&D Systems, AF5034), Smad2/3 (1:1000, CST, 5678), Phospho-Smad2 (Ser465/467)/Phospho-Smad3 (Ser423/425), (1:1000, CST, 8828), Smad4 (1:1000, CST, 38454) and Phospho-Smad4 (Thr276), (1:1000, Thermo Fisher Scientific, PA5-64712). The next day, blots were washed in TBST and then incubated at room temperature for 1 h with a horseradish peroxidase labeled secondary antibody. Following secondary antibody incubations, blots were washed multiple times with TBST, exposed to a chemiluminescent reaction, Pierce™ ECL Western Blotting Substrate (Thermo Fisher Scientific, Rockford, IL), and were exposed to film. Optical densities of films were quantified (sample minus background) using ImageJ.

Measurement of cytokines Cell culture supernatants from indicated in vitro experiments, graft infiltrating cell culture supernatants obtained ex vivo, or serum samples were analyzed for the following cytokines: IFNγ, TNFα, IL-17A, total TGF-β1, latent TGF-β1, and free-active TGF-β1, enzyme-linked immunosorbent assay (ELISA) kits were purchased from Biolegend (San Diego, CA). For detection of TGF-β2, ELISA kit was purchased from R&D Systems (Minneapolis, MN).

RNA Extraction and qPCR CD4+ T cells in the dLN or spleens of grafted mice were purified using EasySep PE Positive Selection Kit (Stemcell Technologies, 18557), and total RNA was isolated using miRNeasy kit (Qiagen, Valencia, CA), following manufacturer's protocol. Expression of indicated mRNA and miRNA levels were determined by quantitative real-time PCR (qRT-PCR). Quality and amount of RNA was investigated using Nanodrop 2000 (Thermo Fisher Scientific, Rockford, IL). For miRNA expression analysis, cDNA was made from total RNA using miRNA cDNA Synthesis Kit,

with Poly(A) Polymerase Tailing (ABM, Canada, G902). Two-step with hot-start miRNA qRT-PCR was carried out using EvaGreen miRNA Mastermix (ABM, Canada, MasterMix-mS) with mouse primers for SNORD96A (control), miR-466a-3p, miR-466e-3p, miR-466p-3p, miR-15a-5p, miR-181c-5p, miR-27a-3p and miR-19b-3p (ABM, Canada). Expression levels were normalized to SNORD96A. For mRNA expression analysis, cDNA was made from total RNA using miScript cDNA synthesis kit from Bio-Rad (Hercules, CA). Two-step amplification with a 60° annealing temp. for qRT-PCR was carried out using SsoAdvanced™ SYBR® green supermix from Bio-Rad (Hercules, CA) with mouse primers for TGFβ1, TGFβ2, TGFβR3, PTEN, FoxP3, Smad2, Smad3, TGFβR1 and TGFβ3. All qRT-PCR experiments were carried out on a CFX96 (or 384) Touch Real-Time PCR Detection System (Bio-Rad, Hercules, CA). Expression levels were normalized to β-actin mRNA levels. Fold changes were calculated using the $2^{-\Delta\Delta CT}$ method. Primers are detailed in Table 2.3.

H&E Staining Grafts were excised and fixed by immersion in 4% paraformaldehyde (PFA) in PBS, overnight. Fixed tissues were embedded in paraffin, sectioned and stained with hematoxylin and eosin. Color bright field images and picture montages were taken using a Cytation-5 Imaging Reader (BioTek Instruments, Winooski, VT, USA).

Statistical Analysis Prism 6 and 7 software (Graphpad) were used for statistical analysis. In skin graft experiments, we used groups of at least 7 mice. Data were depicted as means ±SEM. Student's t test was used to compare data between 2 groups. One-way ANOVA with a Tukey post hoc test was used to compare 3 or more groups. A log-rank

(Mantel-Cox) test was used to determine the significance of survival curves. A $p<0.05$ was considered significant.

2.4 RESULTS

Draining lymph node T regulatory cell response to allograft

T regulatory cells (Treg) play a critical role in tolerance and the decrease in their functions is associated with strong inflammation (3-8). To investigate the potential mechanisms that dampen the basal Treg induction during an immune response, we used an allogeneic skin-graft model of transplantation. To that end, C57BL/6 mice (H-2b, BL6), were given age and sex- matched syngeneic (syn) (BL6) or allogenic (allo) C3H (H-2k, C3H) full thickness ~1x1 cm2 tail skin transplants on the dorsal lateral surface. Ten days after transplantation, mice were sacrificed and their draining lymph nodes (dLN) and spleens were harvested and assessed for the type and frequency of Tregs present. Among the main Treg subtypes, we investigated natural Tregs (nTregs), that are demarcated by surface CD4+ and Neuropilin-1 (Nrp1) expression, and express the transcription factor FoxP3 (57,58,60), peripheral Tregs (pTregs) that are CD4+, FoxP3+, Nrp1-, or Nrp1LO (59,60); and Tr1 T cells, which are CD4+, FoxP3 -, CD25-, CD49b+, Lag-3+ (CD223+), and express inducible T-cell costimulatory (ICOS). In addition, these cells express higher latent-associated TGF-β and secrete IL-10 (57,84). In the dLN of allografted mice, but not in the spleen, there was a significant reduction in the percentage of nTregs and pTregs when compared to syngrafted mice (Figure 2.1A-E). In contrast, there were no significant changes in the percentages of Tr1 cells (Figure 2.1F-H). Additionally, when looking at the amount of latent-associated peptide –TGF-β1 (LAP) on CD4+FoxP3+ cells, we observed a notable decrease in the percentages of these Tregs in the allograft dLN (Figure 2.1I). Due

to the requirement of TGF-β1 for pTreg induction, and the decrease in LAP on Tregs after allotransplantation, we looked at TGF-β1 levels in the serum on the day the mice were euthanized and found that its presence was diminished after allotransplantation as well (Figure 2.1J).

A miRNA cluster is altered in dLN CD4+ cells

We next investigated if changes in Tregs were associated with alterations in miRNA expression because miRNA are known to regulate T cell differentiation and plasticity. To that end, we isolated total RNA from purified CD4+ T cells in the dLNs of syn- or allografted mice or naïve mice, pooled the RNA from mice in the same group, and performed a miRNA expression microarray as a preliminary screening tool using an n of 1 per group. Differential fold change expression of 3,164 miRNAs between the naïve, syn and allo groups was performed. A table was constructed of all the miRNA from the array that displayed a 1.5 or greater fold change in the allo group compared the syn group, while also displaying changes between the allo and naïve group, most of which also displayed a fold change greater than 1.5, with miR-7648-3p being the sole exception (Table 2.1). A compelling finding was that 10 of the 27 miRNAs that were found to be up-regulated in the allo group (compared to both naïve and syn groups) all came from the same cluster of miRNA that was contained in the 10th intron of the Polycomb group gene Sex combs on the midleg with four MBT domains-2 (Sfmbt2) on mouse chromosome 2, henceforth referred to as Chromosome 2 miRNA cluster (C2MC) (Table 2.1). C2MC has also been referred to as the miR-297-669 cluster (61-63).

Validation of miR-466a expression and predicted mRNA targeting

Next, we validated the expression of these miRNA through qRT-PCR (Figure 2.2A). Using TargetScan Mouse 6.2 and microrna.org, several of the miRNA that were up-regulated after allografting were found to target many members in the family of TGF-β signaling, consistent with a clear role for TGF-β1 in the differentiation of naïve CD4+ T cells into pTregs, and tolerance (64-66). These miRNAs and their associated fold changes were input into Ingenuity Pathway Analysis (IPA) to display them alongside their predicted targets (Figure 2.2B). Our data indicating a decrease in pTregs, LAP+ Tregs, and circulating TGF-β1 (Figures 2.1A, D, I, J) suggested that the TGF-β1 pathway may be attenuated after allotransplantation, an avenue that was further pursued. Among the up-regulated miRs, the specific miRNA from C2MC with the highest validated mean expression in CD4+ T cells draining from the allograft was miR-466a-3p (Figure 2.2A), henceforth referred to as miR-466a. This miRNA was chosen as the main miRNA of interest, both because of its noteworthy upregulation (Figure 2.2A), and because the seed sequence of miR-466a is identical to miR-297(a/b/c)-3p, miR-446d-3p, miR-467g and miR-669d-3p, other members of C2MC. Upregulation of miR-466a after allotransplantation was specific to dLN CD4+ cells, as it was not significantly altered in splenic CD4+ cells or other peripheral LN CD4+ cells (Figure 2.2C). Predicted targets of C2MC in (Figure 2.2B) were validated through qRT-PCR (Figure 2D) to be down-regulated in allograft dLN CD4+ cells. We next investigated the mRNA specifically targeted by miR-466a. Predicted target, binding, and miRSVR score of miR-466a - mRNA interactions are displayed in a Table (Table 2.2). We cloned the 3'-untranslated region (3' UTR) of several mRNA of interest (Smad2, Smad3, TGF-β2 and TGF-βR3) as well as a

mutated 3' UTR, immediately downstream of luciferase in a luciferase reporter assay. EL-4 cells were transfected with the luciferase reporters or a control vector lacking any 3' UTR inserts in the presence of either a miR-466a mimic or a scramble control. We found that in the presence of miR-466a mimic, the luciferase activity of the reporter with the TGF-β2 3' UTR cloned into its sequence was significantly lower, while such a decrease was not seen in the presence of the scramble control, any of the other cloned 3' UTRs, or in the mutated control group (Figure 2.2E). This finding was consistent with the predicted 7mer-m8 seed match shared between miR-466a and TGF-β2.

miR-466a targets Treg polarization through TGF-β2

To directly test the role of miR-466a on Treg differentiation, we used an in vitro Treg polarization model. To that end, purified naïve CD4+ T cells cultured with cytokines were transfected with either mock (empty vector), scramble control (25nM), mimic (25nM), or mimic + inhibitor (100nM). The data showed that transfection with mimic, but not any of the other conditions, could suppress the generation of Tregs as demarcated by the co-expression of CD4 and FoxP3 (Figure 2.3A-C). It was worth noting that the mimic caused a robust decrease in the total number of Tregs generated in culture when compared to controls (Figure 2.3C). Transfection efficiency was validated with qRT-PCR (Figure 2.4A). We next quantified the mRNA and protein levels of the predicted targets of miR-466a after transfection and found that the mRNA expression of Smad2, Smad3, TGF-β1, TGF-β2 and TGF-βR3 were all reduced after mimic transfection compared to the other conditions (Figure 2.4B). However, upon examining the protein level, although both Smad2 and Smad3 showed active phosphorylation, as is to be expected upon TGF-β signaling, the only protein examined whose levels were decreased after mimic transfection

was TGF-β2 (Figure 2.3D-G). Continued Smad signaling despite the reduction in TGF-β2 is likely due to persistent signaling through TGF-β1. Additionally, there was a decrease in the amount of free-active TGF-β1 in the cells transfected with miR-466a mimic, and this alteration was reversed with the addition of the inhibitor (Figure 2.4C).

Next, we examined the effect of miR-466a inhibition in a model wherein there was no exogenously administered TGF-β1. To that end, naïve CD4+ cells were purified and stimulated in vitro with anti-CD3/CD28 Ab in the presence of a locked nucleic acid (LNA), designed specifically to inhibit miR-466a/b/c/d/e/p-3p (will be referred to as LNA-466), or a control that was designed not to target any known miRs (LNA-ctrl). Cells treated with LNA-466 exhibited an increase in the number of CD4+CD25HILAP+FoxP3+ Tregs compared to controls (Figure 2.3H). To confirm that TGF-β2 can have a pronounced effect on Treg polarization, naïve CD4 cells were polarized with either TGF-β1 (5ng/mL) or TGF-β2 (5ng/mL). Both culture conditions induced the polarization of naïve T cells into Tregs, but TGF-β2 induced Tregs had increased expression of inducible T-cell costimulatory (ICOS), a marker of Treg fitness (82), compared to TGF-β1 induced Tregs (Figure 2.3I).

miR-466a inhibitor decreases pro-inflammatory and increases anti-inflammatory cells after coculture with alloantigen

To mimic more closely the in vivo environment of transplantation, we implemented an in vitro coculture model wherein naïve LN cells were cultured with either syngeneic antigen or alloantigen (50μg/mL). LN cells cocultured with syngeneic antigen died between days 3-5; however, LN cells cultured with alloantigen persisted and expanded. Coculture with alloantigen provoked a robust increase in expression of miR-466a at several

time points compared to cells cultured with syngeneic antigen (Figure 2.5A). Next, LN cells were cocultured with alloantigen and LNA-466 or control inhibitor and cells were analyzed by flow cytometry. LNA-466 addition resulted in a decrease in pro-inflammatory T helper 1 (Th1) cells that were CD4+IFNγ+, cytotoxic effector CD8+ IFNγ+ cells (Tc1), and CD4+ IL-17A+ T helper 17 (Th17) cells (Figure 2.5B). In the same cultures, LNA-466 induced increased proportions of CD4+CD25HI cells, and concomitantly increased FoxP3+ expression among that population, compared to controls (Figure 2.5C, D).

LNA-466 attenuates inflammatory markers after allogenic skin transplantation

Because LNA-466 was effective in attenuating inflammatory T cells induced by alloantigen in vitro, we investigated its effect in vivo. To that end, C57BL/6 mice were given either C57BL/6 (syn) or C3H (allo) skin grafts and were administered LNA-466 or LNA-ctrl at a dose of 10 mg/kg starting 1 day before allografting, and every 3rd day thereafter, until termination of the study. While LNA-466 caused a slight delay in allograft rejection, it was statistically not significant (Figure 2.6A). However, mice given the allograft + LNA-466 did exhibit a significant decrease in the size and total cellularity of draining lymph nodes, thereby indicating decreased host-versus-graft response and inflammation (Figure 2.6B, C). In the same experiment, LNA-466 failed to induce significant changes in the size and cellularity of the spleens (Figure 2.7A, B), thereby demonstrating that LNA-466 was targeting the dLNs, the primary site of immune response against alloantigen, and the site of mir-466a upregulation. To determine if LNA-466-mediated effect on Tregs was having a functional impact on inflammatory cytokines, dLN cells harvested from LNA-466-treated mice were cultured overnight and the supernatants

were examined for cytokines. The data showed that LNA-466 derived cultures had significantly lower effector cytokines such as TNFα and IFNγ levels when compared to cells derived from allograft + LNA-ctrl treated mice (Figure 2.6D, E).

Mice receiving LNA-466 exhibited no significant changes in the amounts of circulating TGF-β1; however, consistent with the ability of miR-466a to target TGF-β2, the LNA-466 group demonstrated increases in circulating TGF-β2 when compared to syn or allograft + LNA-ctrl groups (Figure 2.6F, G). Corroborating this finding, we found an increase in the number of circulating memory Treg cells (Figure 2.6H, I) in the LNA-466 group, surpassing the number of memory Tregs in the syn group.

When we performed histopathological analysis of the grafts, we noted that allograft + LNA-466 mice showed a decrease in the levels of cellular infiltration and graft damage compared to allograft + LNA-controls (Figure 2.6J).

LNA reduces intragraft effector cells and cytokines

Next, we directly studied the nature of cells and cytokines seen within the graft after LNA-466 or LNA-ctrl treatment. To that end, the grafts were excised minced and digested to retrieve graft infiltrating cells (GICs), which were either immediately stained, or plated for 24hr in complete media to obtain GIC culture supernatants. The data revealed that LNA-466 treated animals had a decrease in effector CD4+ and CD8+ GICs compared to the LNA-ctrl group (Figure 2.8A-C). LNA-466 treatment also resulted in an increase in the percentage of graft infiltrating CD4, CD62L, FoxP3+ Tregs, compared to the LNA-ctrl group (Figure 2.8D, E). Graft culture supernatants revealed that LNA-466treatment led to reduced levels of effector inflammatory cytokines, TNFα (Figure 2.8F) and IFNγ (Figure 2.8G), as well as increases in total TGF-β1 and TGF-β2 (Figure 2.8H & I).

TGF-β2 induced Tregs are as potent as TGF-β1 induced Tregs in attenuating allograft rejection response

To study the role of TGF-β2-induced Tregs in suppressing inflammation, CD4+ cells from C57BL/6 FoxP3GFP reporter mice were isolated and cultured with splenic APCs from allogenic mice along with anti-CD3ε (10μg/mL), anti-CD28 (4μg/mL) and IL-2 (10 ng/mL). TGF-β1 is conventionally used to stimulate the production of both polyclonal and antigen-specific induced Tregs (iTregs) (4-8). Here, we tested the effect of culture with either TGF-β1 (5ng/mL) or TGF-β2 (5ng/mL) on iTreg generation. Similar to the polarization findings in Figure 2.3I, after 3 days of culture, we found that TGF-β2 was able to induce the generation of iTregs (Tβ2-iTregs) to the same extent and phenotype as TGF-β1 (Tβ1-iTregs) (Figure 2.9A, B). To test the efficacy of these cells at delaying acute rejection in vivo, after 3 days of co-culturing, iTregs were sorted for CD4+, FoxP3GFP co-expression and 1x106 cells were intravenously injected into allograft recipient mice 1 day before skin transplantation. Syngenic mice which did not receive any iTregs were used as controls. Tβ2-iTregs displayed potency equivalent to Tβ1-iTregs at delaying graft rejection (Figure 2.9C), preventing graft destruction at a rate greater than iTregs generated without the addition of TGF-β1 or TGF-β2. iTregs were verified to be present in the dLN (Figure 2.9D, E) to the same extent among all groups, although iTregs induced with TGF-β1 or TGF-β2 showed greater potential to home to the allograft (Figure 2.9F, G). Indeed, grafts harvested 12 days after allotransplantation that were derived from mice administered Tβ1-iTregs and Tβ2-iTregs showed a decrease in graft infiltrating memory CD4+ cells (Figure 2.9H, I), and a decrease in the number of graft infiltrating memory and effector CD8+ cells (Figure 2.9H, J). In the periphery, Tβ1-iTregs and Tβ2-

iTregs reduced circulating CD4+ and CD8+ cells displaying a memory phenotype but did not cause any change in circulating Tregs (Figure 2.10A-F). Lastly, Tβ1-iTregs and Tβ2-iTregs could significantly reduce the number of graft infiltrating IFNγ-secreting CTLs compared to mice which received only iTregs (Figure 2.9K, L).

2.5 DISCUSSION

Treg generation and administration is rapidly becoming a promising treatment option for patients undergoing end-stage organ failure (3-8). Because alloantigens, unlike conventional antigens, activate a large proportion of T cells and induce a strong inflammatory response, we considered using this model to study the impact of such activation on miRNA expression in T cells leading to induction of proinflammatory T cells, while constraining Tregs. Our results provide a mechanistic perspective on how epigenetic shifts in CD4+ T cell miRNA expression can influence the generation of Tregs by modification of TGF-β2 expression. Our data demonstrated an upregulation of many members of rodent miRNA cluster, C2MC, after allotransplantation in dLN CD4+ cells. Through pathway analyses, these miRNAs, and specifically miR-466a-3p, were predicted to target several members of the TGF-β signaling family. We showed that miR-466a directly binds to the 3' UTR of TGF-β2 through reporter luciferase assays. It should be noted that while miR-466a and its target were validated in this study, there were still several miRNA picked up by the array that were not investigated further and it is possible that such miRNA may contribute to the complex inflammatory cascade perpetuating graft rejection.

Despite being an isoform of the widely studied TGF-β1 (11,14-15,64-68), little information is known about the role of TGF-β2 in the immune system (67,68). Indeed, most of the information concerning TGF-β2 is in regard to its role in development and

function of aorta (69), Loeys-Dietz syndrome (70) and cancer (71-73). Moreover, most studies performed involving TGF-β1 in immune cells have used TGF-βRII deficient cells to highlight the role of TGF-β1, however, this also cancels out any potential TGF-β2 signaling. Thus, our findings that miR-466a regulates TGF-β2, which in turn plays a key role in the generation of Tregs, are novel. This was demonstrated conclusively in our study by altering TGF-β2 levels via transfection of CD4+ cells under Treg polarizing conditions with miR-466a mimics, which led to decreased generation of Tregs, while mimic inhibition reversed this effect. Furthermore, this reduction in Treg generation was associated with decreased mRNA levels of TGF-β family members and signaling molecules Smad2/3; however, at the protein level, while Smad2/3 showed consistent activation status between the groups, only TGF-β2 expression was altered upon mimic transfection. The persistence in Smad signaling despite changes in TGF-β2 expression are likely due to signaling through exogenously administered TGF-β1 in that model of in vitro polarization. Interestingly, we found TGF-β2 to be equally as effective as TGF-β1 at polarizing naïve CD4 cells in vitro, even conferring increased ICOS expression to the polarized Tregs, a marker of Treg fitness (82). To further corroborate the role of miR-466a in T cell differentiation, we used locked nucleic acid (LNA) in a co-culture model to inhibit miR-466a expression and found that LNA-466 caused an increase in CD4+CD25HI FoxP3+ Tregs and a decrease in pro-inflammatory T helper 1 (Th1) cells, CD8+ IFNγ+ cells (Tc1), and CD4+ IL-17A+ (Th17) cells. Mice bearing allograft and treated with LNA-466 exhibited a significant decrease in inflammation, an increase in FoxP3+ Tregs at the grafted site, and an increase in circulating TGF-β2 and circulating memory Treg cells. Together, the current study demonstrates for the first time that allografts induce miR-466a in CD4+ T cells which inhibits Treg

differentiation through suppression of TGF-β2. Our data suggest that in vivo modulation of miR-466a may constitute a novel approach to induce Tregs and thereby inhibit inflammation that is seen in a variety of clinical disorders.

Contrary to our hypothesis that in vivo inhibition of miR-466a using LNA-466 would result in delayed allograft rejection, our data showed that LNA administration failed to delay allograft rejection compared to controls. This may be because allografts activate a larger proportion of T cells compared to conventional antigens, thereby provoking a more robust inflammatory response, and the effect of LNA-466 may be too subtle to quell this pernicious immune response in a model with such a high degree of genetic mismatch. Moreover, in humans, HLA matching eliminates such strong host-versus-graft reactions, which are further controlled by immunosuppressive drugs. Nonetheless, LNA-466 administration significantly altered the immune cell environment towards a more anti-inflammatory phenotype, and this was without altering the circulating levels of TGF-β1. Despite TGF-β1 levels remaining stable in this experiment, we cannot discount the confounding role TGF-β1 may have in these studies. Future work utilizing TGF-β1-/- knockout mice will need to be performed to accurately dissect the specific impact each TGF-β isoform is having on the generation and maintenance of Tregs. Thus, the data presented in this study paint a picture of a complex inflammatory environment wherein modulation of TGF-β2, specifically, via miR-466a downregulation can modify most greatly the inflammatory environment in circulation and within the allograft.

After demonstrating how changes in TGF-β2 levels could alter Treg generation, we investigated the role of TGF-β2 and compared it to its well-studied isoform, TGF-β1, in Treg induction and expansion. TGF-β2 was found to be as effective as TGF-β1 at inducing

Tregs in an allogenic coculture model. Additionally, these Tβ2-iTregs demonstrated an ability to reduce allograft-directed inflammation at a rate comparable to Tβ1-iTregs, and better than iTregs that were not cultured with TGF-β isoforms. This is a novel finding that surely warrants further work – to dissect the differences, if any, between Tregs generated via TGF-β1 or TGF-β2.

miR-466a-3p is a member of C2MC, one of the largest clusters of miRNAs, containing 71 miRNA genes (61-63). C2MC contains subclusters 297~466~467~699, many of which have been implicated in disease processes, from cell fate decision (76), and apoptosis (74) to aging in the heart (75); however, most members of the 466 subcluster have been implicated in immune regulation (76,77). C2MC is under tight, temporal and spatial regulatory control, and exists in Sfmbt2, a region known to be imprinted (62). Sfmbt2 is expressed preferentially in the paternal allele in early embryos, and in later stage extra-embryonic tissue; while CpG islands spanning the transcriptional start site are differentially methylated on the maternal allele during embryogenesis (62,63). The developmental regulation of C2MC is especially germane to this work, because the member of C2MC that was most highly upregulated after alloantigen exposure, miR-466a, was found to target TGF-β2, a protein that is also under considerable governance due to its extensive involvement in proper development (69,70). Another possible mechanism that could be mediating the effects of TGF-β2 on the immune system, other than the direct effect we noticed on CD4+ cells, is the effect of TGF-β2 on antigen presenting cells (APCs). In a model of experimental autoimmune uveoretinitis (EAU) and anterior chamber-associated immune deviation (ACAID), TGF-β2 treated APCs could provoke antigen specific tolerance via Treg induction in vitro and in vivo (78,79). This is an exciting

progression, and is concordant with our finding that increases in TGF-β2 levels occurred in tandem with increased levels of Tregs, and more importantly that TGF-β2 can robustly induce Tregs in an alloantigen coculture model. We found that purified CD4+ T cells, draining the allograft expressed heightened miR-466a; it is quite possible these cells could be secreting their miRNAs in exosomes as a form of cell-cell communication in the dLN microenvironment to dendritic cells. Exosomal trafficking between CD4+ cells and DCs has been well documented, and if CD4+ cells were secreting miRNA-filled exosomes to decrease DC TGF-β2 expression, in accordance with the studies mentioned above, this could result in less Tregs being induced (80). Indeed, Wilson et al. found this form of paracrine exosomal signaling to be dominant in CD4+ cells, specifically in Treg cells (81). Interestingly, in that same study, it was found that several members of C2MC were among the top up-regulated miRs in Treg-derived exosomes (81). Considering clinical transplantation involves lesser HLA incompatibilities than used in our murine model, and due to the salutary effects in vivo manipulation of miR-466a had on allograft rejection, we suggest that miRNA management of TGF-β2 may constitute a therapeutic modality for allograft rejection or other inflammatory diseases - clearly additional studies are necessary to reinforce this point. Our studies also indicate a heretofore unrecognized role for TGF-β2 in the robust induction of T regulatory cells, an observation that could be an additional strategy for decreasing allograft rejection severity without resorting to global immunosuppression.

Table 2.1 miRNA Array Analysis

Transcript ID	Allogeneic vs. Naive	Allogeneic vs. Syngeneic
Mmu-miR-1291	-1.940334	-2.6569
Mmu-miR-5112	-3.72864	-2.11819
Mmu-miR-6368	-2.4931	-2.02958
Mmu-miR-7011-5p	-2.10665	-1.9088
Mmu-miR-1894-3p	-2.03285	-1.78943
Mmu-miR-6912-5p	-2.71246	-1.78591
Mmu-miR-6937-5p	-2.00668	-1.68382
Mmu-miR-6971-5p	-1.83436	-1.64353
Mmu-miR-7016-5p	-2.06684	-1.6174
Mmu-miR-7648-3p	-0.26363	-1.49674
Mmu-miR-324-3p	1.729733	1.5072
Mmu-miR-18a-5p	4.699893	1.531172
Mmu-miR-484	2.595994	1.551924
Mmu-miR-27b-3p	1.819848	1.631183
Mmu-miR-194-5p	1.819848	1.631183
Mmu-miR-181c-5p	6.726528	1.649867
Mmu-miR-128-3p	4.711249	1.682522
Mmu-miR-27a-3p	1.77744	1.685586
Mmu-miR-421-3p	3.317828	1.855922
Mmu-miR-19b-3p	2.20629	1.883595
Mmu-miR-192-5p	4.342631	1.888075
Mmu-miR-182-5p	2.459444	1.889462
Mmu-miR-let-7f-5p	5.910496	1.890165
Mmu-miR-30b-5p	1.916419	2.029614
Mmu-miR-30e-5p	2.124878	2.029614
Mmu-miR-21a-5p	1.916419	2.029614
Mmu-miR-30a-5p	2.191086	2.09029
Mmu-miR-15a-5p	3.724949	2.236029
Mmu-miR-466a-3p	2.332244	2.284712
Mmu-miR-466e-3p	4.058871	2.303314
Mmu-miR-466b-3p	3.908921	2.445917
Mmu-miR-466c-3p	2.474084	2.464956
Mmu-miR-466p-3p	2.452085	2.826219
Mmu-miR-669a-3p	2.601293	2.878352
Mmu-miR-669o-3p	2.129959	2.955524
Mmu-miR-467c-5p	2.129959	2.955524
Mmu-miR-467a-5p	2.97326	2.956093

Table 2.2 miRNA-mRNA Predicted Binding

Predicted miRNA Target	Predicted consequential pairing of miRNA (top) and mRNA target region (bottom)	mirSVR score
TGFβ2	3' agAAUACACACGCAC-AUACAUAu 5' mmu-miR-466a-3p | | ||| : || |||||| 860:5' guUGACCUGU-UUUGAUAUGUAUu 3' Tgfb2	-0.5786
TGFβRIII	3' agaAUACACACGCACAUACAUAu 5' mmu-miR-466a-3p || || | : | |||||| 1649:5' ugaUAAGUAUAU-UCUAUGUAUa 3' Tgfbr3	-0.0256
Smad2	3' agaauacacacgcacaUACAUAu 5' mmu-miR-466a-3p |||||| 29:5' cuccgucguaguauucAUGUAUg 3' Smad2	-0.0256
Smad3	3' agaauacacacgcacaUACAUAu 5' mmu-miR-466a-3p |||||| 660:5' uggcaccacaacccugAUGUAUa 3' Smad3	-0.3307

Table 2.3 List of Primers

Gene	Primer	Sequence (5' – 3')	Accession Number
B actin	Forward Reverse	GGCTGTATTCCCCTCCG CCAGTTGGTAACAATGCCATGT	NC_000071.6
PTEN	Forward Reverse	TGGATTCGACTTAGACTTGACCT GCGGTGTCATAATGTCTCTCAG	NM_008960.2
FoxP3	Forward Reverse	CCCATCCCCAGGAGTCTTG ACCATGACTAGGGGCACTGTA	NM_054039.2
TGF-β3	Forward Reverse	AACAGCCACTCACGCACAGTG GCACAACGAACTGGCTGTCTG	NM_009368.3
TGF-β2	Forward Reverse	CTTCGACGTGACAGACGCT GCAGGGGCAGTGTAAACTTATT	NM_009367.4
TGF-βR1	Forward Reverse	TCTGCATTGCACTTATGCTGA AAAGGGCGATCTAGTGATGGA	NM_009370.3
TGF-βR3	Forward Reverse	GGTGTGAACTGTCACCGATCA GTTTAGGATGTGAACCTCCCTTG	NM_011578.4
TGF-β1	Forward Reverse	GAGAAGAACTGCTGTGTGCG GTGTCCAGGCTCCAAATATAGG	NM_011577.2
Smad2	Forward Reverse	ATTCCAGAAACGCCACCTCC GCTATTGAACACCAAAATGCAGG	NM_010754
Smad3	Forward Reverse	GCGTGCGGCTCTACTACATC GCACATTCGGGTCAACTGGTA	NM_013095.3

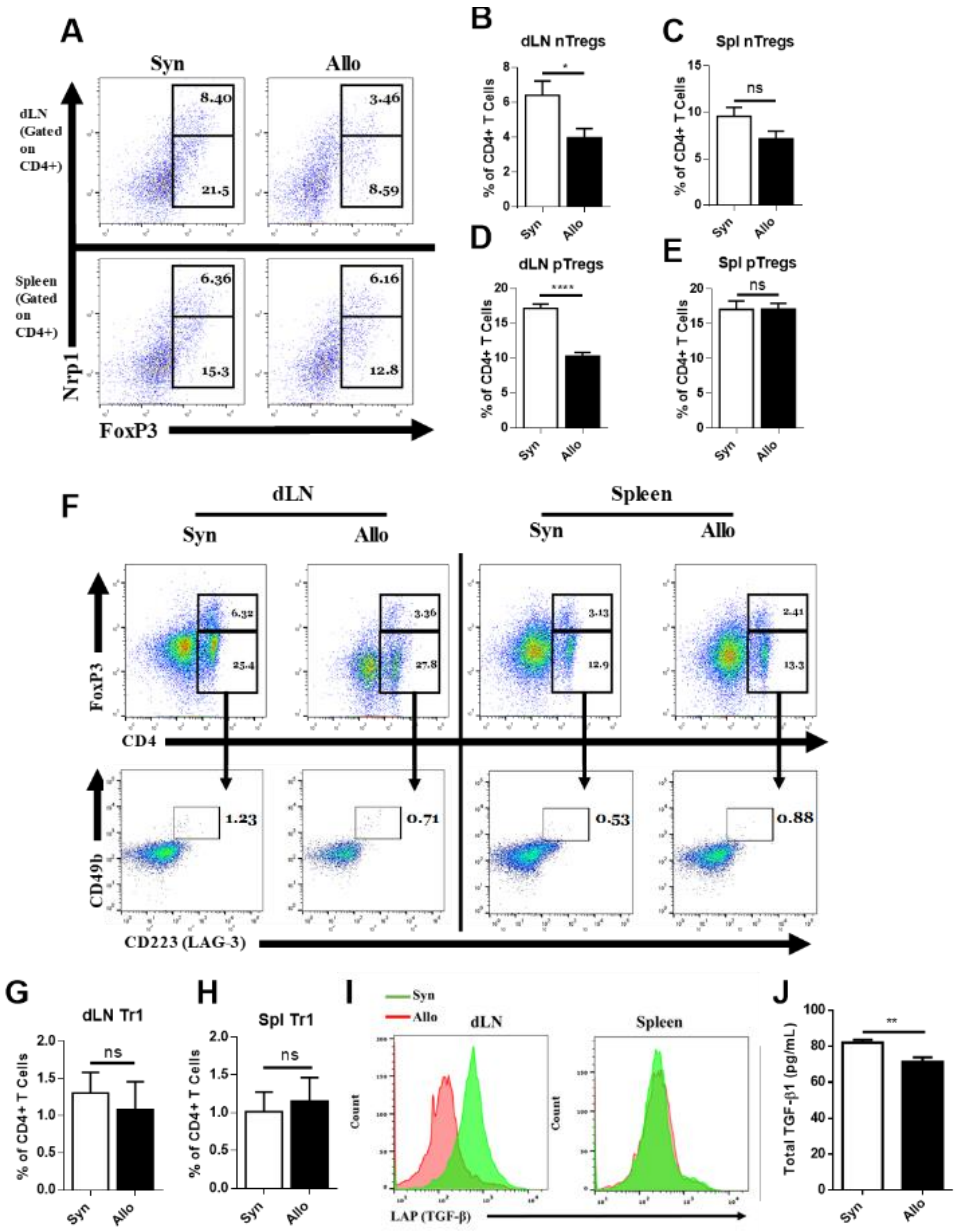

Figure 2.1 ***Allografting alters the dLN T regulatory cell phenotype.*** Ten days after syn- or allografting, mice were sacrificed and organs of interest were harvested. Draining lymph nodes (dLN) and spleens were analyzed for T regulatory cell phenotype by flow cytometry. **A** Representative flow cytometry dot plots gated on CD4+ cells, displaying the percentage of natural Tregs (nTreg) present through co-expression of CD4, FoxP3 and Nrp1 and the percentage of peripheral Tregs (pTreg) that are CD4 and FoxP3 positive, and Nrp1^{LO} or negative. **F** Dot plots (lower panel) gated on CD4+, FoxP3- cells (upper panel), displaying CD223 (LAG-3), CD49b double positive Tr1 cells. **I** Overlaid histograms gated on CD4+FoxP3+ cells, displaying LAP expression. **B, C, D, E, G, H** Quantification of flow cytometry results. **J** ELISA of total TGF-β1 in the serum of mice on the day of sacrifice. n = 12 (Syngeneic) or 18 (Allogeneic) mice per group. Data are

presented as mean ± SEM of three independent experiments. *P<0.05, **P<0.01, ****P<0.0001 by Student's *t*-test.

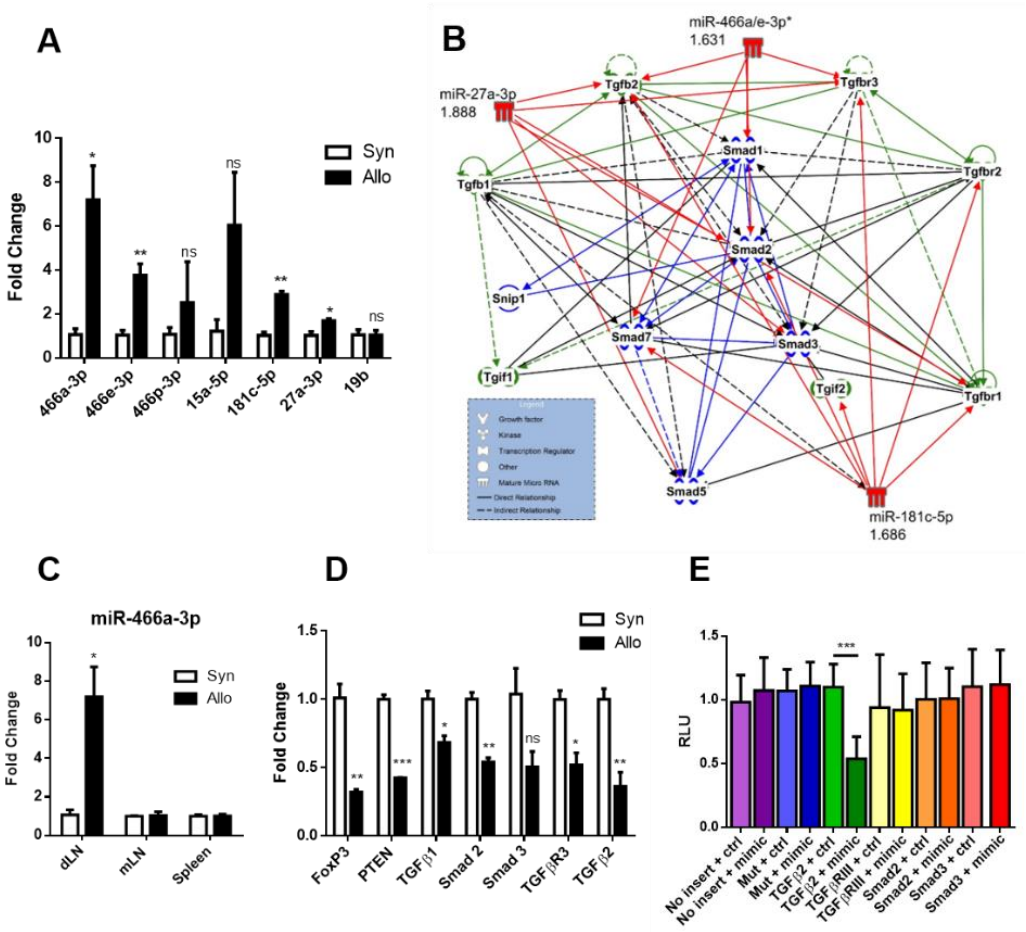

Figure 2.2. ***Alloantigen induced miRNAs target TGF-β family members and signaling molecules.*** Total RNA was extracted from purified CD4+ cells in the dLN of syn- or allografted mice 10 days post-transplant. **A** Validation of microarray results through qRT-PCR. **B** Ingenuity Pathway Analysis (IPA) of seven of the top up-regulated miRNAs and their predicted targets. **C** Fold change miR-466a expression in the dLN, spleen, or mesenteric lymph node (mLN) of purified CD4+ cells derived from syn- or allografted mice. **D** qRT-PCR validation of mRNA expression changes in the dLN CD4+ cells of syn- or allografted mice; n = 8 (Syngeneic) or 12 (Allogeneic) mice per group. **E** Relative luciferase expression in EL-4 cells transfected with luciferase reporter constructs which contained 3′UTR of proteins of interest or a mutated 3'UTR, together with miR-466a-3p mimics or the negative scramble control. A total of 48 h after transfection, luciferase activity was detected. Normalized data were calculated as the quotient of Renilla/firefly luciferase activities and are presented as mean ± SEM of three independent experiments with 2 technical replicates indicating 6 measurements. *P<0.05, **P<0.01, ***P<0.005, ****P<0.0001 by Student's *t*-test.

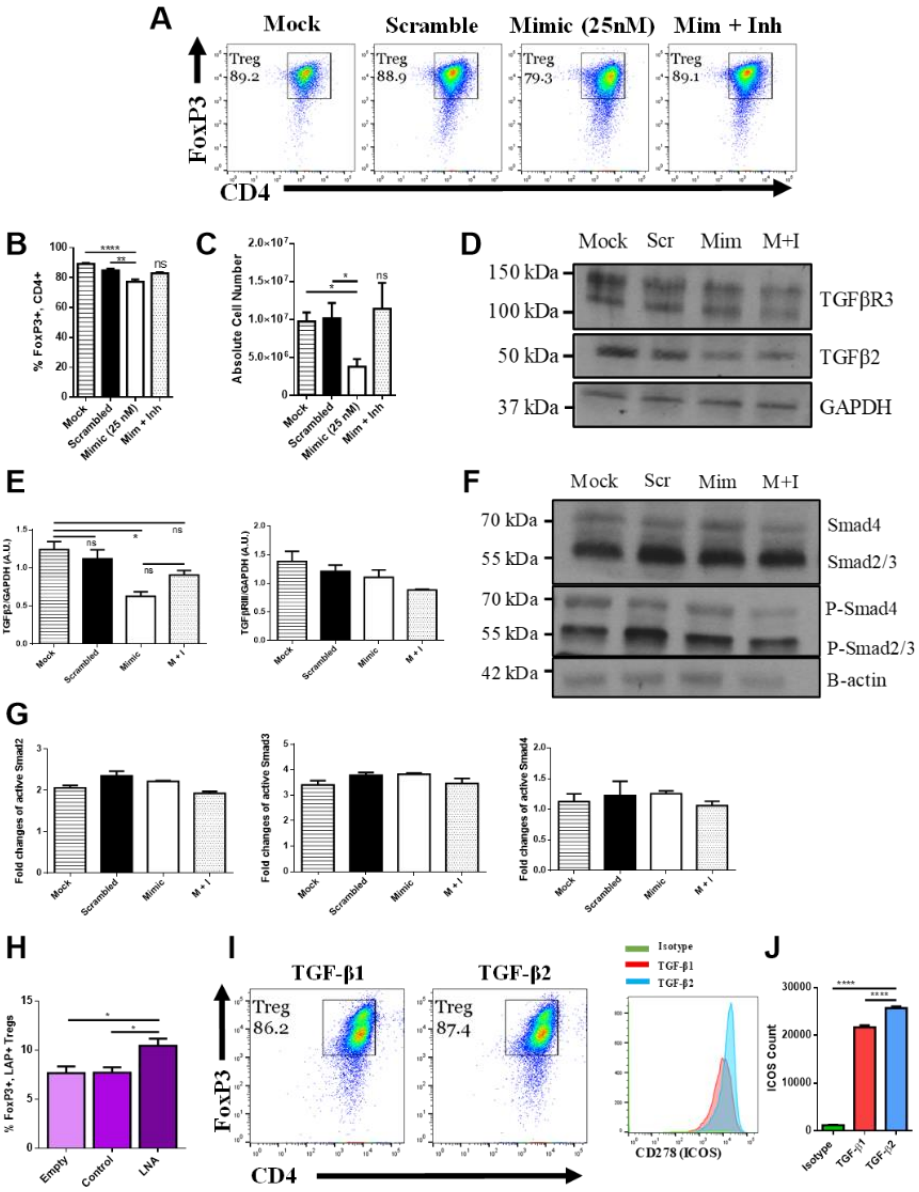

Figure 2.3. ***miRNA 466a-3p transfection inhibits Treg polarization.*** Purified naïve CD4+ T cells were cultured under Treg polarizing conditions along with the indicated mimic, control or inhibitor conditions. Cells were harvested 48 hours after addition of cytokines and miRNA mimics, inhibitors, or controls and subject to flow cytometry, immunoblot and qRT-PCR. Success of Treg polarization is examined as **A** representative dot plots, and quantified in **B** and **C**. Representative immunoblots of indicated proteins are presented in **D** and **F**, along with associated densitometric measurements of TGF-β2 and TGF- βR3 **E**, and quantification of activated Smad 2, 3 and 4 **G**. CD4+ cells were purified from naïve mouse LNs and stimulated *ex vivo* with CD3 (3μg/mL) and CD28 (3μg/mL) for 48 hours and administered LNA or controls at the time of seeding. Quantification of flow cytometry data from LAP expressing FoxP3 positive Treg cells. **H** Purified naïve CD4+ T cells were cultured with either TGF-β1 (5ng/mL) or TGF-β2 (5ng/mL), along with CD3 (3μg/mL),

CD28 (3µg/mL) and IL-2 (5ng/mL) for 5 days. **I** Representative dot plots of FoxP3, CD4 positive Tregs, **J** and their associated CD278 (ICOS) expression. Data are presented as mean ± SEM of three independent transfection experiments. *P<0.05, **P<0.005, ****P<0.0001 by ANOVA with Tukey's multiple comparisons test.

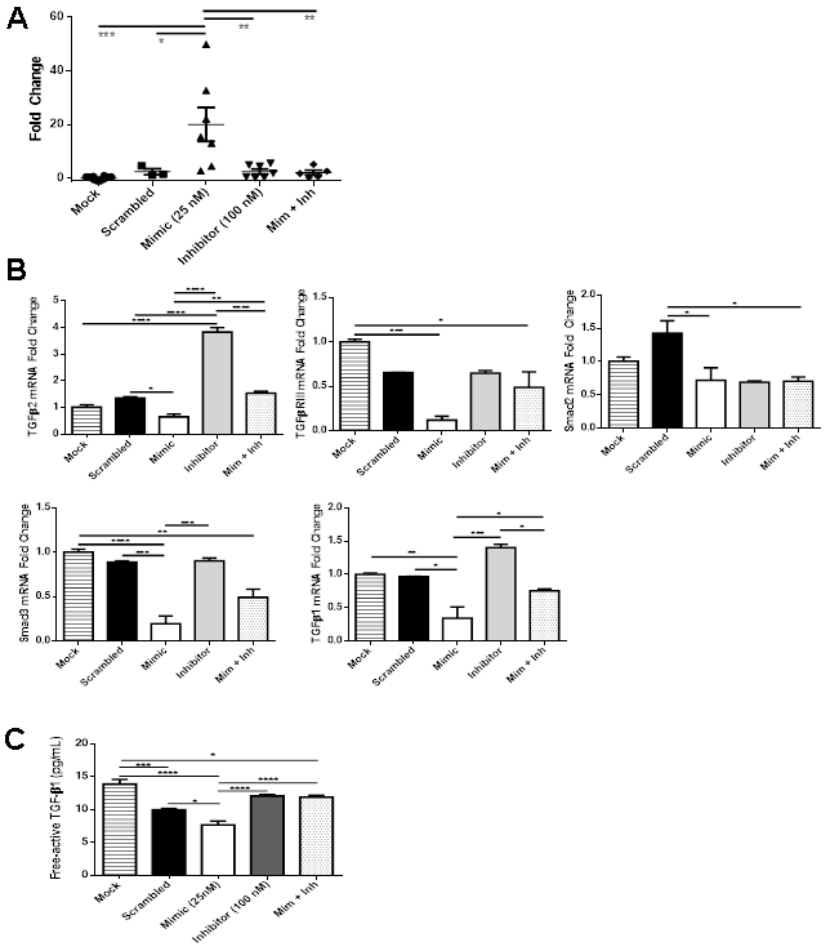

Figure 2.4. ***miRNA-466a-3p transfection in primary mouse CD4+ T Cells.*** CD4+ T cells were isolated from naïve mouse LNs and purified using magnetic bead isolation. CD4+ cells were transfected with empty vector (mock), a scramble control, a miRNA-466a-3p mimic, or an inhibitor specific to miRNA-466a under Treg polarizing conditions for 48 hours in complete media before total RNA was harvested and cell supernatants were collected. Quantitative real-time PCR (qRT-PCR) of miRNA-466a-3p **A,** and indicated mRNAs **B.** ELISA of free-active TGF-β1 in the supernatants of indicated groups **C**. Data are presented as mean ± SEM of two independent transfection experiments indicating six measurements. *P<0.05, **P<0.005, ***P<0.001, ****P<0.0001 by ANOVA with Tukey's multiple comparisons test.

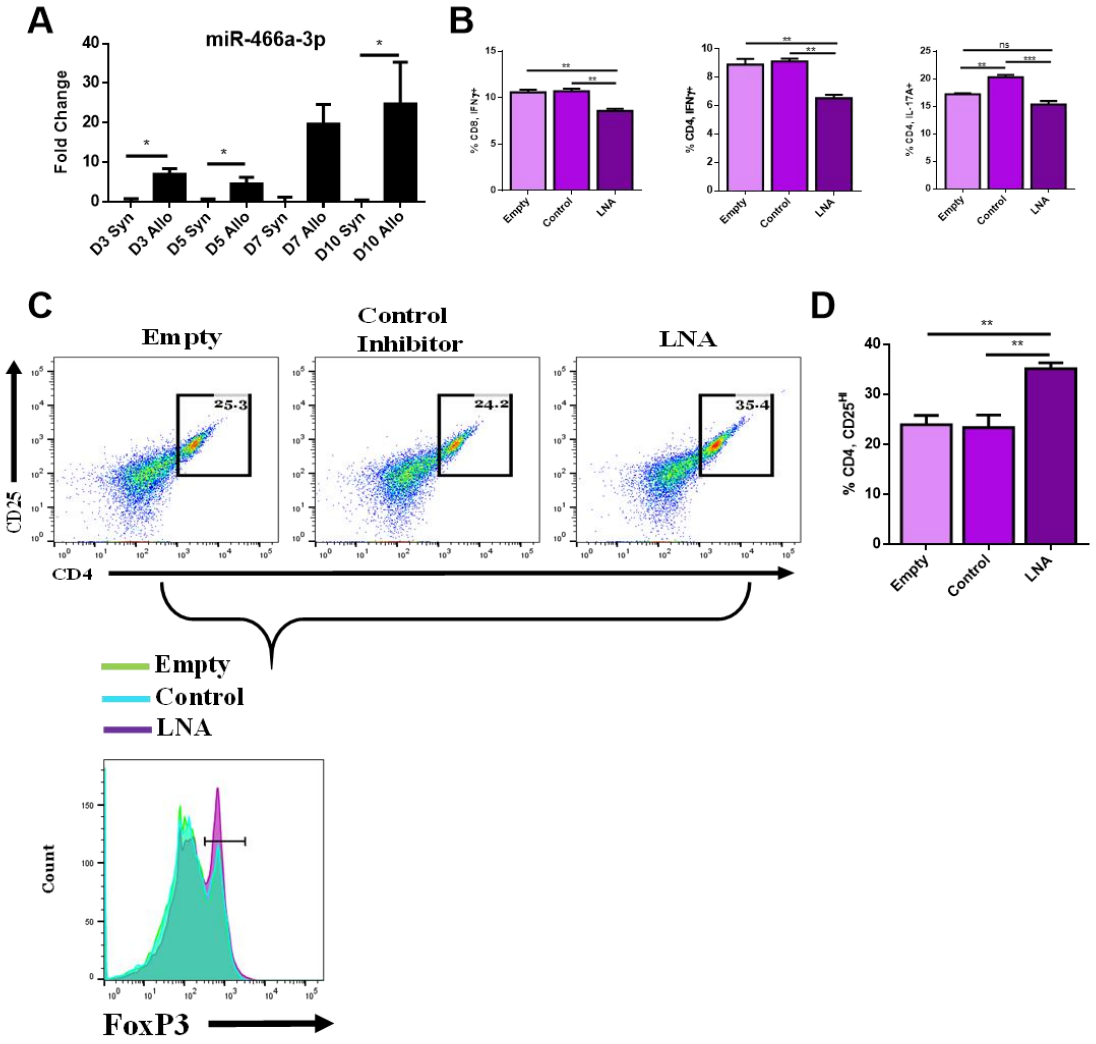

Figure 2.5. ***miR-466a inhibitor decreases pro-inflammatory and increases anti-inflammatory cells after co-culture with alloantigen.*** Co-culture of LN cells with alloantigen increases miR-466a-3p expression compared to LN cells cultured with syngenic antigen at the indicated time points as determined by qRT-PCR **A**. LN cells were administered alloantigen (50µg/mL) for 10 days in complete media. Fresh media and miRNA inhibitors or controls were added every 3 days. Cells were harvested and stained for Tc1, Th1, Th17 and Treg cells. **B** Quantitation of flow cytometry plots**. C** Histogram of FoxP3 expression (bottom row), gated on CD4+, CD25+ dot plots (top row), and quantified in **D**. Data are presented as mean ± SEM of two independent transfection experiments indicating six measurements. *P<0.05, **P<0.005, ***P<0.001, ****P<0.0001 by ANOVA with Tukey's multiple comparisons test.

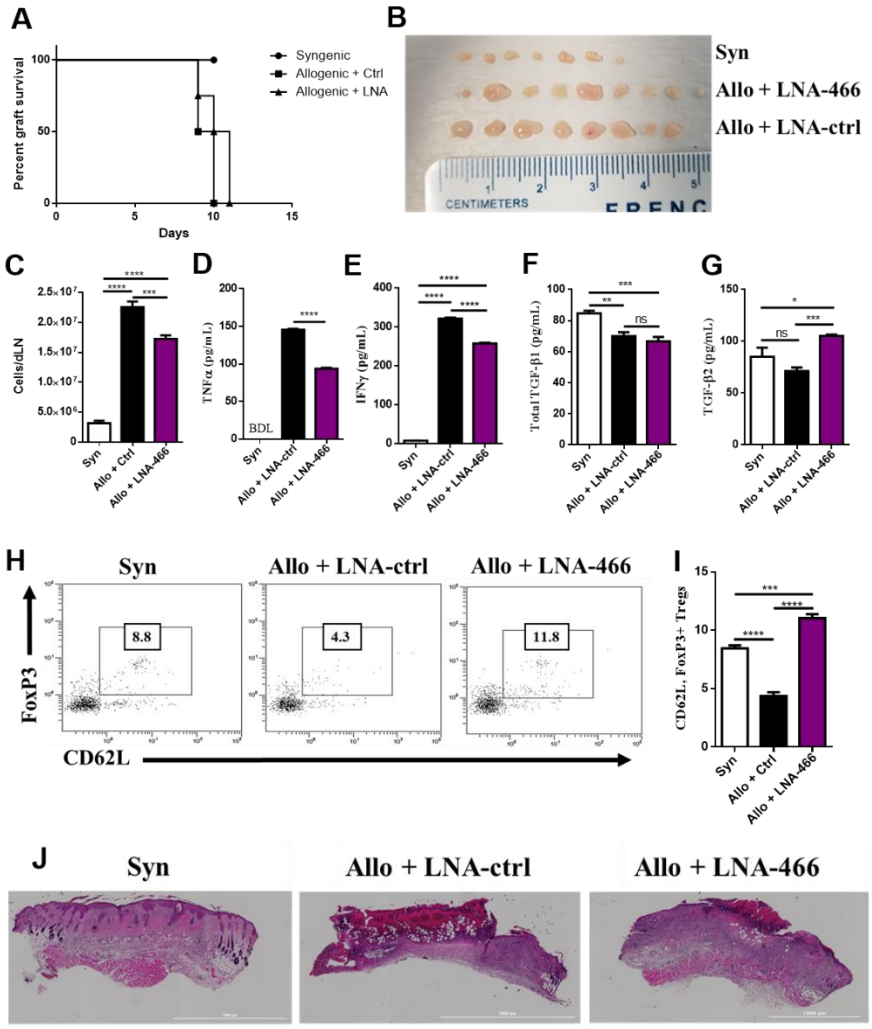

Figure 2.6. ***LNA mitigates dLN effector cell and cytokines*.** Female C57BL/6 mice were given either syn (BL6) or allo (C_3H) tail skin grafts. Mice receiving allografts were given either LNA-466 (10mg/kg) or LNA-ctrl (10mg/kg) i.p. 1 day before skin transplantation, and every 3rd day after that until termination of the study. **A** Survival curve of mice receiving skin transplants and indicated LNA or controls; n = 4 (Syngeneic), 7 (Allogeneic + Ctrl), or 8 (Allogeneic+ LNA). Draining lymph nodes were harvested twelve days after skin transplantation from indicated groups, imaged in **B** and absolute cell counts were taken in **C.** dLN cells were plated overnight in complete media and culture supernatants were harvested and subjected to ELISA for TNFα **D** and IFNγ **E.** Serum was taken upon sacrifice and subjected to ELISA for TGF-β1 **F** and TGF-β2 **G.** Dot plots of circulating cells double positive for FoxP3 and CD62L, data are gated on CD4+ cells **H**, and quantified in **I. J** H&E stains of grafts excised from mice upon sacrifice. Data are presented as mean ± SEM; n= at least 4 per group. *P<0.05, **P<0.005, ***P<0.001, ****P<0.0001 by ANOVA with Tukey's multiple comparisons test.

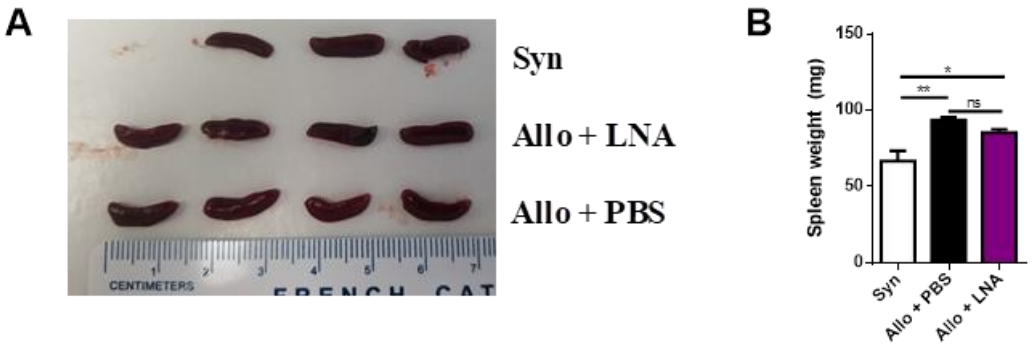

Figure 2.7. ***Splenic inflammation after skin transplantation***. Female C57BL/6 mice were given either syn (BL6) or allo (C_3H) tail skin grafts. Mice receiving allografts were given either LNA (10mg/kg) or PBS i.p. 1 day before skin transplantation, and every 3rd day after that until termination of the study. Image **A** and weight **B** of spleens harvested from mice in indicated groups upon rejection of allografts. Data are presented as mean ± SEM; n= at least 4 per group. *P<0.05, **P<0.005, ***P<0.001, ****P<0.0001 by ANOVA with Tukey's multiple comparisons test.

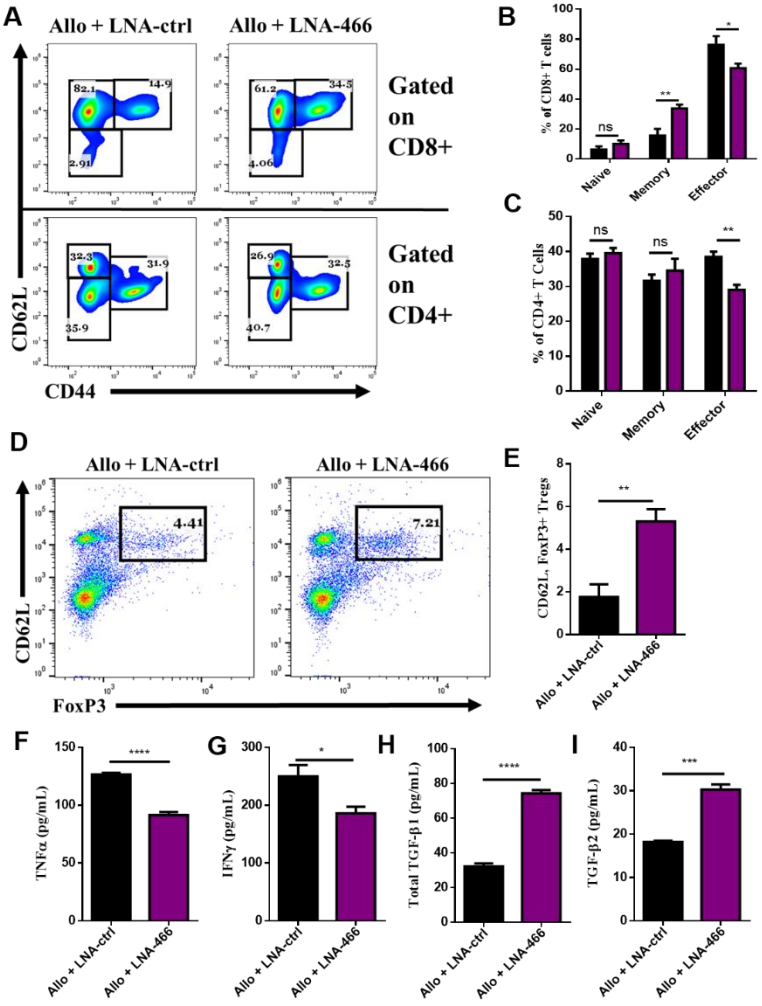

Figure 2.8. ***LNA reduces intragraft effector cells and cytokines***. Female C57BL/6 mice were given either syn (BL6) or allo (C_3H) tail skin grafts. Mice receiving allografts were given either LNA-466 (10mg/kg) or LNA-ctrl (10mg/kg) i.p. 1 day before skin transplantation, and every 3rd day after that until termination of the study. Upon rejection, grafts were aseptically excised, minced and enzymatically digested to dislodge graft infiltrating cells (GICs). GICs were spun down, culture supernatants were collected and live cells were used for flow cytometric analysis. Representative dot plots displaying naïve ($CD62L^{Low}$, $CD44^{Neg}$), memory (CD62L+, $CD44^{HI}$) and effector ($CD62L^{Low}$, $CD44^{HI}$) cell types gated on CD8+ (**A, upper row)** and CD4+ **(A, lower row)** cells. Percentages for CD8+ and CD4+ are quantified in **B** and **C**, respectively. Dot plots of GICs double-positive for FoxP3 and CD62L, data are gated on CD4+ cells **D**, and quantified in **E**; n = 7 (Allogeneic + Ctrl) or 8 (Allogeneic+ LNA). GIC supernatants were collected and subjected to ELISA for the interrogation of effector cytokines TNFα **F** and IFNγ **G**, as well as anti-inflammatory cytokines TGF-β1 **H** and TGF-β2 **I**. Data are presented as mean ± SEM. *P<0.05, **P<0.005, ***P<0.001, ****P<0.0001 by ANOVA with Tukey's multiple comparisons test or a Students *t*-test.

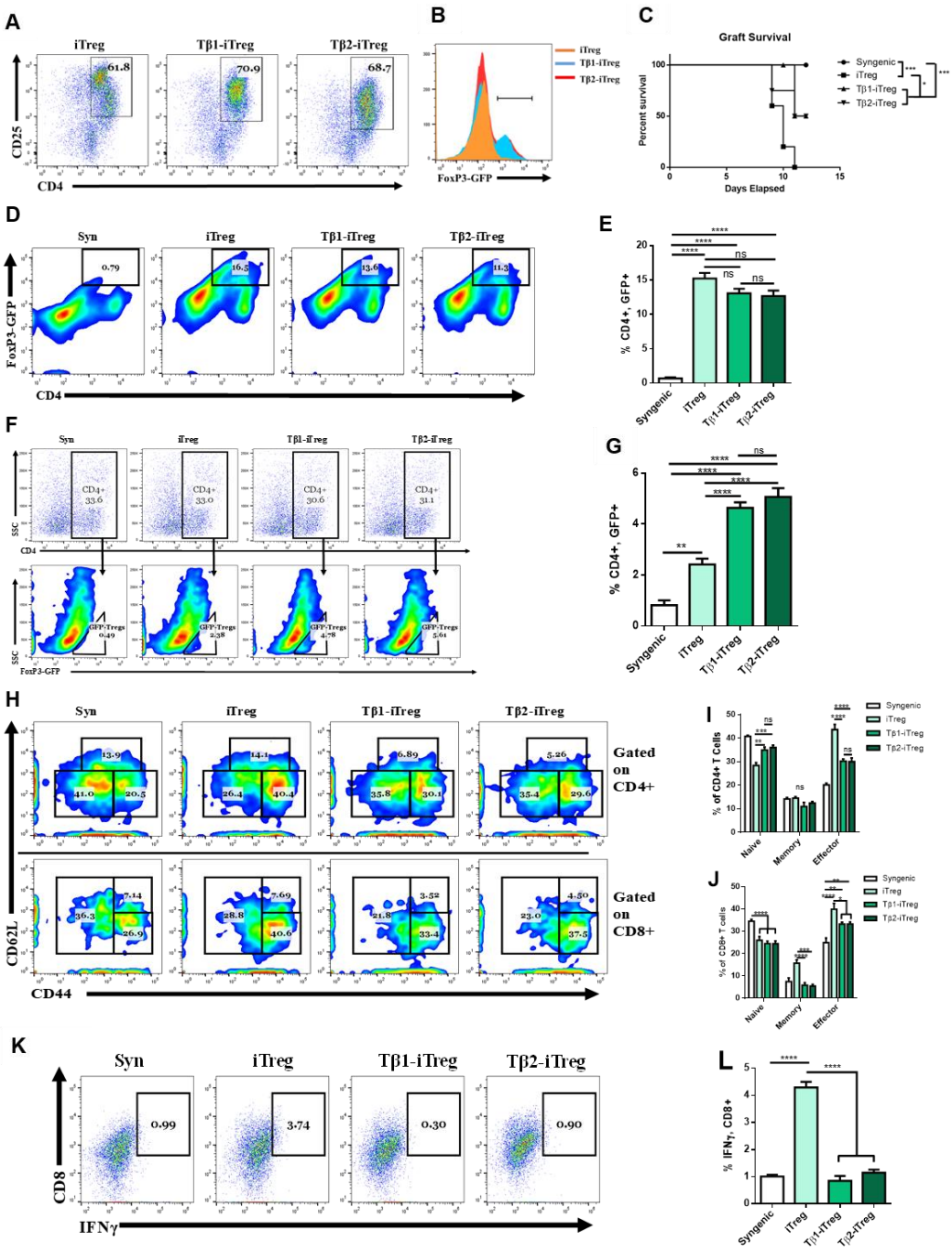

Figure 2.9. ***TGF-β2 induced Tregs are equally as potent as TGF-β1 induced Tregs in ameliorating allograft rejection***. CD4+ cells were purified from naïve BL6 FoxP3^{GFP} mice and cocultured with allogenic splenic APCs along with anti-CD3ε (10µg/mL), anti-CD28 (4µg/mL) and IL-2 (10 ng/mL). Tβ1, and Tβ2-iTregs were also administered TGF-β1 (5ng/mL) or TGF-β2 (5ng/mL), respectively. Coculture proceeded for 3 days at which point the cells were either analyzed for FoxP3^{GFP} expression, or sorted into CD4+FoxP3^{GFP}+ cells and injected intravenously into graft-recipient mice 1d before transplantation. **B** Histograms of FoxP3-GFP expression gated on dot plots of CD4+CD25+ cells in **A**. Female C57BL/6 mice were given either syn (BL6) or allo (C_3H)

tail skin grafts. Mice receiving allografts were administered $1x10^6$ iTregs intravenously 1d before transplant. Grafts were scored starting 7 days after transplantation and continued until mice were sacrificed on day 12. GICs, dLNs and blood were collected for flow cytometric analysis. **C** Survival curve of indicated groups. **D, F** Pseudocolor plots of GFP+, CD4+ co-expressing iTregs in the **D** dLN and **F** among graft infiltrating cells. **H** Pseudocolor plots displaying graft infiltrating CD4+ and CD8+ naïve, memory and effector phenotypes. **K** Dot plots displaying IFNγ, CD8+ CTLs. Flow cytometry results quantified in **B, E, G, I, J, L**. n = 5 (iTreg), 10 (Tβ1-iTreg), or 9 (Tβ2-iTreg) mice per group. Data are presented as mean ± SEM. *P<0.05, **P<0.005, ***P<0.001, ****P<0.0001 by ANOVA with Tukey's multiple comparisons test, or a log-rank (Mantel-Cox) test for the survival curve.

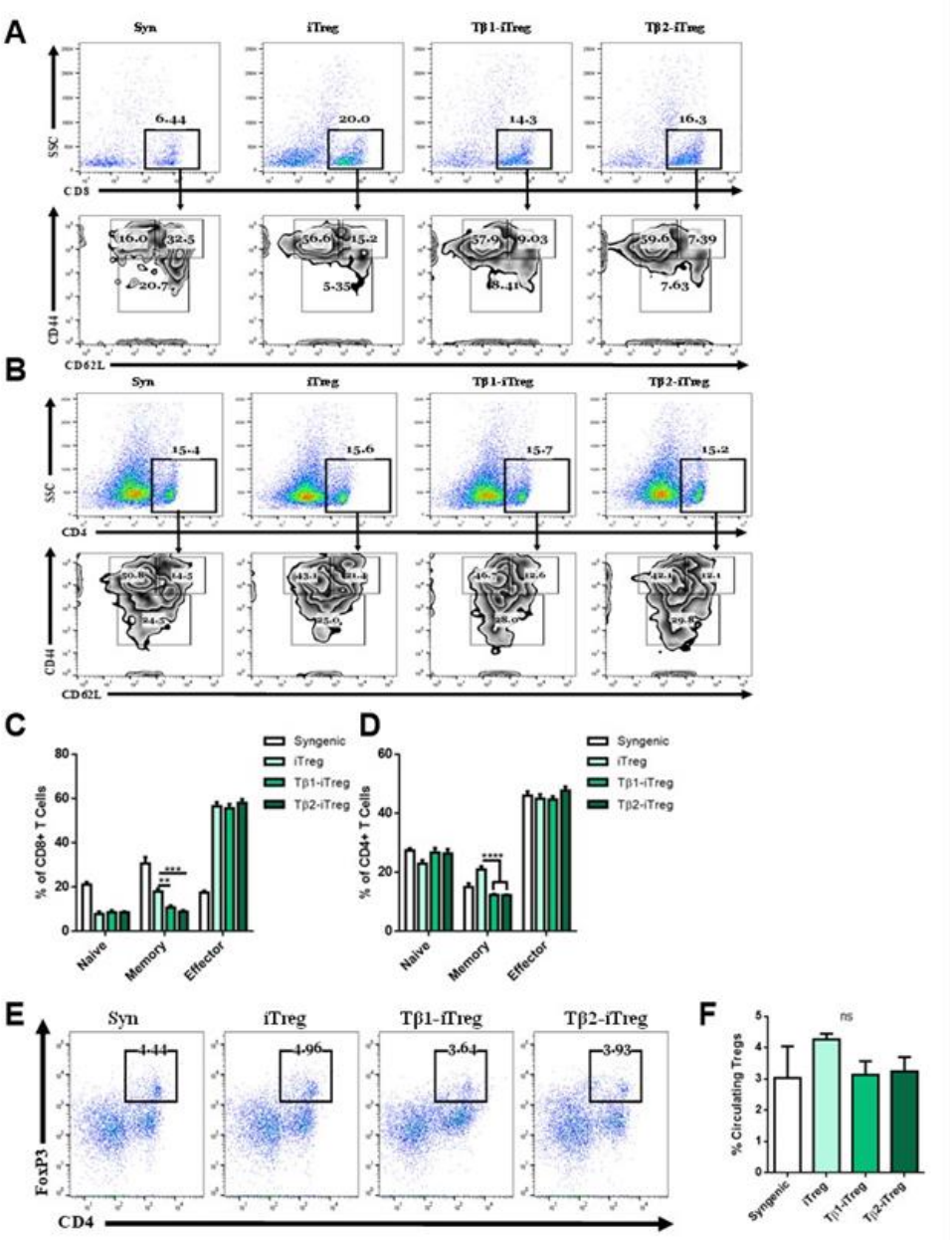

Figure 2.10 ***Circulating inflammatory profile after iTreg administration*****.** CD4+ cells were purified from naïve BL6 FoxP3^{GFP} mice and cocultured with allogenic splenic APCs along with anti-CD3ε (10μg/mL), anti-CD28 (4μg/mL) and IL-2 (10 ng/mL). Tβ1, and Tβ2-iTregs were also administered TGF-β1 (5ng/mL) or TGF-β2 (5ng/mL), respectively. Female C57BL/6 mice were given either syn (BL6) or allo (C_3H) tail skin grafts. Mice receiving allografts were administered 1x10^6 iTregs intravenously 1d before transplant. 12 days post-transplant, mice were sacrificed and exsanguinated. **A, B** Zebra plots displaying naïve, memory and effector phenotypes, gated on CD4+ or CD8+ cells. **E** Dot plot of circulating Tregs. **C, D, F** Quantification of flow cytometry results. Data are presented as mean ± SEM; n= at least 4 per group. *P<0.05, **P<0.005, ***P<0.001, ****P<0.0001 by ANOVA with Tukey's multiple comparisons test.

CHAPTER 3

CANNABINOID RECEPTOR ACTIVATION INCREASES GUT BARRIER INTEGRITY AND INDUCES ANTI-INFLAMMATORY CD103+ DENDRITIC CELLS TO PROTECT AGAINST COLITIS[2]

3.1 ABSTRACT

Intestinal homeostasis consists of the immense responsibility shared between enterocytes and immune cells to tolerate foreign nutrients and commensal microbes, while maintaining vigilance against pathogens. A perturbance to the coordination between host cells and its symbionts can lead to inflammatory bowel diseases, and increased susceptibility to colon cancer. New therapeutic approaches to prevent these disorders are needed to attenuate their increasing global incidence. Cannabinoids are used globally for recreational and therapeutic ends. In the current study, we demonstrate using multiple models of colitis that Δ9-tetrahydrocannabinol (THC) was highly effective in attenuating colitis and colon cancer. Cannabidiol when administered alone was not effective against colitis and a combination of THC+CBD had no noticeable effect. The action of THC was associated with stimulation of colonocyte mucin production and barrier integrity mediated by tight-junction proteins to provide spatial separation between host and commensal

[2] Becker W, Alrafas H, Nagarkatti M, Nagarkatti PS. Cannabinoid receptor activation increases gut barrier integrity and induces anti-inflammatory CD103+ dendritic cells to protect against colitis. Manuscript in preparation.

organisms. In addition, THC modulated dendritic cell (DC) phenotype towards increased CD103 expression in the colonic lamina propria (cLP) and enhanced DC TGF-β1 expression to expand the cLP Treg population, protecting the host from inflammation. Our findings reveal THC's salutary capacity in preventing colonic inflammation by harmonizing the balance between colonocyte and immune cell function. 3.2 INTRODUCTION

Despite the plethora of data from pre-clinical studies on the effectiveness of cannabinoids for IBD, only two clinical studies have been conducted, and there remains a lack of understanding how the myriad functions of cannabinoids work collectively to influence colitis development and progression (53-56). We set out to garner a holistic view of the gut macroenvironment after cannabinoid administration. To accomplish this, the most commonly used cannabinoids, THC and CBD, were used alone or in tandem in several murine models of colitis with disparate etiologies to investigate how the gut immune cells, intestinal barrier, and gut flora work synergistically after cannabinoid treatment to prevent colitis.

3.3 MATERIALS AND METHODS

Mice The University of South Carolina Institutional Animal Care and Use Committee approved all experiments. All mice were housed at the AAALAC-accredited animal facility at the University of South Carolina, School of Medicine (Columbia, SC) under specific pathogen-free conditions and 12 hr dark/light cycles in temperature-controlled rooms and given ad libitum access to water and normal chow diet. Female C57BL/6 and BALB/C mice, aged 8-12 weeks were obtained from Jackson Laboratories (Bar Harbor, ME, USA). Cnr1-/-, Cnr2-/-, and double knockout Cnr1-/-Cnr2-/- mice are

on a C57BL/6 background and were bred and maintained in-house. The number of mice for each experimental cohort is described in the Figure legends.

Colitis induction and treatments For all colitis experiments, unless otherwise indicated, treatments began three days before disease induction with CBD (10mg/kg), THC (10mg/kg) or a combination of THC+CBD (10mg/kg, both), or the vehicle control (ethanol). All treatments were suspended in ethanol and delivered to animals as a ratio of 2:1:18 ethanol:Tween-80:PBS by oral gavage. For the induction of TNBS-induced colitis, BALB/C mice were anesthetized by light isofluorane administration and given an intrarectal administration of 100 μL of 1mg of TNBS (Millipore, Sigma) dissolved in 50% ethanol. Mice were kept vertical for 30s after TNBS administration to keep the TNBS in contact with the colonic mucosal surface. DSS colitis was induced by dissolving 2% DSS (MP Biomedicals) in the drinking water and giving mice ad libitum access until the end of the study or humane endpoints were reached. To induce anti-CD40 colitis, mice were injected i.p. with 100 μL of 200 μg of anti-CD40 IgG2a monoclonal antibody (clone FGK4.5) or isotype rat IgG2a control (both from Bio X Cell), dissolved in PBS. Studies examining the effects of Treg depletion on anti-CD40 colitis progression proceeded as above but with an i.p. injection of rat anti-mouse CD25 (clone PC61, 100 mg/kg) or isotype control (both from Biolegend) one day before anti-CD40 injection.

Assessment of colitis disease parameters For all colitis models, mice were weighed daily, and colon lengths were measured at experimental end-points. Stool scores were measured according to a modified stool scoring system (Table 3.1). Colonoscopy images were taken at indicated time points by anesthetizing the mice and using a high-resolution mouse endoscopic system Karl Storz (Tuttlingen, Germany) Tele Pack Vet X LED

endoscope designed for small animals. The severity of colitis was scored using the mouse endoscopy and murine endoscopic index of colitis severity (MEICS) system, detailed in (Table 3.2). To investigate the levels of proteins clinically relevant to the diagnosis of colitis severity, mice were sacrificed, and blood was taken via the portal vein, allowed to clot, and serum was taken after centrifugation. Serum samples were subjected to sandwich ELISAs for Serum amyloid A (SAA; Abcam), Lipocalin-2 (LCN-2; Invitrogen) and Myeloperoxidase (MPO; Invitrogen), according to manufacturer's instructions.

AOM/DSS model of colitis-induced colorectal cancer C57BL/6 mice aged 8-10 weeks old were injected i.p. with azoxymethane (AOM, MPBIO) (10mg/kg). DSS (1%) was added to the drinking water one week after AOM administration for one week before regular drinking water was returned for two weeks. Three of these DSS (1%)-regular water cycles were completed before mice were kept on regular water and monitored for polyps via colonoscopy until sacrifice. Treatments with VEH, THC (10mg/kg) or THC/CBD (10mg/kg, both) began one week after administration of AOM and continued twice weekly until the end of the last DSS cycle.

Gut permeability assay On day 2 of TNBS-induced colitis, and day 9 of DSS-induced colitis, mice had their food and water removed in the evening. The next morning, mice were gavaged with 600 mg/kg of 4kD FITC-dextran (MilliporeSigma) in 100 μL PBS. Food and water were returned, and 4 hours later, blood was collected by retroorbital bleeding, blood was allowed to clot, and serum was separated after which FITC-dextran concentrations were determined using a PerkinElmer Life Sciences (Boston, MA) spectrophotometer with excitation wavelength at 480 nm.

Histology Proximal colon tissues were excised, rinsed with PBS and fixed by immersion in 3% paraformaldehyde (PFA) for 24 hours. Fixed tissues were embedded in paraffin, sectioned and stained with hematoxylin and eosin. For Periodic Acid-Schiff (PAS) staining, a staining kit purchased from MilliporeSigma was used following manufacturer's instructions. Color bright field images and picture montages were taken using a Cytation-5 Imaging Reader (BioTek Instruments, Winooski, VT, USA).

Tissue Processing Mesenteric lymph nodes (MLNs) and spleens were excised and brought to a single cell suspension. Spleens were subjected to red blood cell lysis before both spleens and MLNs were passed through a 70 μM filter, spun down and re-suspended in FACS buffer for flow-cytometric analyses.

To isolate the colonic lamina propria (cLP), colons were excised and luminal contents were removed by gliding curved forceps down the length of the colon, colons were opened longitudinally and mucus was removed by gentle scraping in sterile 1X PBS. Tissue was cut into 0.5 cm pieces and incubated in pre-warmed sterile 1X HBSS (without Ca2+ and Mg2+) containing FBS (3%vol/vol), 10mM EDTA (Cellgro), and 5mM DL-Dithiotreitol (DTT; MilliporeSigma) for 30 minutes at 37°C while shaking. The intra-epithelial cells (IECs) containing immune cells and enterocytes were recovered by filtering the colon pieces over a 100μM filter. The supernatant containing the IEC fraction was put on ice for at least 10 minutes to allow sedimentation of debris, and the IEC fraction was taken from the upper part of the supernatant. Remaining tissue containing the cLP was incubated in pre-warmed 1X HBSS (with Ca2+ and Mg2+) solution (15mL/colon) containing FBS (3%vol/vol), 1% L-glutamine, 1% penicillin–streptomycin, 10 mM HEPES, 0.5 mg/mL collagenase D (Roche), 0.5 mg/mL Dispase (MilliporeSigma) and 0.04

mg/mL DNase I (MilliporeSigma) for 45 minutes at 37°C while shaking. The supernatant was filtered over a 70μm cell strainer into ice cold sterile 1X PBS. cLP cells were passed through a Percoll (GE Healthcare) gradient (40%/80%(v/v) gradient) and spun at 620xg for 20 minutes with low acceleration and no brake. Cells at the 40/80 interface were collected and washed twice with supplemented FACS buffer and prepared for flow cytometric analysis.

Flow cytometry Relevant tissues were brought to a single cell suspension, then 1-2 x 10^6 cells were washed with PBS and then stained with Live/Dead Fixable Aqua Dead Cell Stain Kit (Invitrogen) for 30 minutes at 4°C to aid in excluding dead cells. Cells were then washed and incubated with TruStain FcX anti-mouse CD16/32 (Biolegend) to block Fc receptors. Extracellular antigens were stained for 20 minutes at room temperature in staining buffer. Cells were fixed and permeabilized with BD Cytofix/Cytoperm (for cytokine restimulations) or BD Transcription Factor Buffer Set (for transcription factor staining) per manufacturer's instructions. Intracellular antigens were stained for 1 hour at 4°C in the appropriate 1x Perm/Wash buffer. Cells were washed with staining buffer and passed through a 100 μm nylon mesh before acquisition on a BD FACSCelesta (Becton Dickinson). Analysis was performed using FlowJo software (FlowJo, BD). All samples were recorded based on the same live cell threshold per tissue. Compensation was set using fluorochrome labeled CompBeads (BD Biosciences). Fluorochrome-conjugated antibodies are detailed in Table 4.

Cell culture and in vitro treatments Cells were cultured in a sterile incubator maintained at 37°C and 5% CO2. Caco-2 and LS174T cells were obtained from American Type Culture Collection (ATCC; Manassas, VA), while MC-38 cells were obtained from

Kerafast (Boston, MA). Cells were cultured in Dulbecco's Modified Eagle Medium (DMEM; Life Sciences) supplemented with 10% fetal bovine serum, 100 U/mL penicillin and 100 U/mL streptomycin, 1% (v/v) non-essential amino acids and 10mM HEPES (all Gibco, Paisley, UK). For experiments involving the addition of compounds, all cell lines were used at a population doubling (PD) between 10-20. Cells were seeded at 0.5 x 106 cells/well in a 6-well plate. Upon ~80% confluence, media was removed and replaced with media containing vehicle with THC, CBD, AM251, SR144528 or a combination (all at 10μM). Primary cells were cultured in complete RPMI supplemented with 10% FBS, 100 U/mL penicillin, 100 U/mL streptomycin, 10mM HEPES (Gibco, Paisley, UK), and 50 μM β-mercaptoethanol (MilliporeSigma, Gillingham, UK) (complete medium).

Bone marrow dendritic cell generation and DC: T cell coculture Naïve bone marrow cells were collected from the femurs of 10-week-old C57BL/6 mice and plated at a density of 1x106 cells/mL in 24-well plates with GM-CSF (20ng/mL) and IL-4 (10 ng/mL) supplementation to generate bone-marrow dendritic cells (BMDCs). 18 hours after initial plating, debris and non-adherent cells were removed and media containing GM-CSF was replaced and cells were monitored for 7 days until the end of culture. VEH or THC (10μM) were added to wells at initial plating and at media changes. On day 7, floating cells were collected and analyzed by flow cytometry, recovered supernatants were subjected to ELISA for TGF-β1. On day 6, floating cells were collected and DCs were purified by magnetic sorting for CD11c (EasySep, STEMCELL Technologies). Some purified DCs were re-plated in complete media for another day before supernatants were collected. Concurrently, naïve C57BL/6 mice were sacrificed, spleens and lymph nodes were harvested and brought to a single cell suspension before CD3+ T cells were isolated via

magnetic sorting and pulsed with CFSE (5μM). CD11c purified BMDCs treated with VEH or THC were plated with naïve T cells in 48-well plates at a ratio of 1:5 DCs to T cells with either 50 μg IgG control (Biolegend) or 50 μg anti-CD40 (BioXCell). Co-cultures continued for 3 days and select wells were harvested daily for examination of T cell proliferation.

RNA extraction and qPCR After isolation and purification, tissues of interest were snap frozen in liquid N2, or placed in RNAlater (Qiagen) and transferred to -80°C until ready for processing. Total RNA was isolated using RNeasy kit (Qiagen). Quality and quantity of RNA was determined by Nanodrop 2000 or Qubit fluorometer (both Invitrogen). Lithium chloride precipitation was carried out on tissues derived from DSS-treated mice to remove DSS contamination from RNA samples according to (100). Total RNA was used to make cDNA using miScript cDNA synthesis kit from Bio-Rad. qRT-PCR was carried out using SsoAdvanced SYBR green supermix from Bio-Rad. All qRT-PCR experiments were carried out on a CFX96 (or 384) Touch Real-Time PCR Detection System (Bio-Rad), using two-step amplification with a 60°C annealing temperature. Expression levels were normalized to 18S mRNA levels in mouse tissue samples; samples derived from MC38 cells were normalized to a combination of β-actin and 18S expression. Caco-2 samples were normalized to a combination of B2M and RPLPO expression, based on (101) and stable expression between treatment groups. Fold changes were calculated using the 2-ΔΔCT method. Primers for genes of interest are detailed in (Table 3.3).

Short Chain Fatty Acid Quantification using GC-MS At sacrifice, cecal contents were snap frozen in liquid N2 until ready for processing. Cecal contents were weighed and homogenized in ultrapure water to a concentration of 250 mg/mL. 1:4 volumes of 25%

metaphosphoric acid was added to samples for 30 minutes on ice. Acidified samples were centrifuged at 12,000xg for 15 minutes at 4°C before filtering the supernatant over Ultra-free MC columns (MilliporeSigma) using the same spin. An internal standard (IS) of 2-ethylbutyric acid was added to all samples and standards at a concentration of 0.1mM before addition of methyl tert-butyl ether (MTBE). Acidified and filtered samples with IS and MTBE were vortexed, spun down at 200xg for 5 minutes at room temperature, and the organic layer was recovered and subjected to a HP 5890 gas chromatograph configured with flame-ionization detectors (GC-FID). Stabilwax®-DA Column (fused silica) of 30 m × 0.32 mm i.d. coated with 0.50 μm film thickness was used. Helium was supplied as the carrier gas at a flow rate of 15 mL/min. The temperature was programmed to achieve the following run parameters: initial temperature 100°C, hold for 0.5 min, ramp 20°C/min, final temperature 250°C, maintain for 5 min. The injected sample volume for GC analysis was 1 μL splitless and the total run time was 18.0 min. Calibration standards were prepared as aqueous stock solutions using these fatty acids at the given concentration; acetic, propionic, and n-butyric at 400 mM, isovaleric and valeric 200 mM, isobutyric 100 mM, caproic and n-heptanoic 50 mM (all from MilliporeSigma). Each standard was injected to identify their retention times. Standard mixture was prepared at several concentrations suitable for the samples. Response factors (RF) were calculated via dividing the peak areas of the responses by the respective concentrations of the standards. To quantify the peak area in terms of concentration, the relative response factor (RRF) was used. The RRF was calculated using the formula RRF = RFStandard/RFIS. The concentration of the samples was calculated using the following equation, Conc. samples = Peak AreaSample x (Conc. IS/ Peak AreaIS)(1/RRF).

Antibiotic treatment BL6 mice were randomized and subjected to antibiotics in their drinking water for at least 3 weeks. Antibiotics included: ampicillin (1g/L), metronidazole (1g/L), neomycin (1g/L) and vancomycin (0.5g/L). Fresh antibiotic water was replaced every week. At the end of the antibiotic treatment, stool was collected, DNA was extracted, and PCR using Eubacteria primers was conducted and analyzed via agarose gel electrophoresis to determine extinction of bacterial DNA from post-antibiotic treated mice compared to pre-antibiotic mice. Fecal transfer donor mice (3-4 per group) were given at least three administrations of THC (10mg/kg) or vehicle before being moved to clean cages. After finishing their antibiotic regimen, recipient mice were then randomized again and placed into the old donor mouse cages with their used bedding. Three days after the end of antibiotic treatment, donor mice were placed in clean cages, stool was collected and re-suspended in PBS to 120mg of feces/mL of sterile PBS. Stool was homogenized by vortexing and shaking and spun down at 800xg for 6 minutes at room temperature. Supernatant was passed through a 40μM filter and administered to recipient mice in 200μL by oral gavage for 3 days before beginning DSS colitis.

16S Sequencing Fecal pellets were collected on indicated days and stored at -80°C. For isolation of mucus-associated bacteria, colons were excised upon sacrifice, luminal contents were removed, colons were opened longitudinally and gently rinsed in a petri dish with PBS. Mucus was then scraped from the luminal surface of the colons and stored at -80°C. Colon-associated bacteria was harvested by taking a ~1cm piece of the proximal colon after the mucosal lining was removed and snap freezing it in liquid N2. Bacterial DNA was extracted using the QIAamp Fast DNA Stool Mini Kit (Qiagen). Double-stranded DNA was quantified by Qubit Fluorometer (Invitrogen). Primers for the V4 region

of the 16S rRNA bacterial gene were used for amplification, then samples were individually barcoded to label each sample according to Illumina 16S Sample Preparation Guide (Illumina). Amplified 16S rDNA was sequenced using Illumina MiSeq. Sequence data were processed using QIIME. Read pairs were quality filtered and joined to form a complete V4 amplicon sequence. Operational taxonomic units (OTUs) were selected by clustering reads at 99% sequence similarity in relation to the Greengenes reference database using the consensus method implemented in QIIME.

Statistical Analyses Data were analyzed using GraphPad Prism software with the statistical test and number of experimental repetitions indicated in the respective Figure legends. Unless otherwise stated, data are presented as individual dots for each sample/mouse, a line for mean, and bars indicating SEM. Tests were always 2-sided where applicable; $P < 0.05$ was considered significant.

3.4 RESULTS

Cannabinoids ameliorate TNBS-induced colitis and reduce effector cell phenotypes.

We investigated the beneficial effects of cannabinoids on intestinal inflammation by examining a murine model of acute colitis that mimics the human symptoms of ulcerative colitis. BALB/c mice were injected intrarectally with 100 mg/kg of 2,4,6-Trinitrobenzenesulfonic acid (TNBS) in 50% ethanol. To test if cannabinoid treatment would prevent the onset of the diseases, we initiated the treatment 3 days before disease induction. We used 4 groups of mice: TNBS+Vehicle, TNBS+CBD, TNBS+THC and TNBS+THC+CBD. We used 10mg/kg of THC or CBD or 10 mg/kg each of THC and CBD in the combination group. We used THC+CBD because these cannabinoids are found together in Cannabis and may offer beneficial effects when combined. THC and

THC+CBD treatment was able to reduce the body weight loss compared to VEH control, while CBD alone failed to reduce weight loss (Figures 3.1A, B). Colonoscopy revealed significant inflammation, bleeding and ulcers in the VEH and CBD groups, which was diminished in the THC and THC+CBD groups (Figure 3.1C, 1D, 3.2A). The VEH group had significant colon shortening attenuated with THC or THC+CBD treatment but not with CBD alone (Figures 3.1E, F). Inflammatory markers including serum Amyloid A (SAA), Lipocalin-2 (LCN2) and Myeloperoxidase (MPO) were all reduced in the THC or THC+CBD group mice, when compared to vehicle controls, with less striking effects in MPO levels, while CBD alone failed to have significant effect (Figures 3.1G-I). Periodic acid-Schiff's staining showed that VEH and CBD groups had significant tissue damage, more immune cell infiltration, and less mucus deposition compared to THC and THC+CBD groups (Figure 3.1J). To characterize the immune cell populations, the colonic lamina propria (cLP) cells were subjected to flow cytometric analysis. Gating strategy are detailed in (Figures 3.2B-E). THC and THC+CBD reduced the number of CD8+IFNγ+ cytotoxic T cells (CTLs) compared to VEH and CBD groups (Figures 3.1K-, L). There was no change in CD4+ IL-17A secreting Th17 cells (Figure 3.1L, M); however, THC and THC+CBD increased the FoxP3+ T regulatory cells in the cLP compared to VEH and CBD groups (Figure 3.1O, P). Overall, these data demonstrated that while CBD alone at the dose tested (10mg/kg) was not effective in attenuating TNBS-mediated colitis, THC or a combination of THC+CBD were highly effective. Also, THC alone was as effective as THC+CBD.

Cannabinoids prevent DSS-induced colitis and reduce effector cell phenotypes.

Due to the success of THC and THC+CBD in ameliorating TNBS-induced colitis, we next sought to investigate how cannabinoids may benefit a model of colitis with a different etiology, dextran sodium sulfate (DSS)-mediated colitis. C57BL/6 mice were treated with VEH or cannabinoids for 3 days before disease induction via 2% DSS in the drinking water and body weight, stool parameters and colonoscopies were performed periodically throughout the 13-day disease course. THC or THC+CBD were efficacious at preventing weight loss and bloody diarrhea when compared to VEH controls while CBD alone was not effective (Figures 3.3A, B; 3.4B). The colonoscopies revealed less inflammation and a thicker mucus layer in the THC and THC+CBD groups than the VEH and CBD groups throughout the study (Figures 3.3C, D; 3.4A). Colon lengths were measured at sacrifice and provided further evidence of the disease-preventative effects of THC and THC+CBD (Figures 3.3E, F), bolstered by the serum biomarkers SAA and LCN-2 that were also reduced in treatment groups (Figures 3.3G, H), while MPO was not (Figure 3.3I). Overall, CBD alone was ineffective except for reducing SAA (Figure 3.3G). PAS stains of the proximal colon exhibited prominent immune cell infiltration in the VEH and CBD groups and decreased mucus production from goblet cells which was reversed in the THC or THC+CBD groups (Figure 3.3J). Flow cytometry of cLP effector immune populations revealed a reduction in the THC and THC+CBD groups of inflammatory Th17 cells, CD8+IFNγ+ cells (Figures 3.3K-N), and an increase in Tregs (Figure 3.4C, D). Additionally, we found a reduction in T-bet+ Th1 cells but no significant change in Gata3+ Th2 population in THC or THC+CBD groups when compared to VEH group (Figure 3.3O,

P). Overall, these data are consistent with the findings from the TNBS-induced colitis model in that while CBD alone was not effective in attenuating DSS-induced colitis, THC alone or a combination of THC+CBD was highly effective. Also, THC was as effective as THC+CBD suggesting that CBD, at the dose tested, provided no additional benefit.

Cannabinoid receptor 1 activation leads to increases in gram-negative bacteria and short-chain fatty acid dysregulation that are inconsequential to DSS progression.

To examine whether the anti-colitic effects of cannabinoids such as THC are due to any changes in the gut flora, we first performed studies using naïve mice. Stool was collected from a pool of naïve mice before (Pre-Tx) and after five administrations of either VEH (VEH 5X) or THC (THC 5X, 10 mg/kg, oral gavage), DNA was extracted and 16S rRNA sequencing was performed. Short-term THC administration, compared to Pre-Tx mice and VEH 5X mice, showed increases in gram-negative Bacteroidetes and Proteobacterial phyla (Figures 3.5A-C). The specific Proteobacteria altered after THC administration belonged to the classes alpha- and gammaproteobacteria (Figure 3.5D). To assess how acute (1X) and short-term (5X) THC administration altered levels of bacterial metabolites heavily implicated in homeostatic host functioning, analysis of short-chain fatty acids (SCFAs), was performed on the cecal contents. The data showed an increase in acetate and butyrate 24 hours after a single (1X) administration of THC compared to VEH (Figure 3.5E), however, this increase was transient, as there were no differences in cecal SCFA levels after short-term (5X) THC administration (Figure 3.5F). To identify if changes in gut microbiota were mediated through cannabinoid (CB) receptors, CB1 (Cnr1-/-), CB2 (Cnr2-/-) or double CB receptor knockout (Cnr1-/-Cnr2-/-) mice were utilized. Administration of THC 5X in Cnr2-/- mice led to similar bacterial community changes as

seen in WT mice, with an increase in the THC 5X group of bacteroides and gammaproteobacteria, suggesting a CB2-independent mechanism through which they are increased (Figure 3.5G). Despite similar changes in bacterial composition in Cnr2-/- and WT mice given THC, Cnr2-/- mice given THC short-term had reduced levels of butyrate in their cecal contents (Figure 3.5H), and this was not seen after acute administration (Figure 3.6A). In Cnr1-/- mice given THC, we saw an opposite trend wherein THC, acutely and after short-term administration, reduced acetate and proprionate levels in the cecum (Figures 3.6B, C), and short-term THC administration led to increases in gram-positive Firmicutes classes (Figure 3.6D). Notedly, it is through the CB receptors that THC exerts its flora-altering effects, because short-term THC administration in Cnr1-/-Cnr2-/- mice showed inconsequential effects on bacterial community shift or SCFA production compared to VEH or Pre-Tx mice (Figures 3.6E, F).

Next, we investigated how cannabinoids impact the microbial balance in the DSS-induced colitis model. We found that despite some overlap between all groups, the THC and THC+CBD group, in which colitis was attenuated, were clustered closer together and farther away from the VEH and CBD groups, that developed severe colitis (Figure 3.5I). Concordantly, the THC and THC+CBD groups had higher levels of acetate, proprionate and butyrate in their cecal contents when compared to the VEH and CBD groups (Figure 3.5J). To test whether the changes in bacterial community seen with THC administration are the mechanism of protection against colitis development, we did a fecal transfer (FT) experiment wherein naïve mice were given antibiotics (ABX) in their water for 4 weeks to deplete their microbiota. Then they were taken off ABX water and placed in cages with the used bedding of mice that had received short-term VEH or THC administration which

would be the FT donor mice. After 3 days in the used cages with regular drinking water, stool from donor FT mice was collected freshly and gavaged to recipient mice for 3 days before giving DSS and then for another 5 days after giving DSS. Weight loss was monitored and the data revealed that the fecal bacterial community from THC treated mice could not protect mice from colitis (Figure 3.5K).

Cannabinoids utilize both cannabinoid receptors to specifically increase colonic barrier integrity and mucus production to protect against colitis induction

Because barrier integrity plays a critical role in colitis, we investigated the effect of cannabinoids on this property. On the last day of DSS colitis (day 12) and TNBS colitis (day 4), mice were gavaged with 4kD FITC-Dextran and 4 hours later, serum FITC-Dextran levels were analyzed as a measure of gut permeability. The data showed that cannabinoids were ineffective at reducing gut permeability induced by DSS colitis, compared to VEH group (Figure 3.7A); however, in the TNBS colitis model, both THC and to a lesser extent THC+CBD reduced the gut permeability caused by TNBS (Figure 3.7B). To resolve this incongruity, we recalled that the THC and THC+CBD groups in both DSS and TNBS colitis models evinced increased mucus production via both colonoscopy imaging and PAS staining. To substantiate, mice were given acute or short-term VEH or THC administration, and proximal colons were harvested 24 hours later, and PAS stains were performed to assess mucus deposition in the colonic lumen. We observed a striking increase in mucus emanating from the goblet cells in the THC 1X group into the lumen, that while reduced in vibrance in the 5X THC administration group, was still noticeably increased in the lumen at that time point compared to VEH (Figure 3.7C). We then considered the nature of the DSS and TNBS models and how the DSS model of Crohn's

disease instigates inflammation throughout the entire GI tract, while TNBS colitis is more restricted to the colonic epithelium, akin to ulcerative colitis. Thus, we looked at mucus and tight-junction protein expression in the proximal colon (PC) and small intestine (SI) in VEH (1X) or THC (1X) mice and found that THC increases mRNA expression of gel-forming Muc2 and Muc5ac specifically in the PC (Figure 3.7D). Similarly, increases in tight-junction proteins: Claudin and Zonula occludens-1 (ZO-1), but not Occludin, were specifically seen in the PC after acute THC treatment (Figure 3.7D). Given that mucin expression and the regulation of anti-microbial peptides, β-defensins, are intertwined (95,96), we then examined β-defensin 1 and 3 expression and found that it was also increased after short term THC administration, and specifically in the PC, not in the SI (Figure 3.7D). We tested whether the observed expression increases persist in situations of DSS-induced inflammation and found THC, but not CBD, increases the colonic expression of Muc2, Muc5ac, ZO-1 and β-Defensin 3 (Figure 3.7E). Moreover, this effect was observed in the mouse MC38 adenocarcinoma cell line (Figure 3.7F). Treating the human adenocarcinoma cell line, Caco-2 with THC and CB antagonists AM251 (CB1) and SR144528 (CB2) revealed THC-mediated increases in ZO-1 were through CB1, as they were reduced in the THC+AM251 group (Figure 3.7G). Contrary to the work in mice, β-Defensin 1 expression was reduced by THC and was dependent on both CB receptors (Figure 3.7G). THC administration to Caco-2 cells was able to increase Muc2 and Muc5ac expression in this cell line, and this is also dependent on both CB receptors, because only with a combination of AM251 and SR144528 are expression levels returned to the level of the vehicle (Figure 3.7G). Further evidence that THC requires both CB receptors to increase mucus and defensin production is mirrored by work in Cnr1-/- and Cnr2-/- mice

where THC has no effect (Figure 3.6G). To approximate how the increased colonocyte barrier integrity caused by THC effects disease initiation and prevention, TNBS and DSS colitis models were initiated as was done previously, but with a THC pre-treatment group (Pre-Tx), that began receiving treatment 3 days before disease initiation, and a treatment group (Tx), that received treatment concurrently with disease initiation. Although both methods display efficacy in reducing disease parameters, THC pre-treatment was significantly more effective than concurrent treatment at preventing colitis in both TNBS and DSS-colitis models as evidenced by a decrease in weight loss and colon shortening (Figure 3.7H-K).

THC treatment reduces αCD40 colitis severity through a reduction in dendritic cell activity.

TNBS and DSS-induced colitis result from luminal damage to the enterocyte layer, while anti-CD40 Ab injection is known to trigger colitis resulting from robust intestinal inflammation stemming from the macrophage and DC activation (97,98). Importantly, this model acts solely on the immune system, and is independent of the microbiota or intestinal permeability to stimulate inflammation (93,97,98). To study the effect of cannabinoids in this model, 3 days before disease induction, we began treatment with VEH or THC as done in previous colitis models, and then a single injection of αCD40 Ab or IgG control Ab was administered intraperitoneally (ip). Disease severity peaked 3 days post αCD40 Ab injection and treatment continued until 7 days post disease-induction at sacrifice. Both VEH and THC treated mice lost significant weight compared to IgG controls, some losing up to 15% in 3 days; there was no ameliorative effect of THC on weight loss caused by disease (Figure 3.8A). However, spleen weight used as a marker of systemic inflammation

and mesenteric lymph node cellularity, were both significantly reduced by THC treatment (Figures 3.8B, C). THC treatment was also able to reduce levels of serum pro-inflammatory cytokines, IFNγ and TNFα (Figure 3.8D). In this model, the levels of Th2 cytokines such as IL-4, IL-5, and IL-13 were low and remained unchanged after THC treatment. Colonoscopy at peak of disease on day 3 also revealed decreased inflammation in the THC treated group when compared to VEH group, and once again noticeable mucus deposition was seen in the lumen of THC treated mice (Figure 3.8E, F). Immune cell phenotyping in the cLP showed a decrease in the percentage and numbers of infiltrating CD45+ immune cells in THC group when compared to VEH group (Figures 3.8G-I). Also, there were less cLP macrophages in the THC treated group (Figures 3.8J, K); however, there was no difference in the activation markers CD80 or CD86 on the macrophages (Figures 3.9A, B). Dendritic cells (DCs), by comparison, were not reduced in percentage in the cLP (Figures 3.8L, M), but their levels of activation marker CD80 were reduced in the THC group (Figures 3.9C, D). In the mLN, THC treatment reduced IFNγ secreting CD8+ cells and CD4+ Th1 cells, when compared to VEH (Figures 3.9E-H), while there were no observed differences in CD4+ IL-17A, IL-10 or IL-4 secreting cells, or in DC phenotype (Figures 3.9I-L). To assess how cLP DCs played a role in disease, we characterized the subsets of DCs known to heavily influence intestinal inflammatory balance. We phenotyped DCs for their expression of surface markers CD103 and CD11b, because DCs with higher expression of CD103 have been shown to play a role in promoting an anti-inflammatory response through Treg induction (88), whereas DCs with more CD11b expression are catalysts for T cell and innate lymphoid cell (ILC) inflammatory

responses (99). THC treatment caused an increase in CD103+ DCs and a concurrent decrease in CD103+CD11b+ DCs at sacrifice compared to VEH mice (Figure 3.8N, O).

Dendritic cell re-programming and not Treg induction are the mechanism through which THC ameliorates αCD40-induced inflammation.

Considering the observed DC phenotype switch, we examined the numbers of Tregs in the cLP of αCD40 and IgG control mice after VEH or THC administration. Flow cytometric analysis of Treg phenotype revealed that αCD40 Ab treated mice had an increase in Helios+FoxP3+ natural Tregs (nTregs), when compared to control mice, and THC treatment further enhanced this population (Figure 3.10A, B). Because an increase in FoxP3+ Tregs was seen in the TNBS and DSS model as well after THC and THC+CBD treatment, we considered this as a possible mechanism through which THC exerts its anti-colitic effects. However, depleting Tregs using an anti-CD25 antibody (clone PC61, 100 mg/kg) one day before disease induction with αCD40, proved to be an unlikely mechanism through which THC acts, as there was no change in the body weight loss or spleen weight between αCD40 mice treated with THC with or without an intact Treg pool (Figures 3.10C, D). In the TNBS, DSS and αCD40 models, we observed a THC-mediated phenotypic change towards increased DC CD103 expression (Figure 3.11A-D). Therefore, we shifted our focus back towards THC's effects on DCs and looked at how THC affects intestinal DCs acutely, in situations without overt inflammation. Acute (1X) THC treatment increased the percent of CD103+ single positive and reduced the percent of CD103+CD11b+ double positive DCs in the cLP 24 hours after a single THC administration (Figure 3.10E, F). One mechanism through which CD103+ DCs can influence Treg induction is through TGF-β1 secretion (88), and supernatants recovered

from cLP cells harvested from THC or VEH 1X mice and plated overnight revealed a trend towards increased TGF-β1 production in THC-treated mice (Figure 3.10G). The increase in CD103+ DCs seen in the cLP after THC administration was not noticed in the mLN of these mice (Figure 3.10H, I), and the increase in TGF-β1 seen in the cLP after THC treatment was also not seen in the mLN (Figure 3.10J), suggesting a cLP specific effect. Because DCs traffic between the cLP and mLN, their temporal and spatial activity after THC treatment is important to understand their functioning. CCR7 expression is linked to trafficking between the mLN and cLP (98), therefore, we looked for CCR7 expression on cLP and mLN DCs after THC 1X exposure and found that THC acutely reduced DC CCR7 expression in the cLP but especially in the mLN (Figure 3.10K, L), suggesting that DCs were migrating less between the immune tissues in the intestines. To isolate the effects of THC on DCs specifically, bone-marrow dendritic cells (BMDCs) were generated by addition of GM-CSF and IL-4 to a culture of naïve bone marrow cells treated with VEH or THC. The data showed THC treated BMDCs had more TGF-β1 in their supernatant when compared to controls (Figure 3.10M). Although there were equivalent percentages of DCs in the VEH and THC treated cultures, a BMDC culture is a mixed population of cells, and thus on day 6 of BMDC culture, CD11c+ DCs were purified and plated overnight, and analysis of their supernatant revealed that TGF-β1 levels were increased from the THC-treated BMDCs compared to VEH controls (Figure 3.10N). We observed a decrease in DC CD80 expression, but not CD86 expression in THC treated cultures; and THC-treated DCs reduced CD4 and CD8 T-cell proliferation in vitro (Figures 3.11E-G). Furthermore, THC administration increases the number of cLP Helios+FoxP3+ nTregs in a CB2 dependent manner, and while DC phenotype is consistent between knockout and WT mice, there are

significantly reduced numbers of total DCs in the cLP of Cnr2-/- mice (Figure 3.12A-D). Next, we analyzed other immune cell changes that occur after acute THC administration under naïve conditions and found that THC does not affect the percentage of innate lymphoid cells (ILCs): ILC2, NCR or LTi ILC3s in the cLP, nor the number of macrophages, although there was an increase in FCεRI+c-Kit+ mast cells in the cLP after THC administration, which appeared to be mediated through CB2 (Figures 3.12E-J). Moreover, THC 1X treated mice whose cLP was isolated and plated overnight showed only small differences in cytokine production by an increase in IL-2 and IL-6 compared to VEH treated mice (Figure 3.12K).

Cannabinoid receptor activation stems the progression of colitis-induced colon cancer by reducing IL-22 production in the epithelial microenvironment.

Given the well-established propensity for colitis to lead to the development of colon cancer (29,30), we next investigated the effect of THC or THC+CBD on a murine model of colitis-associated colon cancer. To induce colon cancer, we used the well-established model of carcinogen injection, azoxymethane (AOM, 10 mg/kg, ip), followed by three cycles of DSS to induce colon carcinogenesis. We halted cannabinoid treatment after the third DSS cycle to examine the effects of cannabinoids solely on cancer initiation, and not the potential direct effects of cannabinoids on tumors. Disease progression and experimental schematic is detailed in (Figure 3.13A), revealing that mice given DSS+AOM to induce colon cancer (CC group) but treated with cannabinoids, lost less weight compared to the CC + VEH group (Figure 3.13A). At termination of the study, colonic tumors and spleen weights were increased in the CC + VEH group compared to both CC + THC and CC + THC+CBD groups (Figure 3.13B-D). Colonoscopies revealed

reduction in inflammatory severity as well as tumor induction in CC + THC and CC + THC+CBD groups when compared to CC + VEH group (Figure 3.13E, F). Notable was that consistent with earlier data shown in (Figures 3.1C, D; 3.2C, D; 3.7C) where we saw that the colons of both disease and naive control mice given THC or THC+CBD had increased colonic mucus, here we see mucus deposition persists after many weeks of treatment (Figure 3.13E, F). Since CC + THC and CC + THC+CBD mice did not develop any tumors, we looked at immune parameters relevant to carcinogenesis that might be differentially regulated in the treatment groups. IL-22 is a cytokine produced by Th22 cells and ILCs that is critical to the development, maintenance, and stemness of inflammation-induced colon cancer (105-107). The CC + VEH group had a significant increase in the amount of CD4+IL-22+ Th22 cells in the intra-epithelial cell fraction (IEC) of the colon compared to CC + THC and CC + THC+CBD groups, while there was no change in cLP CD4+RORγt+ cells (Figure 3.13G-I). Taking the cells from the cLP and IEC and plating them overnight to collect supernatants revealed that the increase in IL-22 seen in the CC+VEH group in the colonic microenvironment is coming specifically from cells in the IEC (Figure 3.13J, K), not the cLP.

3.5 DISCUSSION

The synergy between immune cells, enterocytes and symbiotic and pathogenic microbes in the GI tract requires a delicately balanced network that can adapt as new signals are acquired. A disruption in that balance can lead to chronic inflammation. Recent epidemiological evidence suggests this disruption in the form of colitis is on the rise in developing nations and its current burden in North America and Europe is daunting (26-28). New strategies that can safely tip the gut equilibrium toward host defense without sparking inflammatory cascades or leave the host vulnerable to other maladies will be the

most effective strategy for preventing disease. In the current study, we demonstrated the potential for cannabinoids in the prevention and amelioration of gut inflammation. Previous reports have found that cannabinoids acting through CB1 can reduce gut motility (49,85) and gastric acid secretion (86), and increase barrier integrity (49,51). Studies from our lab and others have demonstrated the CB2 dependent anti-inflammatory properties of cannabinoids working directly through immune cells (46, 48-50, 87). The work herein builds on those studies to provide a comprehensive evaluation of how the most commonly used cannabinoids, positively influence host gastrointestinal homeostasis through increased coordination between immune cells, colonocytes and gut flora.

The most commonly consumed cannabinoids come in the form of recreational marijuana, whose primary bioactive components are CBD and THC (41,42). With cannabis legalization and public consumption of marijuana and CBD extracts increasing, it is important to parse out the scientifically proven beneficial effects of these compounds to cut through the noise of increasing anecdotal reports (41, 108, 112). Purified forms of CBD come as the FDA-approved drug Epidiolex for epilepsy, and purified THC comes as Dronabinol to treat spasticity and pain, among others (43, 108). A combination of THC and CBD is sold under the trade name Sativex and is prescribed to treat the symptoms of multiple sclerosis (42, 43). Numerous reports from animal studies and one prospective placebo-controlled human study tout the effectiveness of cannabinoids for ameliorating colitis (41, 42, 48-54). Our goal was to understand how each component, CBD and THC, can affect disease course to best understand the therapeutic potential of these compounds. To accomplish this, we used three models of colitis and one model of inflammation induced

colorectal cancer, looking at gut immunity, barrier function and host-microbiota interactions to gain a clear view of where the efficacy of cannabinoid in treating colitis lie.

In the TNBS and DSS model of colitis, THC and a combination of THC+CBD were effective at preventing the symptoms of colitis, but CBD was not. Our results align with a human trial on CBD for Crohn's disease (55); however, their sample size was low, and it is possible that in both cases the dose of CBD used was too low, as there are reports of CBD being effective for treating inflammatory pain (108,109) and liver inflammation (110,111). Nonetheless, THC was significantly more effective than CBD at protecting against TNBS and DSS-induced colitis, with no significant benefit added when combining CBD with THC. TNBS and DSS colitis are both induced via luminal delivery of xenobiotics that induce colitis by damage to the epithelial layer and allowing microbes to infiltrate host tissue in the case of DSS, and by disrupting the luminal mucus layer with ethanol and haptenizing colonic proteins in the case of TNBS. In examining tissues from THC and THC+CBD treated mice, we noticed less inflammation than the VEH and CBD groups but also more mucus deposition into the luminal layer. We confirmed that THC alone stimulates the production of Muc2 and Muc5ac after a single administration in naïve mice, as well as in inflamed DSS-diseased mice. In addition to increasing mucus production, THC also increases the expression of tight-junction proteins ZO-1 and Claudin. Importantly, this effect was specific to the colon. This explains why, despite similarly improved clinical parameters of disease, DSS mice treated with cannabinoids had gut leakage comparable to VEH mice, while TNBS mice treated with cannabinoids did not. DSS delivered in the drinking water will also break up the epithelial lining of the small intestine and other parts of the GI tract, leading to leakage, while TNBS induced damage

is specific to the colon. Using cannabinoid receptor (CB) knockout mice, MC38 and Caco-2 adenocarcinoma cell lines, we were able to show that CB1 is responsible for the THC-mediated increases in tight-junction proteins, confirming work by others (51). Novel to this study was that the increase in mucus and β-defensins that occurs after THC administration is dependent on both CB1 and CB2. The increase in mucus expression was prevalent in mouse tissue, cell lines and human cell lines, but Caco-2 cells given THC had the opposite trend in β-defensin production when administered THC, this could be attributable to the nature of that cell line or a non-conserved mechanism. Regardless, additional human data is needed to support this finding. The observed increases in colonic barrier integrity were shown to be important for disease prevention, as mice pre-treated for 3 days with THC developed less severe TNBS and DSS colitis compared to mice whose treatment began concurrently with disease induction.

Importantly, the THC-mediated increase in tight-junction proteins and mucus were seen only in the proximal colon samples, but not in the small intestine where there is less contact with microbes. Mucus is a glycoprotein, that once deposited into the lumen polymerizes into a polysaccharide gel. This gel is an excellent source of defense from microbes and has been protective in colitis and colon cancer (95,96); however, it also acts as fuel for microbes. The increase in mucus production and deposition after THC administration may be why the changes in bacterial composition seen after THC administration favor the gram-negative phyla of Bacteroidetes and Proteobacteria, two phyla well known for their voracious appetite for carbohydrates (90). This would also explain why those bacteria, which are commonly thought of as pathogenic with colitis (90, 91), were not disease promoting in our THC treated mice, because those bacteria were not

opportunistic pathogens, simply a result of increase in their preferential food source. Further support for this notion is the finding that acute administration of THC caused a small increase in acetate and butyrate levels in the cecum, that is diminished after short-term administration, indicating an initial burst of microbial mucus metabolism that wanes. It would also explain why the fecal transfer from THC-treated mice was ineffective at suppressing colitis progression. Yet another compensatory mechanism in this complex interplay at the luminal surface is that the increased mucus production is balanced by an increase in defensin production, as seen from both our in vivo animal experiments and in vitro MC38 cells.

By increasing the mucus production from goblet cells, and the observed increases in tight junction message expression, THC likely prevented the mechanism of action of disease induction in TNBS and DSS colitis; consequently, we used the αCD40 model of colitis to isolate the effects of THC on GI immunity. Injection of αCD40 causes acute wasting disease and colitis dependent on secretion of inflammatory cytokines TNF-α, IL-12 and IL-23 (97,98). We found THC reduced inflammation systemically and in the colon in the αCD40 colitis model via reduction in gross intestinal pathology and circulating pro-inflammatory cytokines IFNγ and TNFα. Flow cytometry of the cLP and Treg-depleting studies revealed in this inflammatory model, the most likely immune cell through which THC exerts its most potent anti-inflammatory effects are DCs.

DCs are the master antigen-presenting cells, and a reduction in their ability to stimulate other immune cells stops the overwhelming inflammatory cascade before it can start. Acting through CB2, we demonstrated that THC can modulate DC phenotype towards a more anti-inflammatory state, characterized by decreased expression of CD80 in

vitro as well as in vivo in αCD40 colitic mice. DCs in the cLP can promote the expansion of T regulatory cells. Several studies have examined this mechanism, suggesting that DCs, primarily CD103+ DCs, upregulate CCR7 to migrate to the mLN where they secret TGF-β1 and retinoic acid to induce T regulatory cells (88). Our results showed that THC administration in naïve mice and after αCD40 induced colitis caused a decrease in CCR7 expression on DCs in both the cLP and mLN, suggesting THC reduces DC migration between gastrointestinal lymph tissue. In addition, we found that BMDCs treated with THC and cells from the cLP of mice treated with THC exhibited increased levels of TGF-β1. Taken together these data indicate that THC causes DCs to, instead of migrating to the mLN and induce Tregs, remain in the cLP, secrete TGF-β1, and increase the percentage of Tregs and influence other local cell types through the anti-inflammatory actions of TGF-β1. Indeed TGF-β1 is critical for intestinal homeostasis. Global TGF-β1-/- mice develop spontaneous colitis around 3-4 weeks of age, and DC specific knockout of TGF-β1 also results in spontaneous colitis (102,103). Moreover, DCs are an important source and activator of TGF-β1 in the intestine, necessary for controlling Treg and Th17 differentiation (103) and colonocyte homeostasis (104). The effect of THC on DCs is consistent with the observation that THC treatment reduces APC activity in vitro in human cells (44).

A frequently observed finding in studies examining the effect of cannabinoids on the immune system is the ability of CB receptor activation to switch T helper phenotype from Th1 to Th2 (47,48). We did not find evidence in our models for this switch to be occurring. THC reduced Th1 activity, although there was no evidence through flow cytometric analysis of CD4+Gata3 expression or in IL-4, IL-5 or IL-13 production that a

Th2 phenotype was being induced. This suggested that in the gut, the effect of THC may be different in that down-regulation of Th1 cells may not result from a switch from Th1 to Th2 but mere suppression of Th1 cells by TGF-β, as shown in other studies (47,48,103).

Taken together these data indicate a sophisticated network of mechanisms through which THC promotes cooperation and balance in the colonic macroenvironment. THC-mediated decreases in DC activation reduce effector cell generation, while DC secretion of TGF-β1 increases Tregs locally to promote tolerance. The decrease in immunogenicity from cLP immune cells is counterbalanced by increased barrier integrity, mucus production and antimicrobial peptide release that stave off unwanted microbial interference, while still allowing for the uptake of their beneficial metabolites (Figure 3.14). We also showed, crucially, these effects can last long term. In the AOM+DSS model of colorectal cancer, THC and THC+CBD maintained a thick mucus layer and was able to reduce the amount of intra-epithelial-infiltrating IL-22 producing Th22 cells. IL-22 has recently gained attention for its carcinogenic properties in human patients as well as in animal models of colon cancer by promoting cancer stemness through STAT-3 activation (99, 105-107). Our results show THC decreased the amount of tumorigenic IL-22 in the colonocyte microenvironment where cancer initiation and progression occur. Ultimately, the presented data provide robust evidence for the multi-faceted efficacy of THC in colitis prevention.

Table 3.1. Macroscopic scoring of colitis models.

Feature	Description	Score
Stool score	Normal, solid pellets	0
	Loosely-shaped, moist pellets	1
	Diarrhea	2
	Occult blood present[a]	3 → 5

Table 3.2. Mouse endoscopy and murine endoscopic index of colitis severity (MEICS).

Parameter	Description	Score
Translucency of the Colon Mucosa	Transparent	0
	Moderate	1
	Marked	2
	Non-transparent	3
Vascular Patter	Normal	0
	Moderate	1
	Marked	2
	Bleeding	3
Fibrin Visible	None	0
	Little	1
	Marked	2
	Extreme	3
Stool Consistency	Normal + solid	0
	Still shaped	1
	Unshaped	2
	Spread	3

Table 3.3. List of Primers

Gene Name	Accession Number	Primer	Sequence 5' → 3'
mMUC2	NM_023566	Forward	CTACCATTACCACCACTAC
		Reverse	GTCTCTCGATCACCACCATTT
mMUC5ac	NM O88715	Forward	CTGTAACACCCAGTGTCCTAAG
		Reverse	AGGCTGGTAGAAGTAGGTAGAG
m18S	NR_003278	Forward	CGTCGTAGTTCCGACCATAAA
		Reverse	TTTCAGCTTTGCAACCATACTC
mβ-actin	NM_007393	Forward	GGCTGTATTCCCCTCCATCG
		Reverse	CCAGTTGGTAACAATGCCATGT
mβ-Defensin 1	NM_007843	Forward	CACAGGCTTCCTGGGATATAAA
		Reverse	CGCTCTGGTTGGACAACTTA
mβ-Defensin 3	NM_013756	Forward	TTGAGGAAAGGAGGCAGATG
		Reverse	CGGGATCTTGGTCTTCTCTATTT
mZO-1	NM_009386	Forward	GCCGCTAAGAGCACAGCAA
		Reverse	TCCCCACTCTGAAAATGAGGA
mClaudin18	NM_001194921	Forward	TGGGTTTTGTGGTGTCACTG
		Reverse	GGTAGTTGAATACAGCGGTCAC
mOccludin	NM_001360536	Forward	TTGAAAGTCCACCTCCTTACAGA
		Reverse	CCGGATAAAAAGAGTACGCTGG
mLyz-1	NM_013590	Forward	CCTCCAAGTAACAGGACTTCAG
		Reverse	CTGACTGACAAGGGAGACTTTG
mLyz-2	NM_017372	Forward	AGTTCTTCAGCCAGGAAGTG
		Reverse	CCAAGATCAACTGGTCTCCTATAA
hB2M	NM_004048	Forward	GAGGCTATCCAGCGTACTCCA
		Reverse	CGGCAGGCATACTCATCTTTT
hRPLPO	NM_053275	Forward	CCATTCTATCATCAACGGGTACAA
		Reverse	TCAGCAAGTGGGAAGGTGTAATC
hDEFB1	NM_005218	Forward	GGTGGGTCAAAATGTGTGAGT
		Reverse	GCTGTGGTAGGTCAGGCTTC

hDEFB103A	NM_001081551.3	Forward	TGCTCTTCCTGTTTTTGGTGC
		Reverse	TGCCGATCTGTTCCTCCTTT
hZO-1	NM_001301025	Forward	CGGTCCTCTGAGCCTGTAAG
		Reverse	GGATCTACATGCGACGACAA
hMUC2	NM_002457	Forward	CACCTGTGCCCTGGAAGGC
		Reverse	CGGTCACGTGGGGCAGGTTC
hMUC5AC	NM_017511	Forward	CGGGTCCACGAGGAGACGGT
		Reverse	GCTTCTGCAGCCAGGCACGA
hGAPDH	NM_002046	Forward	GAAGGTCGGAGTCAACGGATT
		Reverse	CGCTCCTGGAAGATGGTGAT

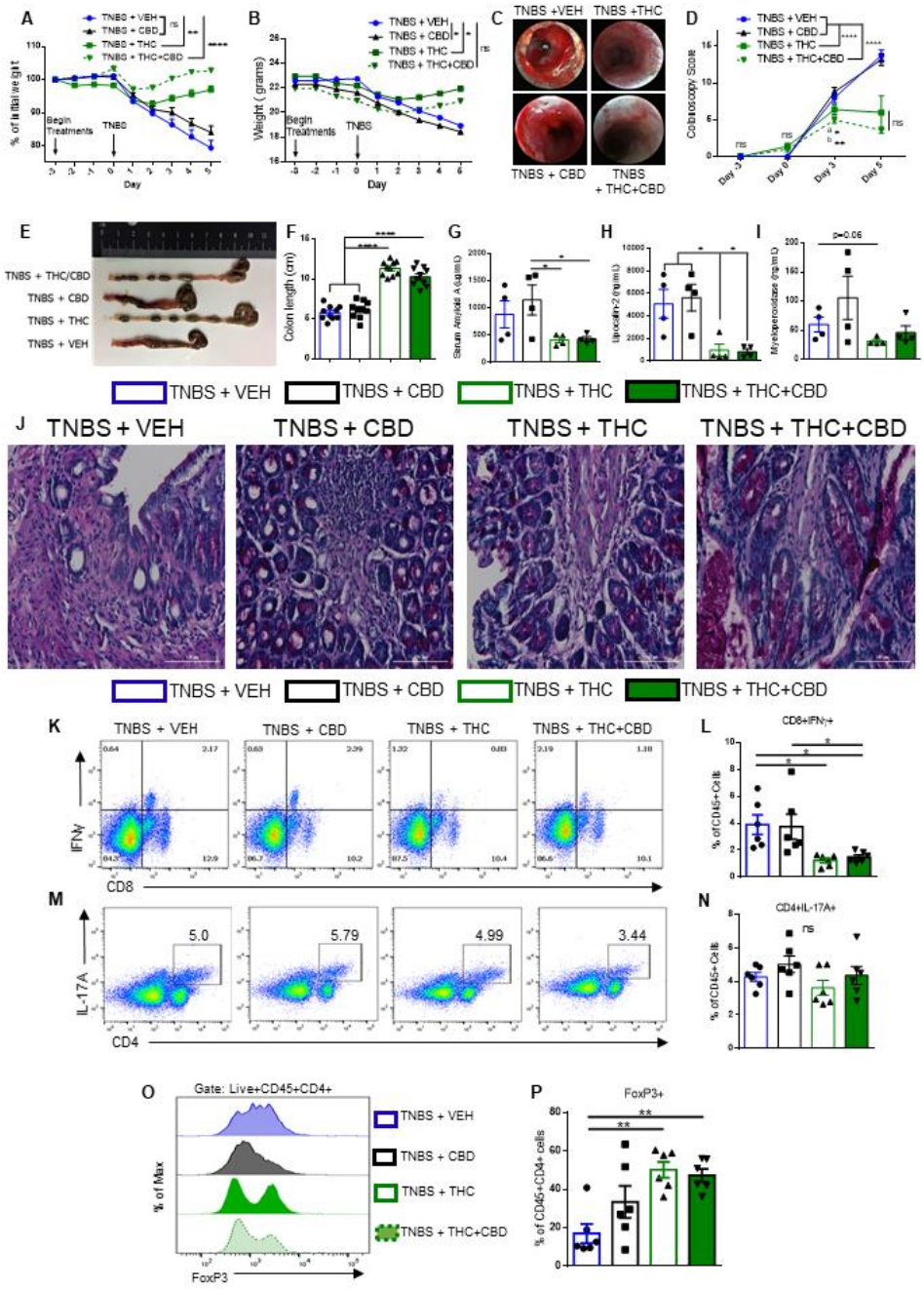

Figure 3.1 ***Cannabinoids ameliorate TNBS-induced colitis and reduce effector cell phenotypes.*** BALB/c mice were injected intrarectally with 100 mg/kg TNBS in 50% ethanol. Starting three days before disease induction and continuing daily, mice were gavaged with either: Vehicle (10% EtOH in PBS+Tween-80), CBD (10 mg/kg), THC (10mg/kg) or a combination of THC and CBD (10 mg/kg, both), (n=10). Mice were sacrificed at 5 days post disease induction and blood as well as organs of interest were harvested and analyzed for colitis-relevant parameters. **(A)** Percent weight change and **(B)** actual weight change over the course of disease. **(C)** Representative colonoscopy

images taken on day 5. **(D)** Quantification of colitis scores at indicated timepoints throughout disease course, (n=5 per group, per time point). **(E)** Representative image and **(F)** length of colons at sacrifice (n=10). **(G-I)** ELISAs from serum at sacrifice quantifying disease relevant biomarkers of colitis severity (n=4-5). **(J)** PAS stain of proximal colons from representative mice taken at sacrifice. **(K, M)** Representative flow cytometry psuedocolor dot plots (gate: Live,CD45+) displaying effector cell types from the lamina propria of indicated mice at sacrifice. **(O)** Offset histograms of FoxP3 expression (gate: Live, CD45+CD4+) in colonic lamina propria at sacrifice. **(L, N, P)** Quantification of flow cytometry results (n=6). Data are presented as mean ± SEM of three independent experiments. *P<0.05, **P<0.01, ****P<0.0001 by Two-way ANOVA with Tukey's multiple-comparisons test.

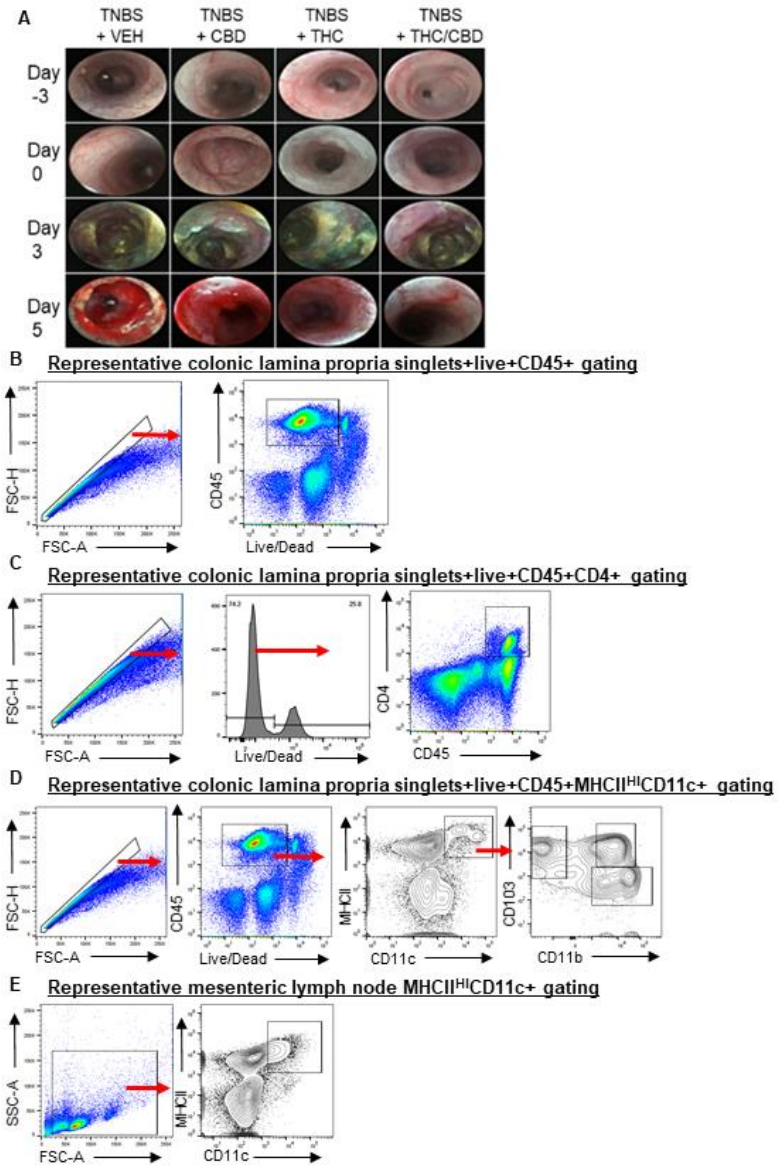

Figure 3.2 ***TNBS-induced colitis treated with cannabinoids supplemental data and representative flow gating strategies*** BALB/c mice were injected intrarectally with 100 mg/kg TNBS in 50% ethanol. Starting three days before disease induction and continuing daily, mice were gavaged with either: Vehicle (10% EtOH in PBS+Tween-80), CBD (10 mg/kg), THC (10mg/kg) or a combination of THC and CBD (10 mg/kg, both), (n=10). **(A)** Representative colonoscopy images from mice at every time point assessed. **(B-E)** Representative flow cytometry gating strategies.

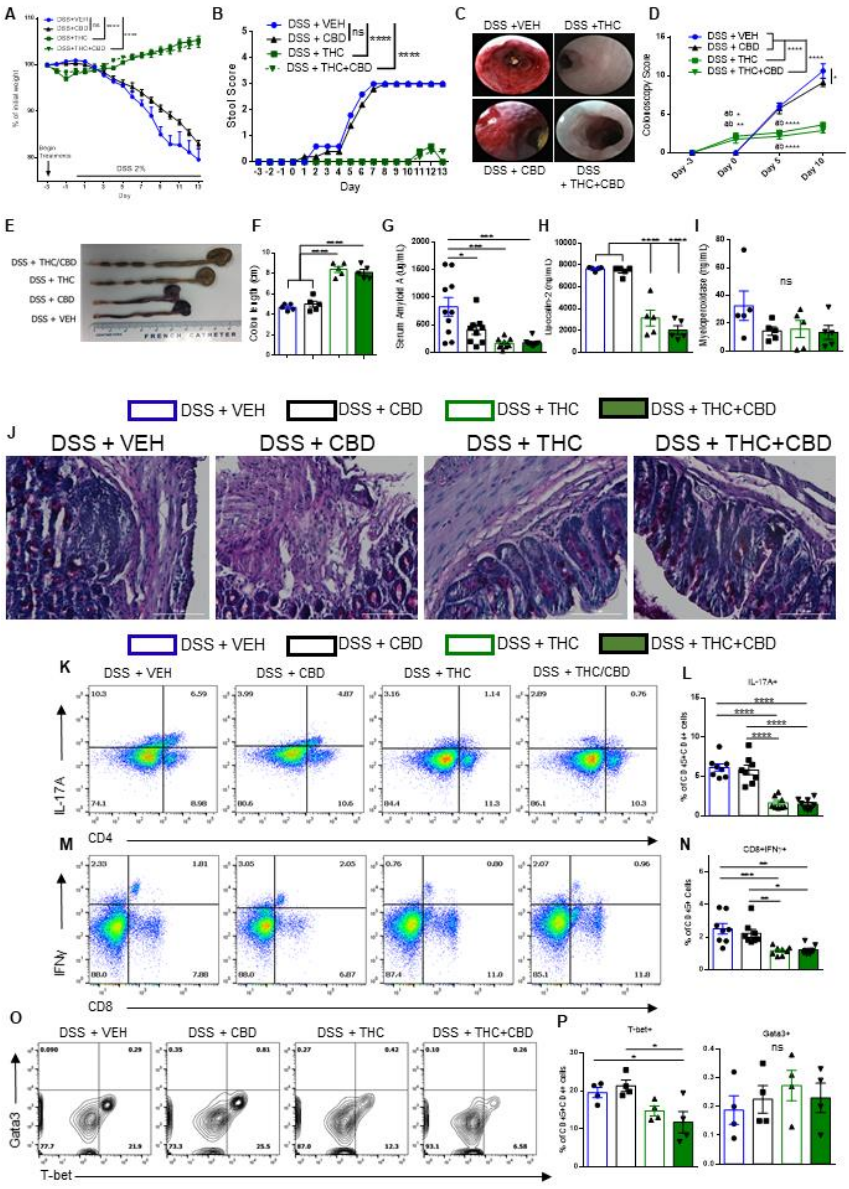

Figure 3.3. ***Cannabinoids prevent DSS-induced colitis and reduce effector cell phenotypes.*** To induce DSS-colitis, C57BL/6 mice were treated with either: Vehicle (10% EtOH in PBS+Tween-80), CBD (10 mg/kg), THC (10mg/kg) or a combination of THC and CBD (10 mg/kg, both) for 3 days before 2% DSS was added to their drinking water. DSS remained in the drinking water until termination of the study 14 days later. Mice were sacrificed at 14 days post disease induction and blood as well as organs of interest were harvested and analyzed for colitis-relevant parameters. (**A)** Percent weight change and (**B)** stool score assessed over the course of disease (n=5). (**C)** Representative colonoscopy images taken on day 10. (**D)** Quantification of colitis scores at indicated timepoints throughout disease course (n=8 per group, per time point). **E** Representative image and (**F)** length of colons at sacrifice (n=5). (**G-I)** ELISAs from serum at sacrifice quantifying disease relevant biomarkers of colitis severity (n=10, SAA; n=5, LCN-2,

MPO). **J** PAS stain of proximal colons from representative mice taken at sacrifice. (**K, M, O)** Representative flow cytometry psuedocolor dot plots (gate: Live,CD45+) displaying effector cell types from the lamina propria of indicated mice at sacrifice. (**L, N, P)** Quantification of flow cytometry results (n=4-8). Data are presented as mean ± SEM of three independent experiments. *P<0.05, **P<0.01, ****P<0.0001 by Two-way ANOVA with Tukey's multiple comparisons test.

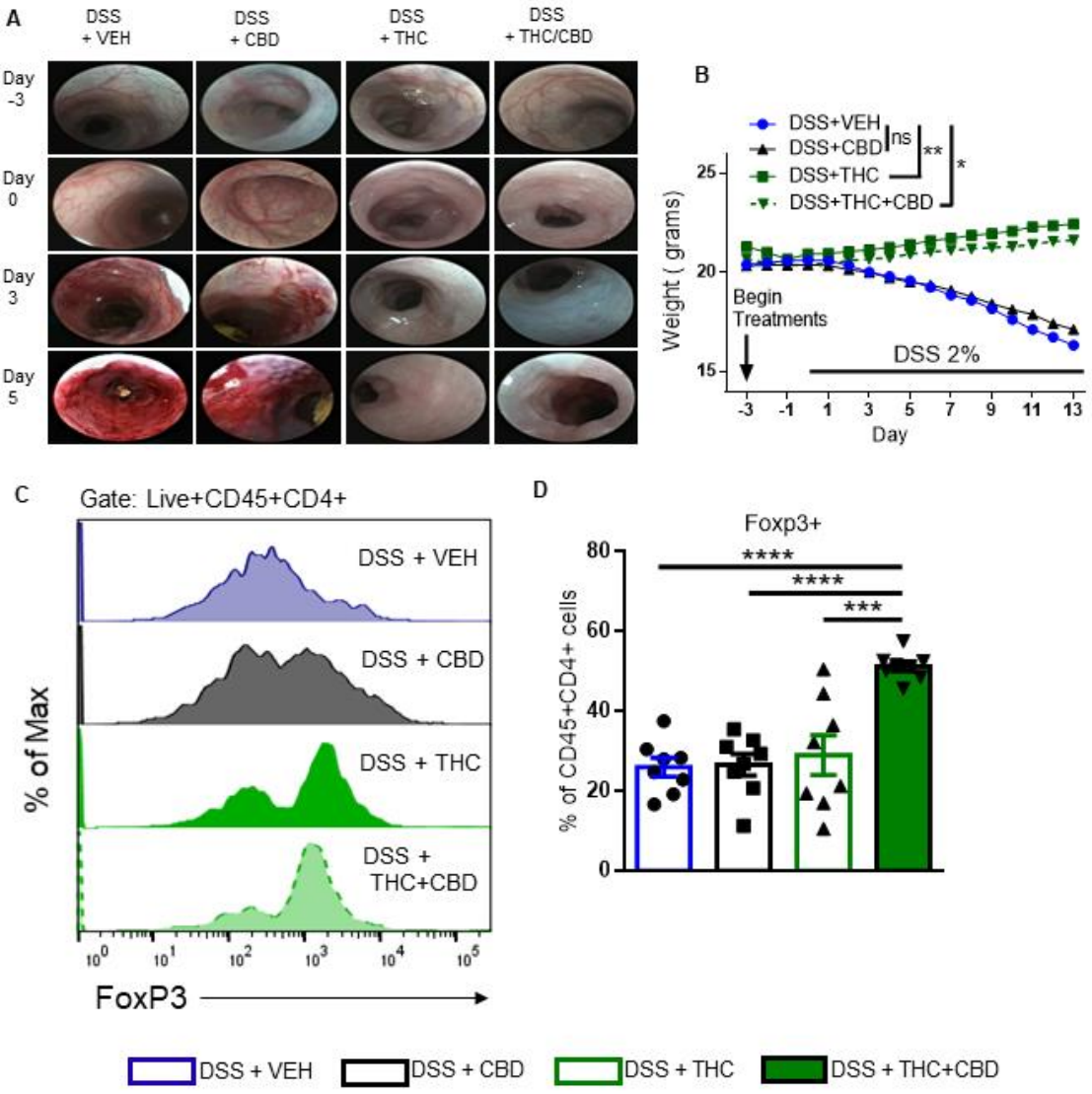

Figure 3.4 ***DSS-induced colitis treated with cannabinoids supplemental data*** To induce DSS-colitis, C57BL/6 mice were treated with either: Vehicle (10% EtOH in PBS+Tween-80), CBD (10 mg/kg), THC (10mg/kg) or a combination of THC and CBD (10 mg/kg, both) for 3 days before 2% DSS was added to their drinking water. DSS remained in the drinking water until termination of the study 14 days later. Mice were sacrificed at 14 days post disease induction and blood as well as organs of interest were harvested and analyzed for colitis-relevant parameters. **(A)** Representative colonoscopy images from mice at every time point assessed. **(B)** Actual weight change throughout the experiment (n=5). **(C)** Representative overlaid histograms displaying FoxP3 expression in the cLP at sacrifice (gate: Live, CD45+CD4+). **(D)** Quantification of flow cytometry results (n=8). Data are presented as mean ± SEM of three independent experiments. *P<0.05, **P<0.01, ****P<0.0001 by Two-way ANOVA with Tukey's multiple comparisons test.

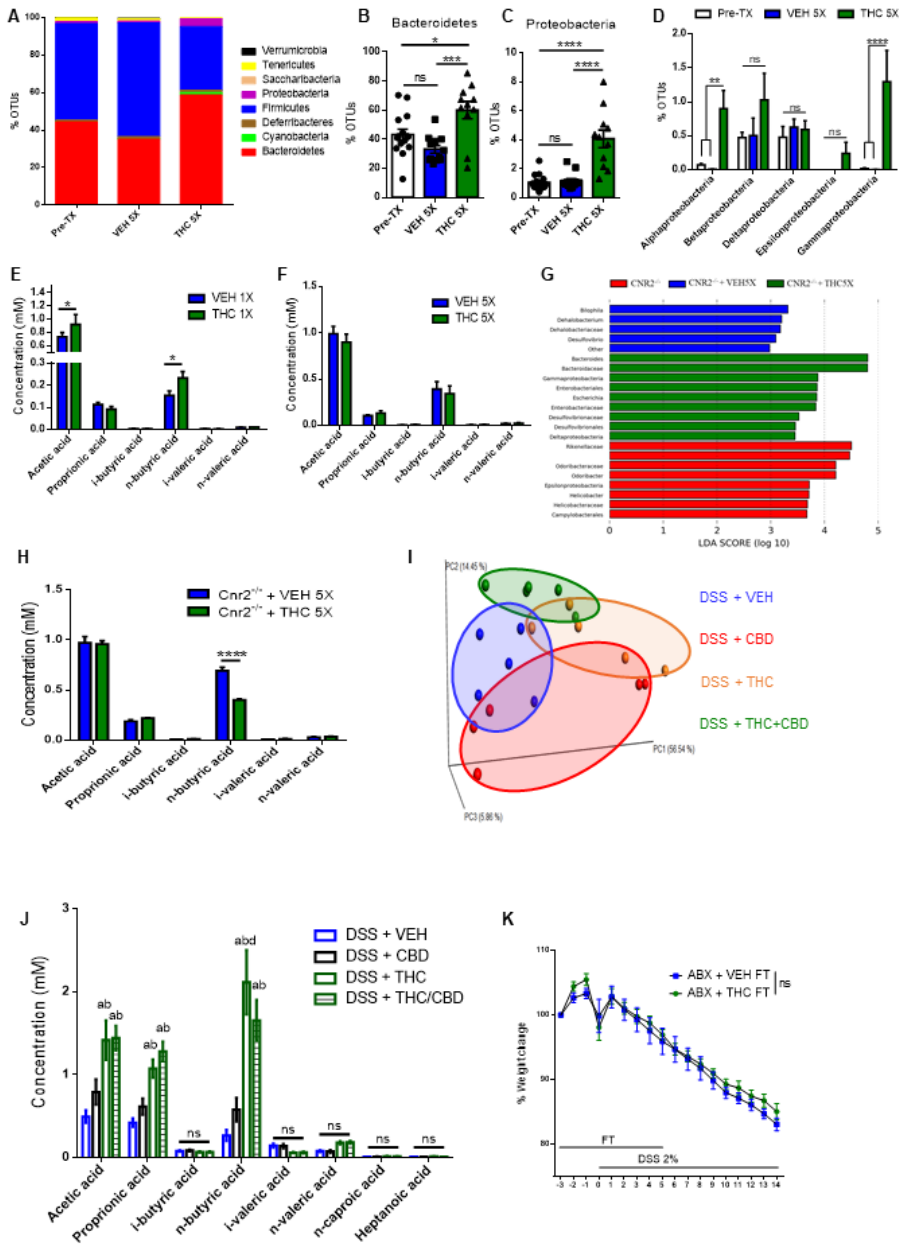

Figure 3.5. ***Cannabinoid receptor 1 activation leads to increases in gram-negative bacteria and short-chain fatty acid dysregulation that are inconsequential to DSS progression*** Stool was collected before any compound administrations (Pre-Tx n=15), and after five administrations of VEH (n=12) or THC (n=11), DNA was extracted and subjected to 16S rRNA sequencing. **(A)** Stacked bar plot displaying % OTUs of phyla of indicated groups. **(B)** % OTUs of the phylum Bacteroidetes and **(C)** Proteobacteria. **(D)** % OTUs of the classes of Proteobacteria. WT mice were given a single (n=10) **(E)** or five (n=9) **(F)** administrations of VEH or THC, sacrificed one day later and cecal contents were analyzed for SCFAs. **(G)** LDA score of Cnr2-/- mice before (n=6) or after five

administrations of VEH or THC (n=3). **(H)** SCFA analysis of Cnr2-/- mice (n=4), given five VEH or THC administrations. **(I)** PCOA plot displaying the bacterial community clustering from indicated mice on day 14 of DSS colitis (n=5). **(J)** Cecal SCFA quantification of indicated mice (n=5). Letters above error bars indicate $p<0.05$ against the indicated group, a=DSS+VEH, b=DSS+CBD, c=DSS+THC, d=THC+CBD. Mice were given antibiotics (ABX) in their drinking water for 4 weeks before antibiotic-free water was returned, mice were placed in the cages of donor fecal transfer (FT) mice containing their used bedding. Three days after cessation of antibiotics, mice were given daily fecal transfers from stool of indicated donor mice. DSS (2%) was administered in the drinking water after three days of fecal transfers and **(K)** body weight was recorded throughout the study (n=7-8 per group). Data are presented as mean ± SEM. Fecal transfer experiment was repeated three times. *P<0.05, **P<0.01, ****P<0.0001 by Two-way ANOVA with Tukey's multiple comparisons test.

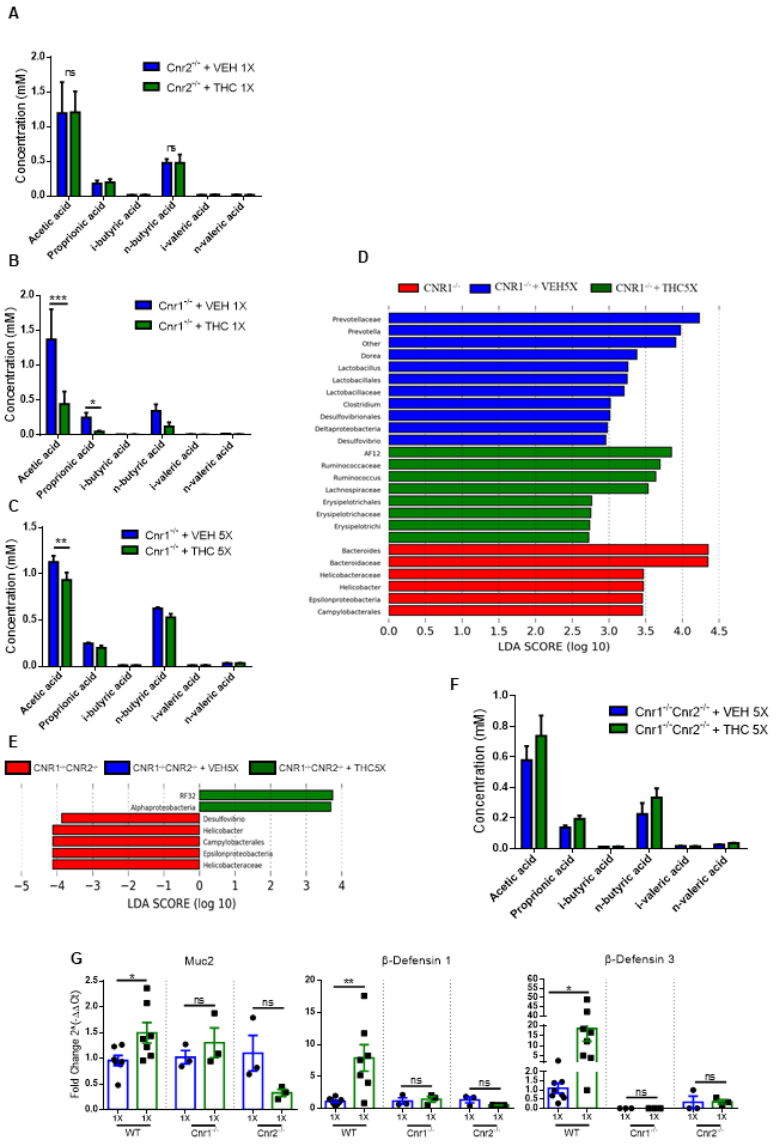

Figure 3.6. ***Cannabinoid receptors mediate the gut flora and short-chain fatty acid changes seen after THC administration*** **(A, B, C, F)** Mice of indicated genotype were given one (1X) or five (5X) administrations of VEH or THC and sacrificed 24 hours later. Their cecal contents were removed and SCFAs were quantified by GC-MS (n=5, all groups). **(D, E)** LDA score of significant bacterial changes occurring between groups. **(G)** qRT-PCR results from PC or SI of WT, Cnr1$^{-/-}$ or Cnr2$^{-/-}$ mice taken 24 hours after one administration of VEH or THC. Data are presented as mean ± SEM of two independent experiments. *P<0.05, **P<0.01, ****P<0.0001 by Two-way ANOVA with Tukey's multiple comparisons test or by Students *t*-test.

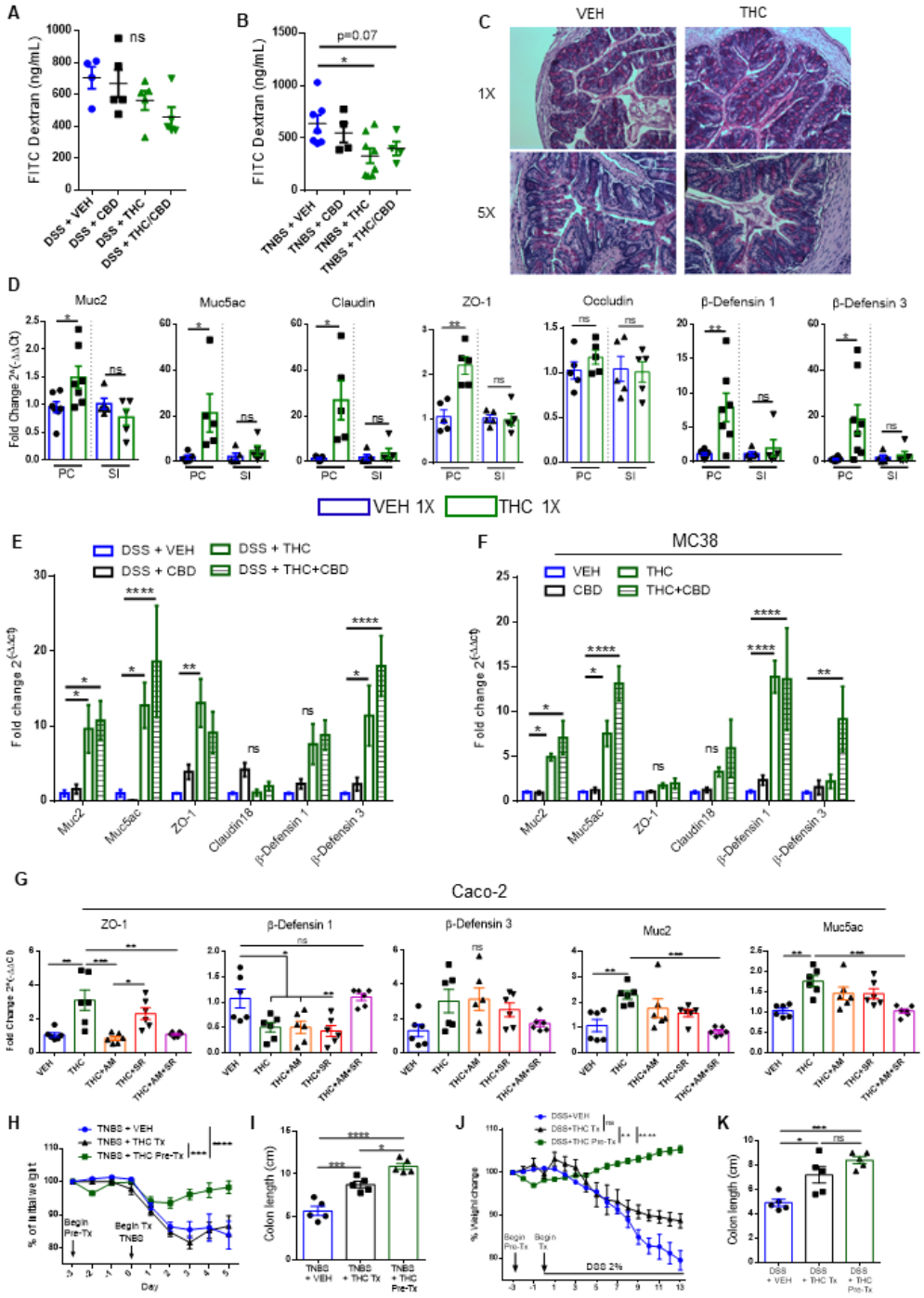

Figure 3.7. ***Cannabinoids utilize both cannabinoid receptors to specifically increase colonic barrier integrity and mucus production to protect against colitis induction*** **(A)** and **(B)** At day 4 of the TNBS-colitis (n=5-10) and day 13 of the DSS-colitis experiment (n=5), mice were fasted overnight and the next morning were gavaged with 100 uL of 4kD FITC-Dextran (600 mg/kg), 4 hours later blood was collected by retroorbital bleed, and serum was analyzed for the presence of FITC-Dextran as a measure of gut permeability. **(C)** PAS stain of proximal colon from mice after one or five VEH or THC

administrations. **(D)** qRT-PCR results from proximal colon (PC) or small intestine (SI) 24 hours after one administration of VEH or THC (n=5-7). **(E)** qRT-PCR results from PC of mice who received DSS (2%) in their drinking water for 13 days. **(F)** MC38 cells were treated with VEH, CBD, THC, or a combination of THC and CBD (all 10μM), for six hours before RNA was collected and qRT-PCR was run on indicated genes (n=4). **(G)** Caco-2 cells were treated with VEH, THC, AM251 (AM) or SR144528 (SR), or a combination where indicated for 12 hours before RNA was collected and qRT-PCR was run on indicated genes (n=6). TNBS and DSS colitis models were induced as was done previously but we used three groups. The VEH and THC Pre-Tx (THC, 10mg/kg, oral gavage) group received treatments beginning three days before colitis initiation, while the THC Tx group began receiving daily treatments the same day colitis was induced. **(H, J)** Percent weight change over the disease course, and **(I, K)** colon lengths at sacrifice (n=5). Data are presented as mean ± SEM. *P<0.05, **P<0.01, ****P<0.0001 by Two-way ANOVA with Tukey's multiple comparisons test.

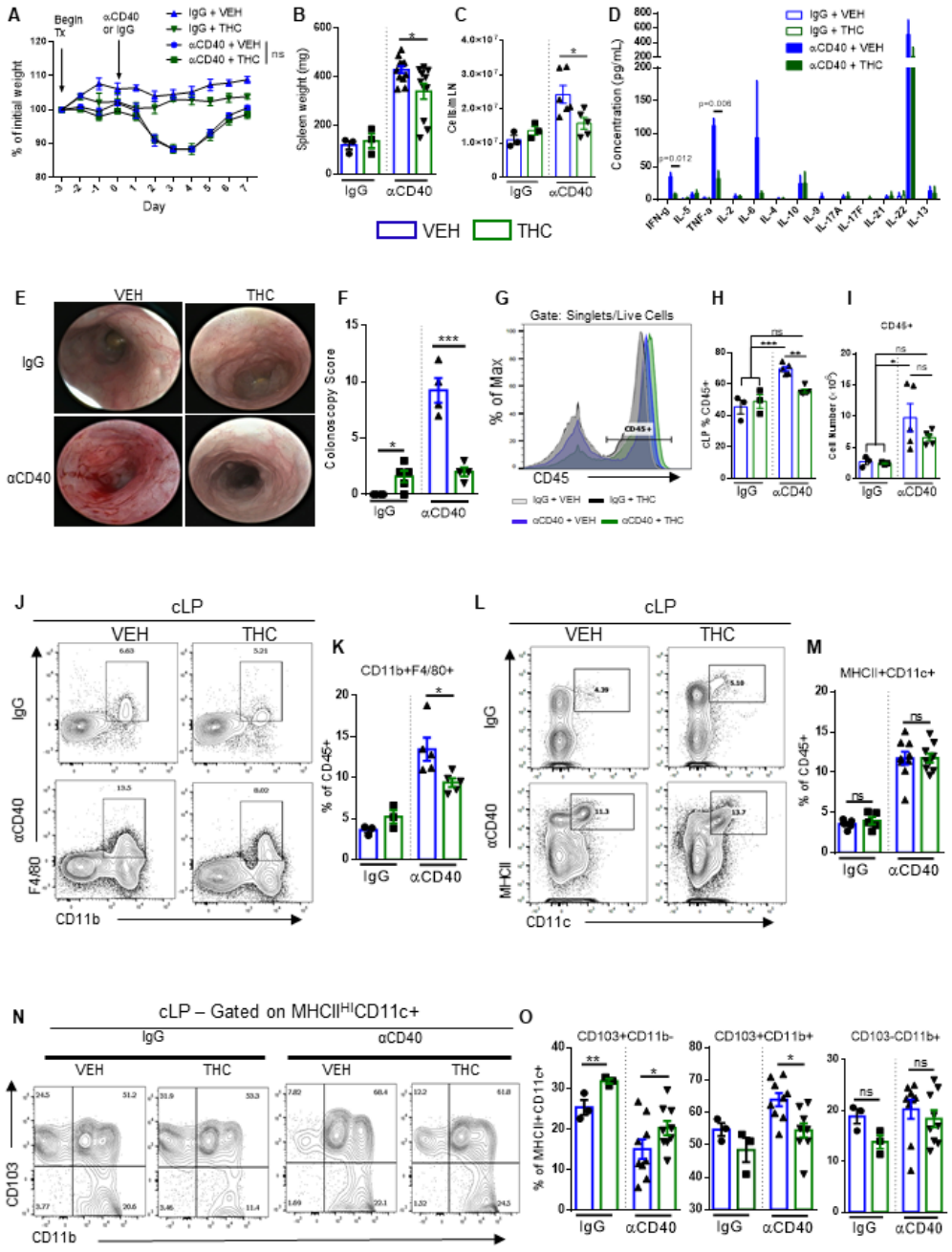

Figure 3.8. ***THC treatment reduces αCD40 colitis severity through a reduction in dendritic cell activity*** Mice were pre-treated daily with VEH or THC (10 mg/kg) for 3 days before intraperitoneal injection of rat anti-mouse IgG (control) or rat anti-mouse αCD40 (200 μg, clone FGK4.5 in PBS) and treatment continued for 7 days post disease induction to monitor progression of inflammatory severity. **(A)** Percent weight change over the course of disease (n=3-10). Spleen weight (n=3-10) **(B)** and absolute mesenteric lymph node cell number (n=3-6) **(C)** were recorded at sacrifice. At peak of disease on

day 3, blood was collected via retroorbital bleed, serum was separated and subjected to Legendplex assay for serum T helper cytokine levels **(D)** (n=3 per group). **(E)** Representative images of colonoscopies performed at peak of disease on day 3, and their quantification in **(F)** (n=4 per group). **(G)** Representative overlaid histograms displaying CD45+ cell percentages from the colonic lamina propria of indicated mice at sacrifice. **(H)** Quantification of CD45 percentages and **(I)** absolute cell counts of CD45+ colonic lamina propria cells. **(J)** Representative contour plots of macrophages (gate: Live, CD45+) (n=3-5) and **(L)** dendritic cells (gate: Live, CD45+) (n=5-8). **(N)** Representative contour plots of cLP dendritic cell subsets at sacrifice (gate: Live,CD45+MHCIIHICD11c+) (n=3-9). **(K, M, & O)** Quantification of flow cytometry results. Data are presented as mean ± SEM. *P<0.05, **P<0.01, ****P<0.0001 by Two-way ANOVA with Tukey's multiple comparisons test.

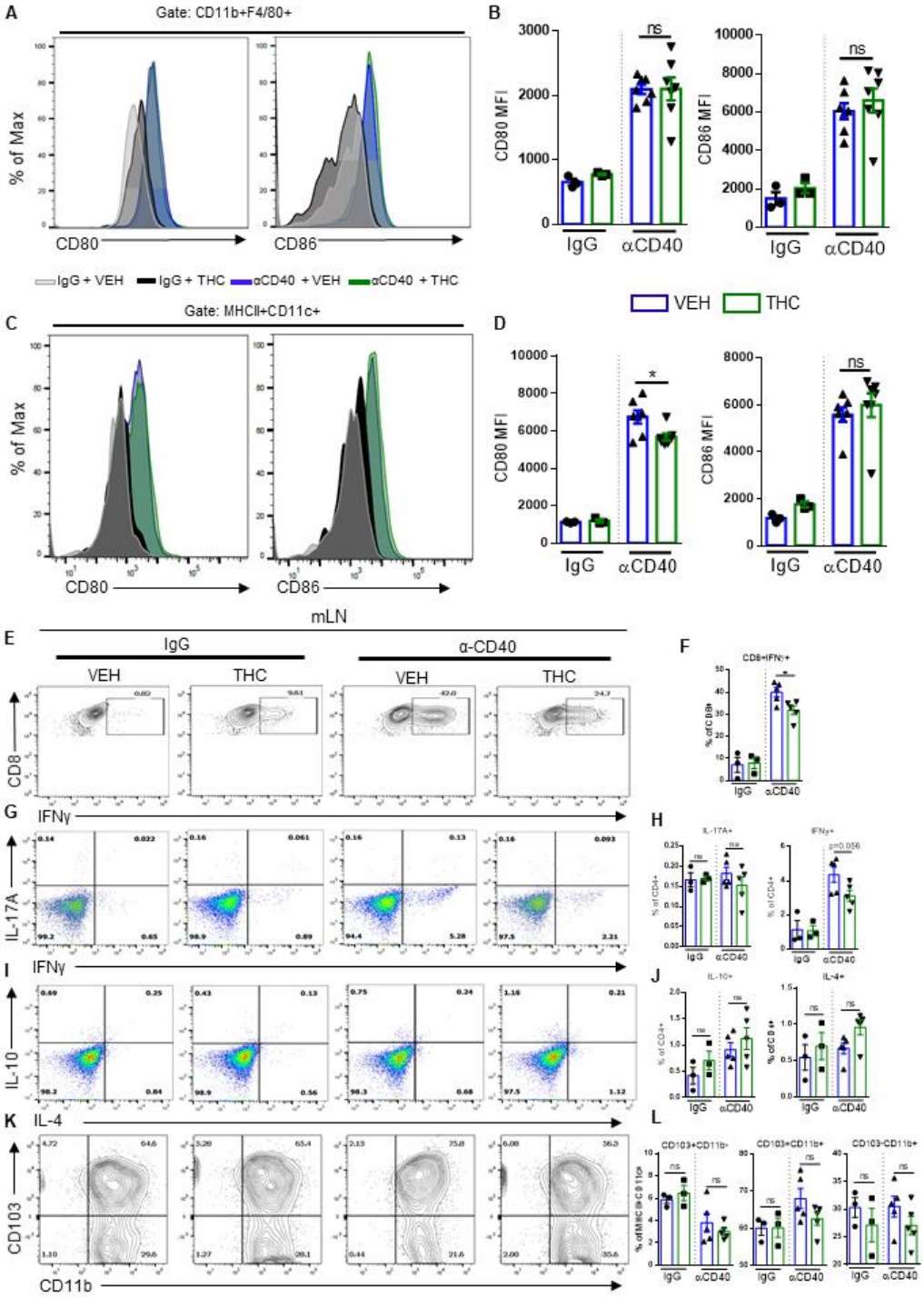

Figure 3.9. ***THC treatment reduces dendritic cell activation lessening the severity of αCD40 colitis*** Mice were pre-treated for 3 days with VEH or THC before disease induction via i.p. injection of 200 µg anti-mouse αCD40 or IgG control. Treatments continued until sacrifice seven days post disease induction. At sacrifice, mLNs or cLPs were taken and analyzed by flow cytometry for immune cells of interest. **(A, C)** Representative overlaid histograms displaying CD80 and CD86 expression in cLP

macrophages, **(A)** (gate: Live, CD45+CD11b+F4/80+), and in cLP dendritic cells **(C)** (gate: Live, CD45+MHCII^{HI}CD11c+). **(E, G, I, K)** Representative flow cytometry plots from the mLN of CD8+IFNγ+ cells **(E)** (gate: CD3+CD4-CD8+); IL-17A and IFNγ single and double positive cells **(G)** (gate: CD3+CD4+); IL-10 and IL-4 positive cells **(I)** (gate: CD3+CD4+); and dendritic cell subsets **(K)** (gate: MHCII^{HI}CD11c+). **(F, H, J, L)** Quantification of flow cytometry results (n=3 IgG groups, n=5-7 αCD40 groups). Data are presented as mean ± SEM of two independent experiments. *P<0.05, **P<0.01, ****P<0.0001 by Two-way ANOVA with Tukey's multiple comparisons test.

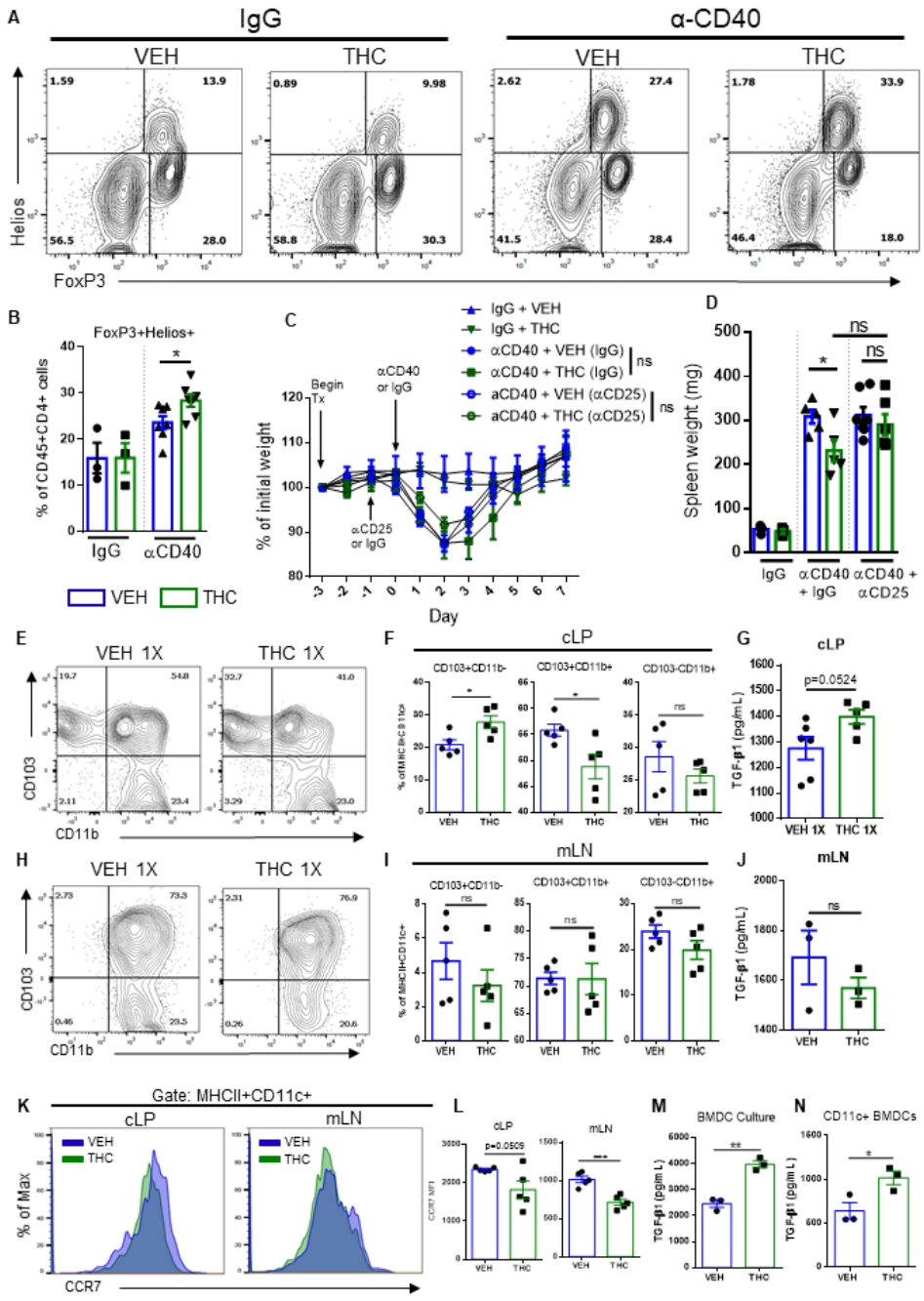

Figure 3.10. ***Dendritic cell re-programming and not Treg induction are the mechanism through which THC ameliorates αCD40-induced inflammation.*** Mice were pre-treated for 3 days with VEH or THC before disease induction via i.p. injection of 200 μg anti-mouse αCD40 or IgG control. Treatments continued until sacrifice seven days post disease induction. **(A)** Representative flow cytometry contour plots of n- and iTregs in the cLP (gate: Live,CD45+CD4+). **(B)** Quantification of flow cytometry results (n=3-8). Mice were pre-treated with VEH or THC for 2 days before depletion of Tregs via i.p. injection of rat anti-mouse CD25 (clone PC61, 100 mg/kg) or isotype control. The next

day disease was induced by i.p. injection of αCD40 or IgG control. **(C)** Weight was monitored, and spleen weight was recorded on day 7 at sacrifice **(D)** n=3 IgG, n=5 αCD40 + IgG, n=7 αCD40 + αCD25). Data are presented as mean ± SEM. *P<0.05, **P<0.01, ****P<0.0001 by Two-way ANOVA with Tukey's multiple comparisons test. Naïve mice were administered VEH or THC once and 24 hours later were sacrificed and cLP and mLN were harvested. Representative contour plots of dendritic cell subsets in the cLP **(E)** and mLN **(H)**, that are quantified in **(F)** and **(I)**, respectively (n=5 per group). 1x106 live cLP or mLN cells from indicated groups were plated in complete media overnight, spun down, and supernatants were collected and subjected to sandwich ELISA for TGF-β1 quantification. TGF-β1 levels in the cLP **(G)** (n=5) and mLN **(J)** (n=3) supernatants of indicated groups. **(K)** Overlaid histograms of CCR7 expression in DCs from indicated mice in the cLP or mLN. **(L)** Mean fluorescence intensity of CCR7 expression (n=5). TGF- β1 levels from the supernatant of BMDCs treated with VEH or THC after 7 days of culture **(M)** or after one day of culture after CD11c+ cell selection **(N)** (n=3 per group). Data are presented as mean ± SEM. *P<0.05, **P<0.01, ****P<0.0001 by Students t-test.

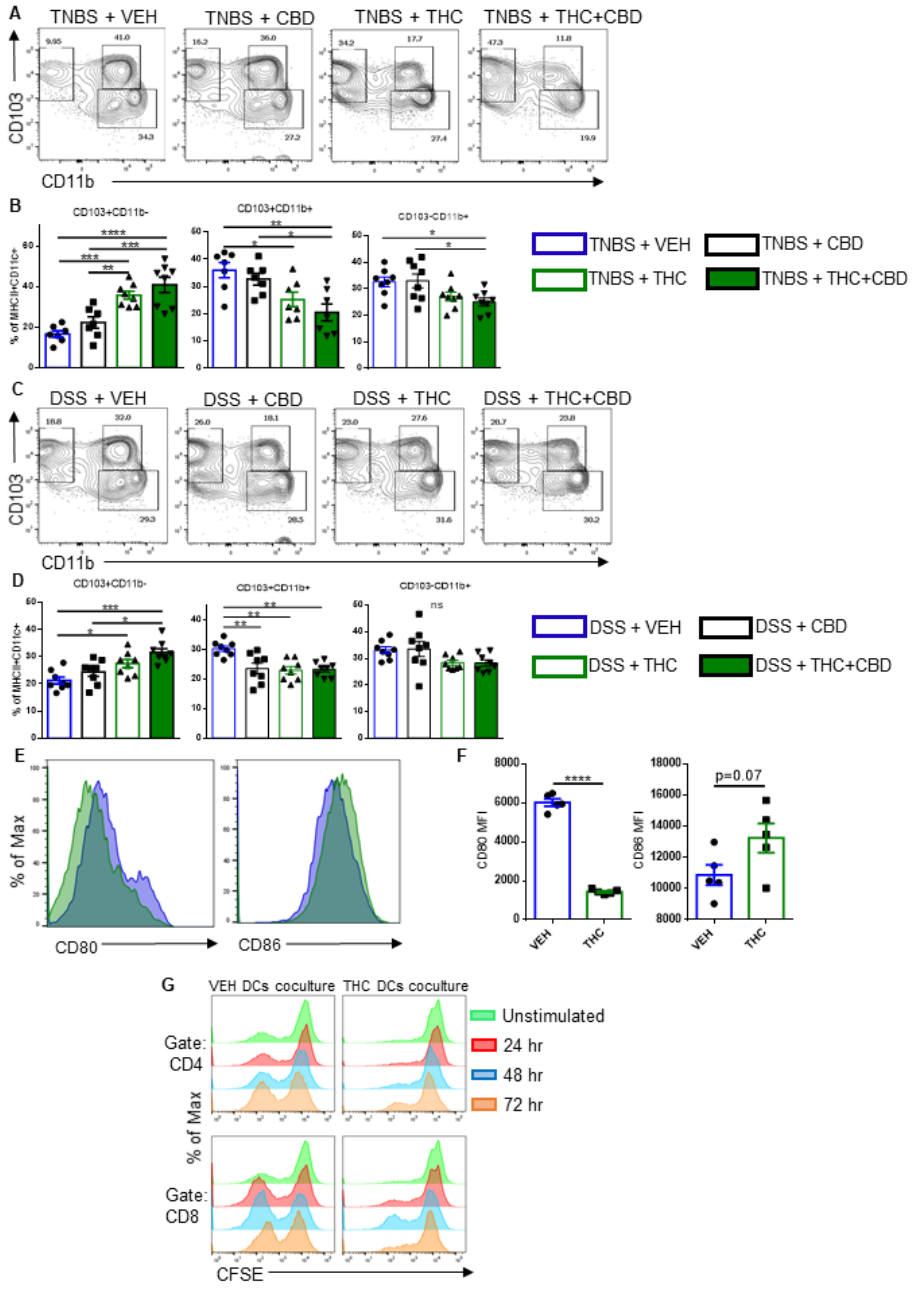

Figure 3.11. ***THC reduces pro-inflammatory DCs and decreases CD80 expression to reduce T cell responses.*** BALB/c mice were injected intrarectally with 100 mg/kg TNBS in 50% ethanol. Starting three days before disease induction and continuing daily, mice were gavaged with either: Vehicle (10% EtOH in PBS+Tween-80), CBD (10 mg/kg), THC (10mg/kg) or a combination of THC and CBD (10 mg/kg, both). **(A)** Representative contour plots of cLP dendritic cell subsets at sacrifice (gate: Live,CD45+,MHCII^{HI}CD11c+) (n=7). C57BL/6 mice were treated with either: Vehicle, CBD (10 mg/kg), THC (10mg/kg) or a combination of THC and CBD (10 mg/kg, both) for 3 days before 2% DSS was added to their drinking water. DSS remained in the

drinking water until termination of the study 14 days later. Mice were sacrificed at 14 days post disease induction and cLP was isolated and stained for markers of dendritic cell phenotype CD103 and CD11b. **(C)** Representative contour plots of cLP dendritic cell subsets at sacrifice (gate: Live,CD45+,MHCII^{HI}CD11c+) (n=7-8). Bone marrow cells were cultured *in vitro* with GM-CSF, IL-4 and either THC (10μM) or VEH for 7 days to induce dendritic cell generation from bone marrow precursors. **(E)** Representative overlaid histograms of CD80 and CD86 expression gated on dendritic cells (MHCII^{HI}CD11c+). **(B, D, F)** Quantification of flow cytometry results. After 6 days of BMDC generation, CD11c+ cells were selected from wells treated with either THC or VEH and then co-cultured with naïve CFSE-pulsed CD3+ T cells at a ratio of 1:5, DCs : T cells. Un-stimulated wells received 50μg of IgG control antibody, while experimental groups received 50μg of anti-CD40. Cells were collected daily for flow cytometric analysis of CFSE dilution among CD4 and CD8 T cell subsets after being co-cultured with VEH or THC treated DCs. **(G)** Representative offset histograms of CFSE expression gated on CD4 cells (upper panel) or CD8 (lower panel) after incubation with VEH or THC treated DCs and stimulated with IgG (control – unstimulated), or anti-CD40. Data are presented as mean ± SEM. *P<0.05, **P<0.01, ****P<0.0001 Two-way ANOVA with Tukey's multiple comparisons test **(A-D)** or by Students *t*-test **(E, F**).

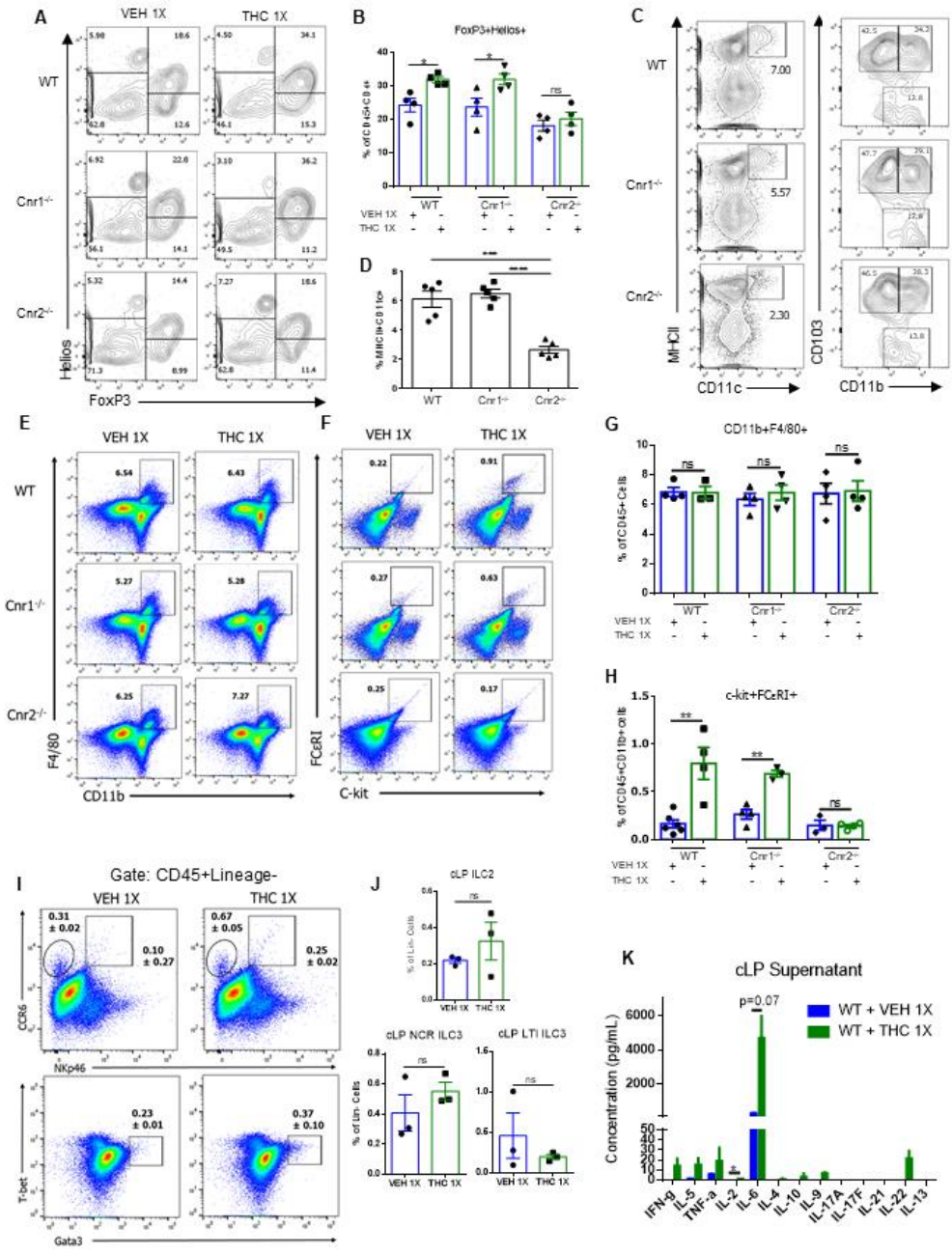

Figure 3.12. ***THC administration causes cLP immune cell phenotype changes through CB2.*** Mice were given one administration of VEH or THC and were sacrificed 24 hours later. cLP was harvested and analyzed via flow cytometry for immune cell populations of interest. **(A)** Contour plots displaying FoxP3+Helios+ nTregs and FoxP3+Helios- iTregs (gate: Live, CD45+CD4+). **(C)** Contour plots displaying total cLP DCs (right column) and DC phenotype (left column, gate: Live,CD45+MHCII^{HI}CD11c+) from indicated mice. **(B, D)** Quantification of flow cytometry results (n=3-5 per group). **(E, F)**

Representative pseudocolor dot plots displaying CD11b+F4/80+ macrophages **(E)** (gate: Live, CD45+), and FCεRI+C-kit+ mast cells **(F)** (gate: Live, CD45+CD11b+) in the cLP. **(G, H)** Quantification of flow cytometry results (n=4 per group). **(I, J)** Histogram and dot plots showing NCR ILC3s (Lineage-CCR6+NKp46+), LTi ILC3s (Lineage-CCR6+NKp46-) and ILC2s (Lineage-Gata3+). **(K)** $1x10^6$ live cLP cells from the indicated groups were plated overnight, supernatants were collected, and subjected to Legendplex assay for Mouse T helper cytokines (n=2 per group). Data are presented as mean ± SEM. *P<0.05, **P<0.01, ****P<0.0001 by Students *t*-test.

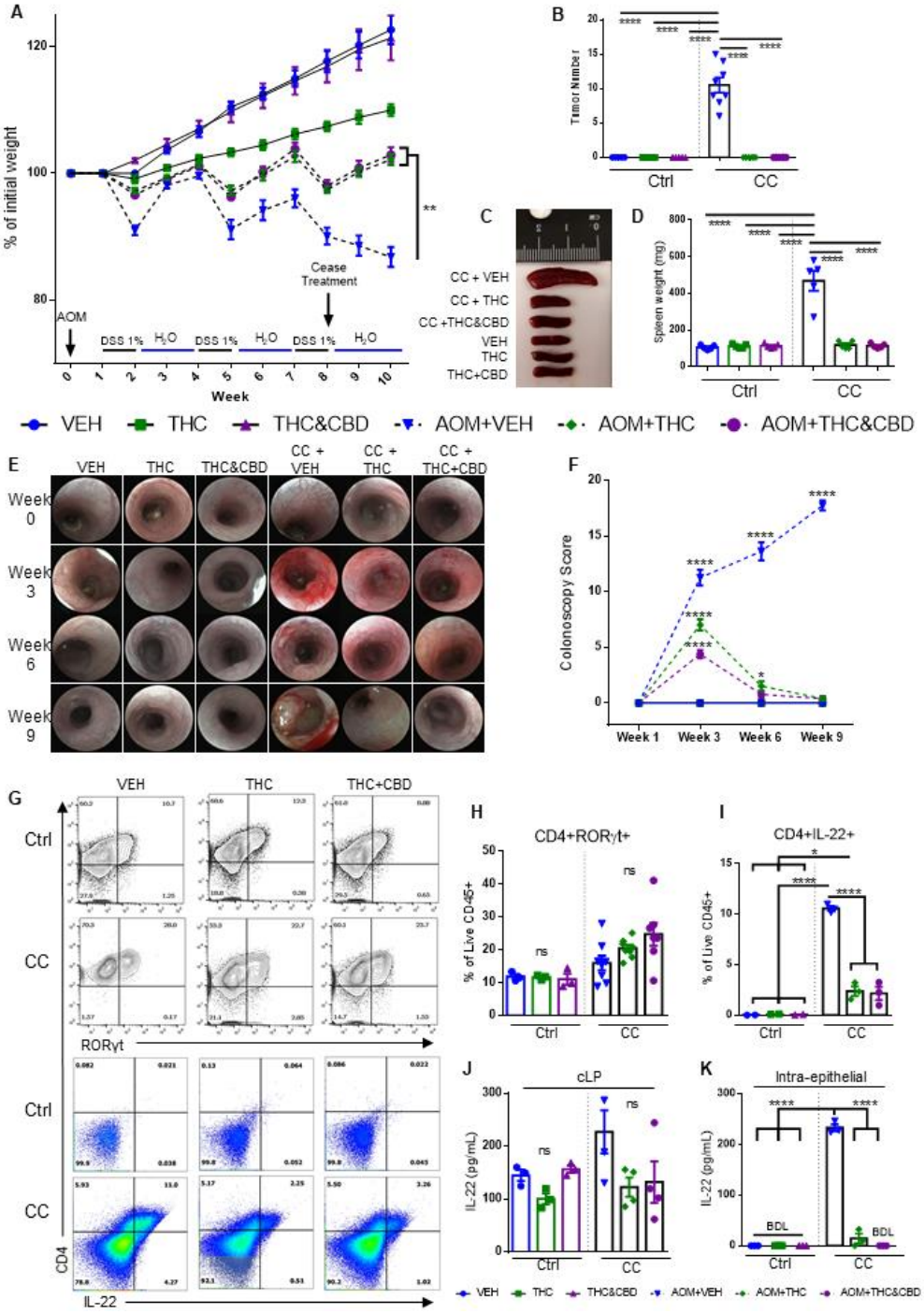

Figure 3.13. ***Cannabinoid receptor activation stems the progression of colitis-induced colon cancer by reducing IL-22 production in the epithelial microenvironment.*** To induce colitis-associated colon cancer (CC), mice were given a single injection of AOM, i.p. (10 mg/kg), then 1 week later treatment started concurrently with the induction of the first cycle of colitis with 2% DSS in the drinking water. Weeklong cycles of DSS (2%) were followed by 2 weeks of regular drinking water for 3 cycles lasting 9 weeks.

Treatment with VEH (10% EtOH in PBS-Tween-80), THC (10 mg/kg) or a combination of THC and CBD (10 mg/kg, both) were given twice a week until the last DSS cycle was completed and then treatments were halted to monitor the effects of cannabinoids on induction of cancer, not the direct effects of the cannabinoids on cancer itself. Control mice were treated twice weekly, but disease was not induced (ctrl). **(A)** Diagram showing percent weight change, treatment schedule and disease course. (n=5, ctrl groups; n=7-9 CC groups). **(B)** Graph showing the number of tumors in each colon at sacrifice. **(C)** Representative photo and **(D)** quantification of spleen weights from indicated mice at sacrifice. Colonoscopies were performed throughout the experiment and representative images are shown in **(E)** and quantified in **(F)** (n=5-8, ctrl groups; n=8 CC groups). cLP and intra-epithelial cell fraction (IEC) was isolated at sacrifice and stained for CD4+RORγt+ and CD4+IL-22+ Th22 cells. **(G)** Representative contour plots displaying CD4+RORγt+ Th17 cells in the cLP (top two panels) and CD4+IL-22+ Th22 cells in the IEC fraction (bottom two panels). **(H, I)** Quantification of flow cytometry plots (n=3, ctrl groups; n=6, CC groups). **(J, K)** $1x10^6$ cells deriving from the cLP or IEC layers from indicated groups were plated overnight, supernatants were collected and subjected to ELISAs for TGF-β1 (n=3, ctrl groups; n=6, CC groups). Data are presented as mean ± SEM. *P<0.05, **P<0.01, ****P<0.0001 by Two-way ANOVA with Tukey's multiple comparisons test. AOM-DSS model was repeated twice. Data presented are from 1 experiment.

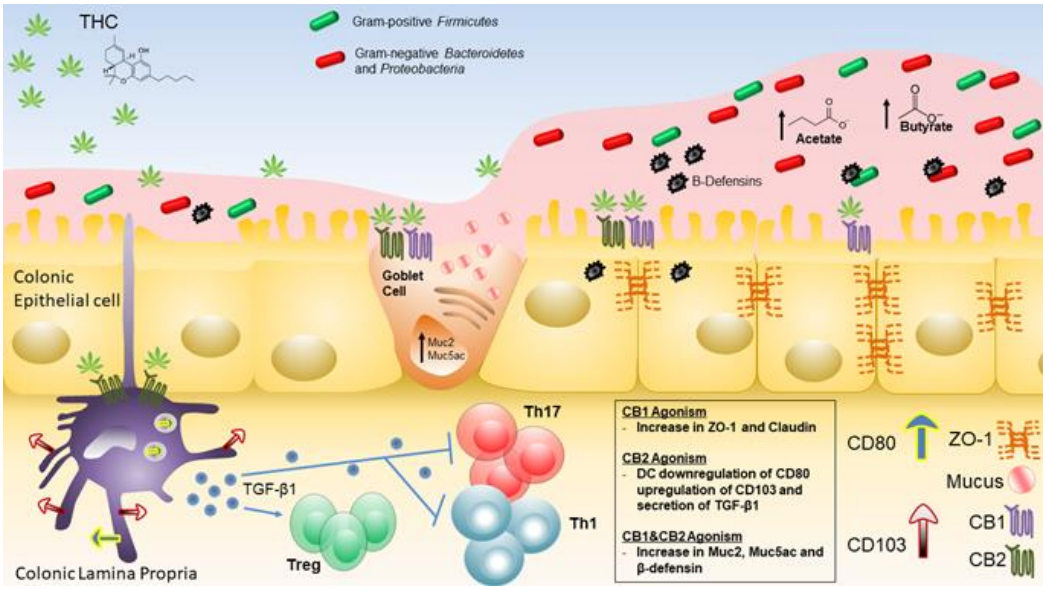

Figure 3.14. ***Graphical abstract of THC-induced effects in the colonic microenvironment***

CHAPTER 4: SUMMARY & CONCLUSIONS

Inflammation is at the heart of a growing number of diseases. Strategies to govern our immune system so that immunogenecity towards symbiotic commensals or the gift of a crucial yet foreign organ transplant are needed. The work presented display how research examining the nature and treatment of disease can reveal innovative strategies for regulating inflammation.

In a model of allogeneic organ transplantation, we examined how a cluster of miRNAs induced after exposure to alloantigen in graft-responding CD4+ T cells work to reduce the activity of anti-inflammatory TGF-β2. We showed that TGF-β2 has the same potency in inducing Tregs as TGF-β1, and that increasing TGF-β2 levels *in vivo* by blocking the interfering miRNA cluster can reduce inflammatory severity. Advances in treating graft rejection may use TGF-β2 to induce Tregs, and we established a new miRNA cluster as a target for alleviating inflammation.

Cannanoids are natural compounds extracted from the *Cannabis sativa* plant. Evidence for their therapeutic efficacy in treating several diseases is growing. The rate of colitis and colon cancer globally are rising, thus new strategies to prevent them are critical. We tested the most frequently consumed cannabinoids, CBD and THC, alone and in tandem to illuminate which component has the greatest therapeutic efficacy in preventing colitis and colitis-associated colon cancer. Our results revealed that THC was very effective at preventing the inflammation induced by three separate models of colitis with disparate

etiologies and one model of colitis-associated colon cancer. We found that CBD had no colitis-preventative value at the dose tested, and if it synergized with THC for a greater effect, the effect was minimal and relegated to longer term models.

THC prevented colitis in two models by increasing the defenses around the colonic microenvironment. THC acted directly on colonocytes and goblet cells to stimulate tight-junction protein and mucus production that are the first line of defense against luminal disturbances and microbes. The increased mucus became a source of food for commensal microbes that led to an increase in the SCFAs acetate and butyrate being secreted after acute THC administration. The changes in bacterial composition seen after THC administration were increases in gram negative *Bacteroidetes* and *Proteobacteria*. While these bacteria were not pathogenic in THC treated mice, they also were not the mechanism through which THC protects against colitis development, as fecal transfers from THC treated mice did not alleviate colitis. THC, working through CB1 and CB2, stimulates the secretion of anti-microbial peptides from colonocytes to balance the increase in gram-negative bacteria. Mice treated prophylactically with THC built up a thicker mucus layer and displayed more protection from colitis than mice who received treatment to alleviate disease.

We utilized a model of colitis that acts solely on the immune system to examine the gut immunological benefits of THC on colitis development. Our work revealed that THC, through CB2, acts directly on dendritic cells (DCs) to stimulate TGF-β1 production that can induce Tregs and directly suppress effector T cells in the colonic lamina propria. THC also reduces DC migration between gut lymphatic tissue, reducing the expansion of T cells induced in anti-CD40, TNBS and DSS models of colitis. In the AOM + DSS model of

colitis-associated colon cancer, THC proved efficacious at preventing colitis and associated cancer in a longer model, displaying prolonged mucus secretion and a reduction in intra-epithelial IL-22 secreting Th22 cells, which can promote cancer. Our data paint a picture wherein THC enacts a sophisticated network of interaction between colonocyte production of mucus and defensins to regulate the gut microbiota, while calming the underlying immune cells from ruinous inflammation through DC secretion of TGF-β1 and the induction of Tregs.

Through an examination of the mechanisms that cause and prevent inflammation, the work described in this dissertation reveal epigenetic, molecular and cellular pathways that regulate inflammation.

REFERENCES

1. Morris, P.J., 2004. Transplantation — A Medical Miracle of the 20th Century. *New England Journal of Medicine* 351, 2678–2680.
2. Marcén, R. Immunosuppressive Drugs in Kidney Transplantation. *Drugs* **69**, 2227–2243 (2009).
3. Tang, Q. & Vincenti, F. Transplant trials with Tregs: perils and promises. *J Clin Invest* **127**, 2505–2512 (2017).
4. Parmar, S., Liu, X., Najjar, A., Shah, N., Yang, H., Yvon, E., Rezvani, K., McNiece, I., Zweidler-McKay, P., Miller, L., Wolpe, S., Blazar, B.R., Shpall, E.J., 2015. Ex vivo fucosylation of third-party human regulatory T cells enhances anti-graft-versus-host disease potency in vivo. *Blood* 125, 1502–1506.
5. Safinia, N., Scotta, C., Vaikunthanathan, T., Lechler, R.I., Lombardi, G., 2015. Regulatory T Cells: Serious Contenders in the Promise for Immunological Tolerance in Transplantation. *Front Immunol* 6, 438.
6. Safinia, N., Vaikunthanathan, T., Fraser, H., Thirkell, S., Lowe, K., Blackmore, L., Whitehouse, G., Martinez-Llordella, M., Jassem, W., Sanchez-Fueyo, A., Lechler, R.I., Lombardi, G., 2016. Successful expansion of functional and stable regulatory T cells for immunotherapy in liver transplantation. *Oncotarget*.
7. Edozie, F.C., Nova-Lamperti, E.A., Povoleri, G.A.M., Scottà, C., John, S., Lombardi, G., Afzali, B., 2014. Regulatory T-cell therapy in the induction of transplant tolerance: the issue of subpopulations. *Transplantation* 98, 370–379.
8. Daniel, V., Wang, H., Sadeghi, M., Opelz, G., 2014. Interferon-Gamma Producing Regulatory T Cells as a Diagnostic and Therapeutic Tool in Organ Transplantation. *International Reviews of Immunology* 33, 195–211.
9. Wang, L., Liu, Y., Han, R., Beier, U.H., Thomas, R.M., Wells, A.D., Hancock, W.W., 2013. Mbd2 Promotes Foxp3 Demethylation and T-Regulatory-Cell Function. *Mol. Cell. Biol.* 33, 4106–4115.

10. Mellor, A.L., Munn, D.H., 2011. Physiologic Control of the Functional Status of Foxp3+ Regulatory T Cells. *The Journal of Immunology* 186, 4535–4540.
11. Gu, A.-D., Wang, Y., Lin, L., Zhang, S.S., Wan, Y.Y., 2012. Requirements of transcription factor Smad-dependent and -independent TGF-β signaling to control discrete T-cell functions. *PNAS* 109, 905–910.
12. Sakaguchi, S., Yamaguchi, T., Nomura, T., Ono, M., 2008. Regulatory T Cells and Immune Tolerance. *Cell* 133, 775–787.
13. Francisco, L.M., Salinas, V.H., Brown, K.E., Vanguri, V.K., Freeman, G.J., Kuchroo, V.K., Sharpe, A.H., 2009. PD-L1 regulates the development, maintenance, and function of induced regulatory T cells. *J Exp Med* 206, 3015–3029.
14. Liu Y, Zhang P, Li J, Kulkarni AB, Perruche S, Chen W. A critical function for TGF-beta signaling in the development of natural CD4+CD25+Foxp3+ regulatory T cells. *Nat Immunol*. 2008;9(6):632–40.
15. Chen W, Jin N, Hardegen W, Lei KJ, Li L, Marinos N, McGrady G, Wahl SM. Conversion of peripheral CD4+CD25- naive T cells to CD4+CD25+ regulatory T cells by TGF-beta induction of transcription factor Foxp3. *J Exp Med*. 2003;198(12):1875–86.
16. Lodish, H.F., Zhou, B., Liu, G., Chen, C.-Z., 2008. Micromanagement of the immune system by microRNAs. *Nat Rev Immunol* 8, 120–130.
17. Murugaiyan, G., da Cunha, A.P., Ajay, A.K., Joller, N., Garo, L.P., Kumaradevan, S., Yosef, N., Vaidya, V.S., Weiner, H.L., 2015. MicroRNA-21 promotes Th17 differentiation and mediates experimental autoimmune encephalomyelitis. *J. Clin. Invest*. 125, 1069–1080.
18. Baumjohann, D., Ansel, K.M., 2013. MicroRNA-mediated regulation of T helper cell differentiation and plasticity. *Nat Rev Immunol* 13, 666–678. doi:10.1038/nri3494
19. O'Connell, R.M., Rao, D.S., Baltimore, D., 2012. microRNA Regulation of Inflammatory Responses. *Annual Review of Immunology* 30, 295–312.

20. Liston, A., Lu, L.-F., O'Carroll, D., Tarakhovsky, A., Rudensky, A.Y., 2008. Dicer-dependent microRNA pathway safeguards regulatory T cell function. *Journal of Experimental Medicine* 205, 1993–2004.
21. Lu, L.-F., Thai, T.-H., Calado, D.P., Chaudhry, A., Kubo, M., Tanaka, K., Loeb, G.B., Lee, H., Yoshimura, A., Rajewsky, K., Rudensky, A.Y., 2009. Foxp3-dependent microRNA155 confers competitive fitness to regulatory T cells by targeting SOCS1 protein. *Immunity* 30, 80–91.
22. Lu, L.-F., Boldin, M.P., Chaudhry, A., Lin, L.-L., Taganov, K.D., Hanada, T., Yoshimura, A., Baltimore, D., Rudensky, A.Y., 2010. Function of miR-146a in controlling Treg cell-mediated regulation of Th1 responses. *Cell* 142, 914–929.
23. Okoye, I.S., Coomes, S.M., Pelly, V.S., Czieso, S., Papayannopoulos, V., Tolmachova, T., Seabra, M.C., Wilson, M.S., 2014. MicroRNA-Containing T-Regulatory-Cell-Derived Exosomes Suppress Pathogenic T Helper 1 Cells. *Immunity* 41, 89–103.
24. Hu, Y., Wang, C., Li, Y., Zhao, J., Chen, C., Zhou, Y., Tao, Y., Guo, M., Qin, N., Ren, T., Wen, Z., Xu, L., 2015. MiR-21 controls in situ expansion of CCR6+ regulatory T cells through PTEN/AKT pathway in breast cancer. *Immunol. Cell Biol.* 93, 753–764.
25. Smigielska-Czepiel, K., van den Berg, A., Jellema, P., van der Lei, R.J., Bijzet, J., Kluiver, J., Boots, A.M.H., Brouwer, E., Kroesen, B.-J., 2014. Comprehensive analysis of miRNA expression in T-cell subsets of rheumatoid arthritis patients reveals defined signatures of naive and memory Tregs. *Genes Immun* 15, 115–125.
26. Lynch, S. V. & Pedersen, O. The Human Intestinal Microbiome in Health and Disease. *New England Journal of Medicine* 375, 2369–2379 (2016).
27. Ng, S. C. *et al.* Worldwide incidence and prevalence of inflammatory bowel disease in the 21st century: a systematic review of population-based studies. *The Lancet* 390, 2769–2778 (2017).
28. Coward, S. *et al.* Past and Future Burden of Inflammatory Bowel Diseases Based on Modeling of Population-based Data. *Gastroenterology* (2019).

29. Baker, K. T., Salk, J. J., Brentnall, T. A. & Risques, R. A. Precancer in ulcerative colitis: the role of the field effect and its clinical implications. *Carcinogenesis* 39, 11–20 (2018).
30. Eaden, J., Abrams, K. & Mayberry, J. The risk of colorectal cancer in ulcerative colitis: a meta-analysis. *Gut* 48, 526–535 (2001).
31. Duerr, R. H. *et al.* A Genome-Wide Association Study Identifies IL23R as an Inflammatory Bowel Disease Gene. *Science* 314, 1461–1463 (2006)
32. Cho, J. H. The genetics and immunopathogenesis of inflammatory bowel disease. *Nature Reviews Immunology* 8, 458–466 (2008).
33. de Souza, H. S. P. & Fiocchi, C. Immunopathogenesis of IBD: current state of the art. *Nature Reviews Gastroenterology & Hepatology* 13, 13–27 (2016).
34. Llewellyn, S. R. *et al.* Interactions Between Diet and the Intestinal Microbiota Alter Intestinal Permeability and Colitis Severity in Mice. *Gastroenterology* 154, 1037-1046.e2 (2018).
35. Desai, M. S. *et al.* A dietary fiber-deprived gut microbiota degrades the colonic mucus barrier and enhances pathogen susceptibility. *Cell* 167, 1339-1353.e21 (2016).
36. Bernstein, C. N. & Shanahan, F. Disorders of a modern lifestyle: reconciling the epidemiology of inflammatory bowel diseases. *Gut* 57, 1185–1191 (2008).
37. Hirata, Y., Ihara, S. & Koike, K. Targeting the complex interactions between microbiota, host epithelial and immune cells in inflammatory bowel disease. *Pharmacol. Res.* 113, 574–584 (2016).
38. Kaplan, G. G. & Ng, S. C. Globalisation of inflammatory bowel disease: perspectives from the evolution of inflammatory bowel disease in the UK and China. *Lancet Gastroenterol Hepatol* 1, 307–316 (2016).
39. Devane, W. A. *et al.* Isolation and structure of a brain constituent that binds to the cannabinoid receptor. *Science* 258, 1946–1949 (1992).
40. Lu, H.-C. & Mackie, K. An Introduction to the Endogenous Cannabinoid System. *Biological Psychiatry* 79, 516–525 (2016).
41. Marzo, V. D. New approaches and challenges to targeting the endocannabinoid system. *Nature Reviews Drug Discovery* 17, 623–639 (2018).

42. Whiting, P. F. *et al.* Cannabinoids for Medical Use: A Systematic Review and Meta-analysis. *JAMA* 313, 2456–2473 (2015).
43. van Amerongen, G. *et al.* Effects on Spasticity and Neuropathic Pain of an Oral Formulation of Δ9-tetrahydrocannabinol in Patients With Progressive Multiple Sclerosis. *Clinical Therapeutics* 40, 1467–1482 (2018).
44. Roth, M. D., Castaneda, J. T. & Kiertscher, S. M. Exposure to Δ9-Tetrahydrocannabinol Impairs the Differentiation of Human Monocyte-derived Dendritic Cells and their Capacity for T cell Activation. *J Neuroimmune Pharmacol* 10, 333–343 (2015).
45. Eisenstein, T. K. Effects of Cannabinoids on T-cell Function and Resistance to Infection. *J Neuroimmune Pharmacol* 10, 204–216 (2015).
46. Sido, J. M., Nagarkatti, P. S. & Nagarkatti, M. Production of endocannabinoids by activated T cells and B cells modulates inflammation associated with delayed-type hypersensitivity. *Eur. J. Immunol.* 46, 1472–1479 (2016).
47. Cabral, G. A., Rogers, T. J. & Lichtman, A. H. Turning Over a New Leaf: Cannabinoid and Endocannabinoid Modulation of Immune Function. *Journal of Neuroimmune Pharmacology* 10, 193–203 (2015).
48. Singh, U. P. *et al.* Cannabinoid receptor-2 (CB2) agonist ameliorates colitis in IL-10−/− mice by attenuating the activation of T cells and promoting their apoptosis. *Toxicology and Applied Pharmacology* 258, 256–267 (2012).
49. Massa, F. *et al.* The endogenous cannabinoid system protects against colonic inflammation. *J Clin Invest* 113, 1202–1209 (2004).
50. Storr, M. A. *et al.* Activation of the Cannabinoid 2 Receptor (CB2) Protects Against Experimental Colitis. *Inflamm Bowel Dis* 15, 1678–1685 (2009).
51. Alhamoruni, A., Lee, A. C., Wright, K. L., Larvin, M. & O'Sullivan, S. E. Pharmacological Effects of Cannabinoids on the Caco-2 Cell Culture Model of Intestinal Permeability. *J Pharmacol Exp Ther* 335, 92–102 (2010).
52. Ahmed, W. & Katz, S. Therapeutic Use of Cannabis in Inflammatory Bowel Disease. *Gastroenterol Hepatol (N Y)* 12, 668–679 (2016).

53. Hasenoehrl, C., Storr, M. & Schicho, R. Cannabinoids for treating inflammatory bowel diseases: where are we and where do we go? *Expert Rev Gastroenterol Hepatol* 11, 329–337 (2017).
54. Naftali, T. *et al.* Cannabis induces a clinical response in patients with Crohn's disease: a prospective placebo-controlled study. *Clin. Gastroenterol. Hepatol.* 11, 1276-1280.e1 (2013).
55. Naftali, T. *et al.* Low-Dose Cannabidiol Is Safe but Not Effective in the Treatment for Crohn's Disease, a Randomized Controlled Trial. *Dig Dis Sci* 62, 1615–1620 (2017).
56. Couch, D. G., Maudslay, H., Doleman, B., Lund, J. N. & O'Sullivan, S. E. The Use of Cannabinoids in Colitis: A Systematic Review and Meta-Analysis. *Inflamm. Bowel Dis.* 24, 680–697 (2018).
57. Peterson, R.A., 2012. Regulatory T-Cells: Diverse Phenotypes Integral to Immune Homeostasis and Suppression. *Toxicol Pathol* 40, 186–204.
58. Sebastian, M., Lopez-Ocasio, M., Metidji, A., Rieder, S.A., Shevach, E.M., Thornton, A.M., 2016. Helios Controls a Limited Subset of Regulatory T Cell Functions. *J. Immunol.* 196, 144–155.
59. Campos-Mora, M., Morales, R.A., Gajardo, T., Catalán, D., Pino-Lagos, K., 2013. Neuropilin-1 in transplantation tolerance. *Front Immunol* 4, 405.
60. Yadav, M., Louvet, C., Davini, D., Gardner, J.M., Martinez-Llordella, M., Bailey-Bucktrout, S., Anthony, B.A., Sverdrup, F.M., Head, R., Kuster, D.J., Ruminski, P., Weiss, D., Schack, D.V., Bluestone, J.A., 2012. Neuropilin-1 distinguishes natural and inducible regulatory T cells among regulatory T cell subsets in vivo. *Journal of Experimental Medicine* 209, 1713–1722.
61. Zheng, G.X.Y., Ravi, A., Gould, G.M., Burge, C.B., Sharp, P.A., 2011. Genome-wide impact of a recently expanded microRNA cluster in mouse. *PNAS* 108, 15804–15809.
62. Inoue, K., Hirose, M., Inoue, H., Hatanaka, Y., Honda, A., Hasegawa, A., Mochida, K., Ogura, A., 2017. The Rodent-Specific MicroRNA Cluster within the Sfmbt2 Gene Is Imprinted and Essential for Placental Development. *Cell Reports* 19, 949–956.

63. Luo, Y., Liu, Y., Liu, M., Wei, J., Zhang, Y., Hou, J., Huang, W., Wang, T., Li, X., He, Y., Ding, F., Yuan, L., Cai, J., Zheng, F., Yang, J.Y., 2014. Sfmbt2 10th intron-hosted miR-466(a/e)-3p are important epigenetic regulators of Nfat5 signaling, osmoregulation and urine concentration in mice. *Biochimica et Biophysica Acta (BBA) - Gene Regulatory Mechanisms* 1839, 97–106.
64. Regateiro, F.S., Howie, D., Cobbold, S.P., Waldmann, H., 2011. TGF-β in transplantation tolerance. *Current Opinion in Immunology, Special section: Cytokines/Immunogenetics and transplantation* 23, 660–669.
65. Chen, W., Konkel, J.E., 2015. Development of thymic Foxp3(+) regulatory T cells: TGF-β matters. *Eur. J. Immunol*. 45, 958–965.
66. Daley, S.R., Ma, J., Adams, E., Cobbold, S.P., Waldmann, H., 2007. A Key Role for TGF-β Signaling to T Cells in the Long-Term Acceptance of Allografts. *J Immunol* 179, 3648–3654.
67. Söderberg, S.S., Karlsson, G., Karlsson, S., 2009. Complex and Context Dependent Regulation of Hematopoiesis by TGF-β Superfamily Signaling. *Annals of the New York Academy of Sciences* 1176, 55–69.
68. Li, M.O., Wan, Y.Y., Sanjabi, S., Robertson, A.-K.L., Flavell, R.A., 2006. Transforming Growth Factor- β Regulation of Immune Responses. *Annual Review of Immunology* 24, 99-146.
69. Lindsay, M.E., Schepers, D., Bolar, N.A., Doyle, J.J., Gallo, E., Fert-Bober, J., Kempers, M.J.E., Fishman, E.K., Chen, Y., Myers, L., Bjeda, D., Oswald, G., Elias, A.F., Levy, H.P., Anderlid, B.-M., Yang, M.H., Bongers, E.M.H.F., Timmermans, J., Braverman, A.C., Canham, N., Mortier, G.R., Brunner, H.G., Byers, P.H., Van Eyk, J., Van Laer, L., Dietz, H.C., Loeys, B.L., 2012. Loss-of-function mutations in TGFB2 cause a syndromic presentation of thoracic aortic aneurysm. *Nature Genet.* 44, 922–+.
70. Ritelli, M., Chiarelli, N., Dordoni, C., Quinzani, S., Venturini, M., Maroldi, R., Calzavara-Pinton, P., Colombi, M., 2014. Further delineation of Loeys-Dietz syndrome type 4 in a family with mild vascular involvement and a TGFB2 splicing mutation. *BMC Med. Genet.* 15, 91.

71. Lu, R., Ji, Z., Li, X., Qin, J., Cui, G., Chen, J., Zhai, Q., Zhao, C., Zhang, W., Yu, Z., 2015. Tumor suppressive microRNA-200a inhibits renal cell carcinoma development by directly targeting TGFB2. *Tumor Biol.* 36, 6691–6700.
72. Niu, G., Li, B., Sun, L., An, C., 2015. MicroRNA-153 Inhibits Osteosarcoma Cells Proliferation and Invasion by Targeting TGF-β2. *PLoS One* 10.
73. Xie, B., Zhang, C., Kang, K., Jiang, S., 2015. miR-599 Inhibits Vascular Smooth Muscle Cells Proliferation and Migration by Targeting TGFB2. *PLoS One* 10.
74. Druz, A., Chu, C., Majors, B., Santuary, R., Betenbaugh, M., Shiloach, J., 2011. A novel microRNA mmu-miR-466h affects apoptosis regulation in mammalian cells. *Biotechnol. Bioeng.* 108, 1651–1661.
75. Zhang, X., Azhar, G., Wei, J.Y., 2012. The expression of microRNA and microRNA clusters in the aging heart. *PLoS ONE* 7, e34688.
76. Ma, F., Liu, X., Li, D., Wang, P., Li, N., Lu, L., Cao, X., 2010. MicroRNA-466l upregulates IL-10 expression in TLR-triggered macrophages by antagonizing RNA-binding protein tristetraprolin-mediated IL-10 mRNA degradation. *J. Immunol.* 184, 6053–6059.
77. Li, Y., Fan, X., He, X., Sun, H., Zou, Z., Yuan, H., Xu, H., Wang, C., Shi, X., 2012. MicroRNA-466l inhibits antiviral innate immune response by targeting interferon-alpha. *Cell. Mol. Immunol.* 9, 497–502.
78. Namba, K., Kitaichi, N., Nishida, T., Taylor, A.W., 2002. Induction of regulatory T cells by the immunomodulating cytokines α-melanocyte-stimulating hormone and transforming growth factor-β2. *J Leukoc Biol* 72, 946–952.
79. Zhang, H., Yang, P., Zhou, H., Meng, Q., Huang, X., 2008. Involvement of Foxp3-expressing CD4+ CD25+ regulatory T cells in the development of tolerance induced by transforming growth factor-β2-treated antigen-presenting cells. *Immunology* 124, 304–314.
80. Mittelbrunn, M., Gutiérrez-Vázquez, C., Villarroya-Beltri, C., González, S., Sánchez-Cabo, F., González, M.Á., Bernad, A., Sánchez-Madrid, F., 2011. Unidirectional transfer of microRNA-loaded exosomes from T cells to antigen-presenting cells. Nat Commun 2, 282.

81. Okoye, I.S., Coomes, S.M., Pelly, V.S., Czieso, S., Papayannopoulos, V., Tolmachova, T., Seabra, M.C., Wilson, M.S., 2014. MicroRNA-Containing T-Regulatory-Cell-Derived Exosomes Suppress Pathogenic T Helper 1 Cells. Immunity 41, 89–103.
82. Redpath, S.A., van der Werf, N., Cervera, A.M., MacDonald, A.S., Gray, D., Maizels, R.M., Taylor, M.D., 2013. ICOS controls Foxp3(+) regulatory T-cell expansion, maintenance and IL-10 production during helminth infection. Eur. J. Immunol. 43, 705–715.
83. Sido, J.M., Nagarkatti, P.S., Nagarkatti, M., 2015. Δ9-Tetrahydrocannabinol attenuates allogeneic host-versus-graft response and delays skin graft rejection through activation of cannabinoid receptor 1 and induction of myeloid-derived suppressor cells. J Leukoc Biol 98, 435–447.
84. Gagliani, N., Magnani, C.F., Huber, S., Gianolini, M.E., Pala, M., Licona-Limon, P., Guo, B., Herbert, D.R., Bulfone, A., Trentini, F., Di Serio, C., Bacchetta, R., Andreani, M., Brockmann, L., Gregori, S., Flavell, R.A., Roncarolo, M.-G., 2013. Coexpression of CD49b and LAG-3 identifies human and mouse T regulatory type 1 cells. Nat Med 19, 739–746.
85. Aviello, G., Romano, B. & Izzo, A. A. Cannabinoids and gastrointestinal motility: animal and human studies. *Eur Rev Med Pharmacol Sci* 12 Suppl 1, 81–93 (2008).
86. Kinsey, S. G. & Cole, E. C. Acute Δ(9)-tetrahydrocannabinol blocks gastric hemorrhages induced by the nonsteroidal anti-inflammatory drug diclofenac sodium in mice. *Eur. J. Pharmacol.* 715, 111–116 (2013).
87. Ke, P. *et al.* Activation of Cannabinoid Receptor 2 Ameliorates DSS-Induced Colitis through Inhibiting NLRP3 Inflammasome in Macrophages. *PLoS ONE* 11, (2016).
88. Schulz, O. et al. Intestinal CD103+, but not CX3CR1+, antigen sampling cells migrate in lymph and serve classical dendritic cell functions. Journal of Experimental Medicine 206, 3101–3114 (2009).

89. Alhamoruni, A., Wright, K. L., Larvin, M. & O'Sullivan, S. E. Cannabinoids mediate opposing effects on inflammation-induced intestinal permeability. British Journal of Pharmacology 165, 2598 (2012).
90. Palmela, C. *et al.* Adherent-invasive Escherichia coli in inflammatory bowel disease. *Gut* 67, 574–587 (2018).
91. Manichanh, C. et al. Reduced diversity of faecal microbiota in Crohn's disease revealed by a metagenomic approach. Gut 55, 205–211 (2006).
92. Britton, G. J. *et al.* Microbiotas from Humans with Inflammatory Bowel Disease Alter the Balance of Gut Th17 and RORγt+ Regulatory T Cells and Exacerbate Colitis in Mice. *Immunity* 50, 212-224.e4 (2019).
93. Bauché, D. *et al.* LAG3+ Regulatory T Cells Restrain Interleukin-23-Producing CX3CR1+ Gut-Resident Macrophages during Group 3 Innate Lymphoid Cell-Driven Colitis. *Immunity* 49, 342-352.e5 (2018).
94. Rizzo, A. *et al.* Smad7 induces plasticity in tumor-infiltrating Th17 cells and enables TNF-alpha-mediated killing of colorectal cancer cells. *Carcinogenesis* 35, 1536–1546 (2014).
95. Kawashima, H. Roles of the Gel-Forming MUC2 Mucin and Its O-Glycosylation in the Protection against Colitis and Colorectal Cancer. *Biological and Pharmaceutical Bulletin* 35, 1637–1641 (2012).
96. Cobo, E. R., Kissoon-Singh, V., Moreau, F. & Chadee, K. Colonic MUC2 mucin regulates the expression and antimicrobial activity of β-defensin 2. *Mucosal Immunol* 8, 1360–1372 (2015).
97. Differential Activity of IL-12 and IL-23 in Mucosal and Systemic Innate Immune Pathology. *Immunity* 25, 309–318 (2006).
98. Barthels, C. et al. CD40-signalling abrogates induction of RORγt+ Treg cells by intestinal CD103+ DCs and causes fatal colitis. Nat Commun 8, (2017).
99. Longman, R. S. *et al.* CX3CR1+ mononuclear phagocytes support colitis-associated innate lymphoid cell production of IL-22. *Journal of Experimental Medicine* 211, 1571–1583 (2014).
100. Viennois, E., Tahsin, A. & Merlin, D. Purification of Total RNA from DSS-treated Murine Tissue via Lithium Chloride Precipitation. *Bio Protoc* 8, (2018).

101. Dowling, C. M., Walsh, D., Coffey, J. C. & Kiely, P. A. The importance of selecting the appropriate reference genes for quantitative real time PCR as illustrated using colon cancer cells and tissue. *F1000Res* 5, (2016).
102. Ihara, S., Hirata, Y. & Koike, K. TGF-β in inflammatory bowel disease: a key regulator of immune cells, epithelium, and the intestinal microbiota. J Gastroenterol 52, 777–787 (2017).
103. Ramalingam, R. *et al.* Dendritic cell-specific disruption of TGF-β receptor II leads to altered regulatory T cell phenotype and spontaneous multiorgan autoimmunity. *J. Immunol.* 189, 3878–3893 (2012).
104. Ihara, S. *et al.* TGF-β Signaling in Dendritic Cells Governs Colonic Homeostasis by Controlling Epithelial Differentiation and the Luminal Microbiota. *The Journal of Immunology* 196, 4603–4613 (2016).
105. Sun, D. *et al.* Th22 cells control colon tumorigenesis through STAT3 and Polycomb Repression complex 2 signaling. *Oncoimmunology* 5, (2015).
106. Kryczek, I. *et al.* IL-22+CD4+ T cells promote colorectal cancer stemness via STAT3 transcription factor activation and induction of the methyltransferase DOT1L. *Immunity* 40, 772–784 (2014).
107. Kirchberger, S. *et al.* Innate lymphoid cells sustain colon cancer through production of interleukin-22 in a mouse model. *J Exp Med* 210, 917–931 (2013).
108. White, C. M. A Review of Human Studies Assessing Cannabidiol's (CBD) Therapeutic Actions and Potential. The Journal of Clinical Pharmacology 0,
109. Philpott, H. T., O'Brien, M. & McDougall, J. J. Attenuation of early phase inflammation by cannabidiol prevents pain and nerve damage in rat osteoarthritis. *Pain* 158, 2442–2451 (2017).
110. Wang, Y. *et al.* Cannabidiol attenuates alcohol-induced liver steatosis, metabolic dysregulation, inflammation and neutrophil-mediated injury. *Sci Rep* 7, (2017).
111. Hegde, V. L., Nagarkatti, P. S. & Nagarkatti, M. Role of Myeloid-Derived Suppressor Cells in Amelioration of Experimental Autoimmune Hepatitis Following Activation of TRPV1 Receptors by Cannabidiol. *PLoS One* 6, (2011).

112. Carliner, H., Brown, Q. L., Sarvet, A. L. & Hasin, D. S. Cannabis use, attitudes, and legal status in the U.S.: A review. *Preventive Medicine* 104, 13–23 (2017).

APPENDIX: PERMISSION TO REPRINT

BELOW IS PERMISSION FROM *FRONTIERS IN IMMUNOLOGY* TO REPRINT DATA PRESENTED IN CHAPTER 2 OF THIS DISSERTATION